Development of Nanomaterials for Drug Delivery and protein binding

Abdelfatah Blau

Submitted to the University of Sheffield

In fulfilment of the requirements for the degree of

Doctor of Philosophy

Supervisor: Dr. Lance J Twyman

Department of chemistry

June 2023

Acknowledgments

Alhamdulillah, I would like to express my deepest gratitude to my supervisor, Dr. Lance Twyman, for his unwavering support, guidance, and kind suggestions. His helpful feedback has been invaluable in completing this thesis. I would like to thank Dr. Marco conte, for his invaluable assistance during my time as graduate teaching assistance. I am grateful for the supportive environment provided by the Twyman research group, who have treated me like family. I would like to thank Mr. Abdullah, Mr. Reyad, Mr. Abdullatif, Mr. Naif, Mr. Khaled, Mrs. Enas, Mrs. Ouhoud, Mrs. Nada, Mrs. Manar, Mrs. Amal, and all my previous students who have been involved in this project.

I dedicate this thesis to my beloved parents, Aisha, and Salem. You have been my greatest source of inspiration and support throughout my academic journey. Thank you for teaching me the values of strength, perseverance, and hard work. Your unwavering love, encouragement, and sacrifices have made this achievement possible. I am forever grateful for everything you have done for me, and I hope that this thesis serves as a small token of my appreciation for your unwavering support.

To my beautiful and genius daughter, Aisha, this is for you! Thank you for still loving Dad, and I deeply apologize for our journey not being as beautiful as we imagined.

I would like to thank all of the staff of the Chemistry Department at the University of Sheffield. Numerous members of staff from the Chemistry Department have helped me in some way and I wish I could thank them all personally.

Finally, I would like to thank the Ministry of Education and Scientific Research in Libya for providing me with the financial assistance that enabled me to pursue this PhD program.

Abbreviations:

PAMAM………………....Poly(amido amine)

PAMAM-OH………………Neutral Hydroxyl Terminated PAMAM

PAMAM-COOH…………..Acid Terminated PAMAM

DCC……………………… Dynamic combinatorial chemistry

DCLs…………………….... Dynamic combinatorial libraries

DCM…………………….... Dichloromethane

DMSO……………………. Dimethyl sulfoxide

EDA……………………… Ethylenediamine

EDC…………………………1-Ethyl-3-(3-dimethylaminopropyl) carbodiimide

DMAP ……………………4-Dimethylaminopyridine

MA…………………………Methyl Acrylate

BTNA….………………....N-benzoyltyrosine-p-nitroanilide

^{1}H NMR………………….... Nuclear Magnetic Resonance Spectrometry

^{13}C NMR…………………...Nuclear Magnetic Resonance Spectrometry

IR/FTIR……………………Infra-Red/Fourier Transfer Infra-Red Spectrometry

ES-TOF MS……………Electron Spray Time-Of-Flight Mass Spectrometry

MALDI-TOF MS…………Matrix Assisted Laser Desorption Ionisation Time of Flight

Chy……………………….*α*-chymotrypsin

NaOH………………………Sodium Hydroxide

K$_2$CO$_3$………………………Potassium Carbonate

UV/Vis……………………...Spectrometry Ultraviolet/Visible Spectrometry

Ɛ …………………….......Extinction coefficient

Nm…………………………Nanometre

GO………………………… Graphene Oxide

L-Tyr……………………… L-Tyrosine methyl ester

L-Val………...................L-Valine Methyl ester

L-PH.................................L-PhenylAlanine

L-Glu.................................L-Glutamic

BTNA.......................…… N-benzoyltyrosine-p-nitroanilide

<u>Table of Contents</u>

Abstract

Graphene oxide (GO) and dendrimers were investigated as ligands for protein binding and drug delivery in this thesis. Amino acids were used to modify protein binding and recognition, exploiting the architecture of these materials. Firstly, functionalized GO was synthesized with amino acids, creating a monomeric and oligomeric GO surface with functional groups. The effects of functionalization on GO binding to Chy were examined, and the results showed that glutamic oligomeric inhibited binding more than the monomeric system or unfunctionalized GO. Competitive inhibition was observed in all cases.

The next area of study focused on dynamic combinatorial libraries for selecting the optimal dendrimer for a given protein. This involved creating dendrimers and thioester-terminated amino acids, followed by introducing the target protein into a solution containing a library of variously sized dendrimers and functionalized amino acids as part of a dynamic combinatorial selection procedure.

The final area of investigation cantered around non-covalent modification of dendrimers. Dendrimers are increasingly popular for delivering hydrophobic and poorly soluble molecules to specific locations. They can host small guest molecules within their internal space, particularly high-generational dendrimers with secondary interactions. However, dendrimers' practical application is limited due to high cost and synthesis time. Hyperbranched polymers (HBP), simpler and more cost-effective alternatives, could be used if they yield comparable results. This study aimed to explore the encapsulation capabilities of various HBPs in conjunction with dendrimers to improve drug delivery efficacy.

The researcher synthesized neutral PAMAM dendrimers for encapsulation investigations, focusing on three generations (G4.0-OH, G3.0-OH, and G2.0-OH). The study found that G3.0-OH exhibited the most effective drug encapsulation. However, HBPAMAM could not be converted into hydroxyl terminal groups. The study observed a decrease in the molecular weight

of HBPAMAM as reaction time increased, levelling off after thirty minutes. The monomeric molar ratio between EDA and MBA did not affect HBPAMAM's molecular weight. Encapsulation experiments were conducted on both HBPs. HBPAMAM-NH$_2$, with amine terminal groups, improved the solubility of ibuprofen at low and high concentrations, but as polymer concentration increased, the encapsulated drug concentration decreased. Dynamic light scattering (DLS) showed that polymer size increased with concentration, and above 0.04 mg/mL, the polymer began to cluster. Dendrimers were more effective than HBPs at increasing ibuprofen concentration, but HBPs were not significantly less effective at drug encapsulation. At a concentration of 0.75 mg/mL, there was no significant difference between the amine-terminated PAMAM dendrimer G3 and the amine-terminated HBPAMAM in drug encapsulation. At a concentration of 0.32 mg/mL, HBPAMAM-NH$_2$ encapsulated substantially more ibuprofen than the G2 dendrimer.

Chapter 1

Introduction

1.1 Introduction

When proteins are interacting with other proteins, they can form two categories of complexes: homocomplexes and heterocomplexes. Although heterocomplexes can be stable, they are typically less stable than homocomplexes as they can be chemically degraded by external factors.[1] The formation of protein-protein complexes plays a vital role in a wide range of biological processes, such as the hormone-receptor, protease-inhibitor and antibody-antigen complexes involved in regulating gene expression and protein degradation.[2] The formation of a reversible non-covalent interaction between two macromolecules, such as proteins, does not imply that the molecules referred to as 'macro' are both similarly large. In molecular biology and biochemistry, macromolecules typically refer to large molecules, but their size can vary significantly. Interactions can occur between molecules of various sizes, when, for example, smaller proteins or even small molecules like ligands bind to larger proteins.[3] In contrast to covalent interactions, non-covalent interactions do not involve the exchange of electrons. Non-covalent bonding relies on electrostatic and hydrophobic forces, in which no electrons are shared by the two or more molecules involved in the chemical bonds and interactions. These complexes may be stable, relying on the intensity of the interaction between the proteins involved.[4] Understanding the molecular mechanisms governing various physiological and pathological processes and devising new therapeutic strategies requires the study of protein-protein complexes, especially if the proteins being studied interact in an unusual manner. Moreover, several cancer treatments involve the disruption of specific protein-protein complexes. In cancers marked by persistent c-Myc activation, an oncogene implicated in diverse tumour types, the elevated expression of the short-lived c-Myc protein drives oncogenic activation. In this context, c-Myc inhibitors emerge as crucial players in disrupting these interactions and potentially impeding disease progression. By effectively targeting c-Myc, these inhibitors have the potential to slow down cancer growth and

metastasis, thus offering hope for improved cancer treatments and enriching our comprehension of this complex disease.[5]

1.2 Protein-Protein Binding

Protein-protein interactions are pivotal in a multitude of biological processes, influencing enzymatic reactions, cell signalling, gene regulation, immune responses, cell adhesion, structural support, molecule transport, apoptosis, cell cycle control, and neurotransmission. These interactions underpin vital functions such as metabolism, growth, and communication within and between cells.[6] Understanding and manipulating these interactions is fundamental in biomedical research and drug development, as they provide key insights into the molecular mechanisms driving health and disease.[7] In order to create compounds capable of interfering with these interactions, it is imperative to gain a more profound understanding of the attributes defining protein-protein interfaces.[7] Through a deep understanding of the distinctive attributes of protein-protein interfaces, researchers have the capacity to create small molecules tailored to bind to these sites, thereby disrupting the interaction. Such understanding opens the way for developing potential therapeutics that use these small molecules to treat a wide array of diseases by disrupting harmful protein-protein interactions. Referred to as protein-protein interaction inhibitors or disruptors, these small molecules hold promise as effective therapeutic drugs, offering targeted and precise treatment options for diverse medical conditions.[8]

Conformational changes are often observed in protein-protein complex formation, and various models have been suggested to elucidate the underlying mechanisms involved. One such model, introduced by Emil Fischer in 1894, is the 'lock and key' model, which proposes that biological interactions, including protein-protein interactions, are regulated by a shape-selective mechanism. According to this paradigm, each protein has a distinct groove or binding site into which its ideal partner fits precisely without requiring substantial conformational changes. According to this model, the binding affinity and specificity of proteins primarily relies on their

complementary geometries and chemical properties. The 'lock and key' paradigm is widely accepted and guides many current investigations of protein-protein interactions. However, the capacity of the 'lock and key' paradigm to explain the interactions between proteins of different shapes is limited. In 1959, Daniel Koshland proposed the 'induced fit' model to resolve this issue.[10] This model suggests that the binding of two proteins is not a rigid process, but rather requires conformational changes in both proteins if a good fit is to be obtained. The binding of a ligand may cause a conformational change in the proteins, allowing it to better align with and bind more strongly to the ligand. The 'induced fit' model is now widely accepted as a more accurate representation of protein-protein interactions, especially when the binding partners have distinct structures.[11] This model suggests that the active site has a degree of flexibility, enabling it to adapt and undergo a conformational change upon ligand binding. Another proposal is that of a pre-existing equilibrium, where the native state of the protein encompasses a range of conformations at the active site. This dynamic ensemble of conformations attracts the ligand, promoting its binding to an active conformation.[12]
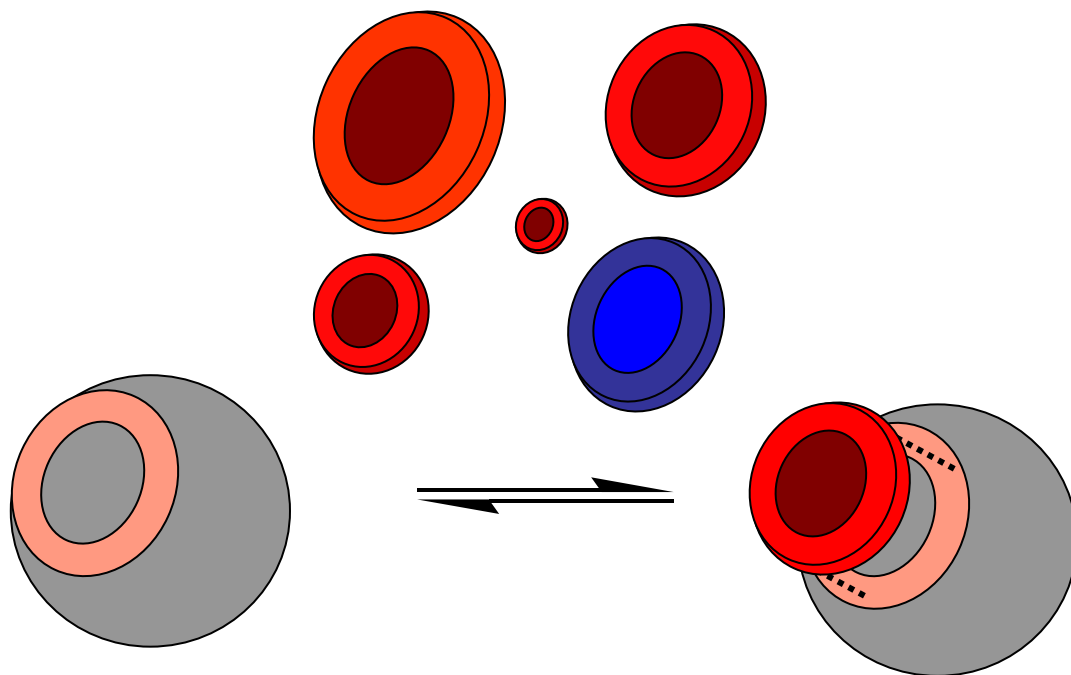
Figure 1.1 The schematic illustrates the "induced fit" model, a recognized mechanism in protein-ligand interactions, where proteins can adapt through conformational changes to enhance binding

with ligands, indicating active site flexibility. Additionally, it illustrates the concept of a pre-existing equilibrium, in which the protein's native state includes diverse active site conformations, one of which enables the ligands to bind.

Protein-protein interactions are complex processes involving a significant surface area of the protein. However, surface area is not the only factor that influences the nature of these interactions; electrostatics and hydrophobicity also play a key part in this determination as well as many specific amino acid/amino acid interactions.[13] The effectiveness of interactions between protein molecules is ultimately decided by the combined effect of these many different factors. Understanding the interaction between these factors is therefore crucial for comprehending the mechanism behind protein-protein interactions.[14] Protein-protein interactions are characterised by a high degree of specificity, with proteins recognising and binding to their best-fitting companion based on a variety of factors, including similarity of interfacial area, three-dimensional geometry, and complementary intermolecular forces. Quantitative terms offer a rigorous framework for assessing and understanding the molecular basis of protein recognition and binding, enabling precise analysis and potential manipulation of these interactions in various biological processes. The method by which two proteins attach to one another is highly selective and requires the presence of a specific combination of components in their simplest form, as well as specific amino acids at the required location.[15] However, if hotspots are unable to form suitable binding sites, the development of allosteric modulators remains a viable option. Most of the identified small molecules that modulate protein-protein interactions (PPIs) are inhibitors. Stabilizing PPIs offers a promising approach to modulation, as it is more energy-efficient to combine existing complexes than to inhibit complex formation. Figure 1.2 depicts a system involving interactions between proteins and gives a simplified illustration of the specificity of partner selectionr.[16]
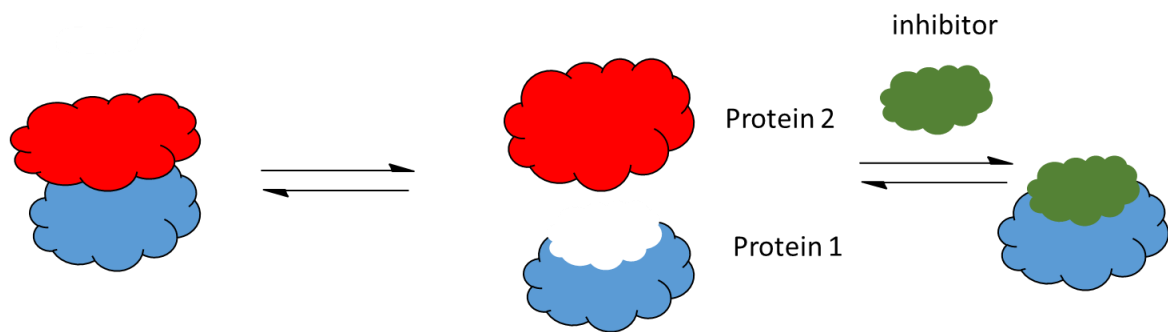
Figure 1.2 Proteins with intricate three-dimensional structures select compatible partners through molecular recognition of molecules with matching binding sites. The proteins connect when a suitable partner is found and thereby initiate crucial biological processes.

The underlying principles that regulate specific protein interactions are not yet completely understood. To gain a deeper understanding of these interactions, Bogan and Thorn used a combination of techniques, including alanine screening and kinetic and thermodynamic measurements to investigate the impact of specific amino acid substitutions on binding kinetics and thermodynamics. They aimed to elucidate the intricate nature of protein-protein interactions and their underlying mechanisms, and determine the role played by each individual residue in the binding process.[12] Clackson and Wells first introduced the concept of the hot spot when they observed that the binding energy between proteins is not evenly distributed across the protein interface.[17] It is instead concentrated in a limited region - the hot spot - made up of specific amino acid residues. These residues are required for the protein complex to be stable and are central in protein-protein interactions.[18]

Bogan and Thorn's study of protein-protein interactions revealed that the hot spots of binding energy are concentrated near the centre of the interface, while peripheral residues rarely contribute to the binding process. Furthermore, the study showed that the residues surrounding the hot spot play a crucial role in keeping bulk solvent away from the interacting residues, which is essential for favourable interactions to occur. Additionally, Bogan and Thorn examined amino acid preferences within the hot spot region and found that tryptophan, tyrosine, and arginine to

14

be the most frequently occurring (with frequencies larger than 10%).[12] The amino acid composition present in hot spots not being random, implied that there was a preference towards certain amino acids in the high energy interactions between two specific proteins in a heterodimer. Understanding the mechanics of protein-protein interactions requires research into protein structures at this level. This understanding is critical for developing strategies to interfere with undesired interactions that lead to disease, such as cancer, neurodegenerative disorders, infectious diseases, and autoimmune diseases.[17]

1.3 Protein-Protein Interaction and Inhibition

The essential role of protein-protein interactions in biological systems makes it possible that we may discover new therapeutic agents by interfering with these interactions.[19] The development of synthetic drugs to disrupt the interactions includes evaluating both small and large molecular weight compounds as prospective protein-protein binding inhibitors. Protein binding relies on various non-covalent interactions, encompassing Van der Waals forces, electrostatic interactions, hydrogen bonds, and hydrophilic/hydrophobic effects, which play crucial roles in the formation and stabilization of protein complexes.[17] A protein's interior active site, which is shielded from the surrounding solvent, or its exterior surface which is exposed, are the two targets in methods for inhibiting protein-protein binding.[20]

1.4 Protein-Protein Inhibition Using Low Molecular Weight Synthetic Agents

1.4.1 Small Synthetic Inhibitors

Most research within the pharmaceutical industry in this field has involved designing small molecules as potential inhibitors. Small molecules are typically created to interact with an enzyme's active site or another specific location. As hydrogen bonds, electrostatic interactions, and salt bridges make up most of the functional components involved the interactions of a protein's active site, small compounds that resemble drugs and have hydrogen bond donor groups

or hydrophilic motifs, may be plausible candidates for therapeutics.[14] It is crucial to note that creating synthetic drugs that are specifically aimed at protein-protein interactions faces several difficulties. At first, the area needed for recognition is large (ranging between approximately 700-1500 Å^2 per protein). Selective targeting is challenging since interacting surfaces have been determined to be shallow voids with no distinctive features.[21] The nature of the binding sites on the interacting protein partners poses an additional challenge. As these binding sites are typically non-contiguous, conventional synthetic peptide mimicry approaches may prove ineffective. Furthermore, the surfaces involved in protein-protein interactions are more intricate than those of enzyme-ligand interactions, and specific structural features on their surfaces, such as pockets and protrusions, are essential for their binding. This complexity can hinder the effectiveness of inhibitors designed to target these interactions, as the inhibitor may struggle to simultaneously bind to both proteins when one has a pocket requiring occupation and the other presents hindering surface features.[22] Additionally, to be considered potential therapeutic molecules, small compounds must be efficient in vivo (as statins and metformin are in their widely-used role as therapeutic agents for cholesterol management and diabetes control). Antibiotics, chemotherapy drugs, and antidepressants are also small molecule treatments effective against bacterial infections and cancer. Any therapeutics must also exhibit low toxicity and high absorption in addition to strong activity against the target protein. Typically, compounds exhibiting "drug-like" properties have molecular weights below 500. Progress was made in developing small molecule inhibitors in the late 1990s when Quershi and colleagues successfully synthesized a non-peptide antagonist.[23]
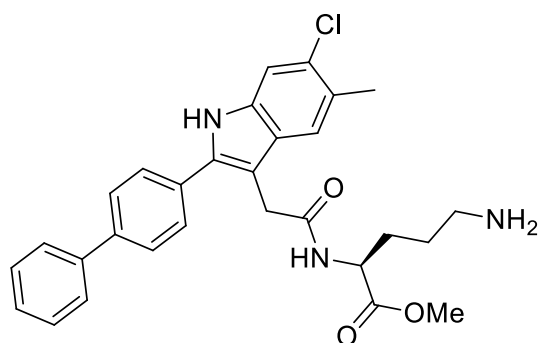
Figure 1.3 The schematic depicts the chemical structure of a non-peptide erythropoietin antagonist, which was identified through screening a chemical library of inhibitors of human erythropoietin binding to the erythropoietin receptor's extracellular region. This led to the discovery of a biphenyl indole derivative with significant inhibitory efficacy.

Inducible nitric oxide synthase is a crucial target protein (iNOS), making particular iNOS inhibitors potentially useful for therapeutic purposes. The enzyme nitric oxide synthase produces nitric oxide, a chemical that is essential for neurotransmission. Combinatorial chemistry was employed by McMillan and colleagues to create the compound, an inhibitor of iNOS. Studies using X-ray crystallography proved that the dimerization interface and substrate binding site have been disrupted. Through an allosteric mechanism, the inhibitor functions by interrupting the dimer formation through an allosteric mechanism, preventing the pairing of two molecules. In this process, the inhibitor binds to a site on the protein, causing a conformational change that hinders the dimerization, ultimately blocking the interaction between the two molecules. Studies conducted in vivo on rats show that the inhibitor demonstrated action with ED_{50} values < 2 mg/kg. These outcomes highlight the therapeutic potential of these inhibitors.[24]
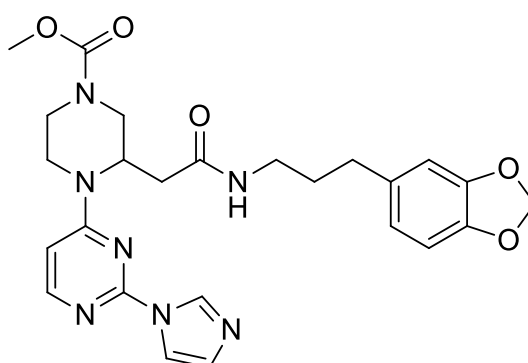
Figure 1.4 Inducible nitric oxide synthase (iNOS), a significant protein target. iNOS, a vital player in signal transduction, is produced by the dimeric enzyme nitric oxide synthase and is linked to tissue damage in autoimmune diseases. Consequently, the development of an iNOS inhibitor holds substantial clinical promise for addressing these conditions.

Another important target is the tumour necrosis factor alpha (TNF-α). TNF-α is also a member of the cytokine family and is involved in systematic inflammation. Despite the successful development and utilization of inhibitory antibodies like Enbrel, Remicade, and Humira for treating rheumatoid arthritis, there is still a preference for small molecule inhibitors due to their cost-effectiveness and ease of administration. By displacing a subunit and generating an inactive dimer, He et al. developed a potent small molecule inhibitor of TNF- that disrupts the biologically active trimer.[25]
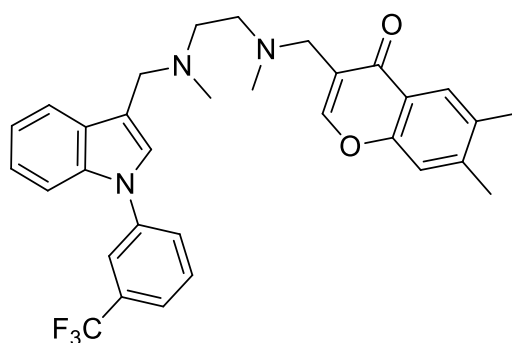
Figure 1.5 The structural arrangement illustrates a small-molecule inhibitor tailored for the specific targeting of the protein tumour necrosis factor (TNF-). This inhibitor induces the displacement of a subunit within the biologically active TNF- trimer, leading to the formation of an inactive dimer.

1.5 α-Helix Mimetics

A breakthrough within this field was the discovery of the important role helical segments play in a range of protein-protein interactions and the flexibility of protein structures that allows proteins to adopt different conformations when binding to different partners. Consequently, the synthesis of helical mimics has significant potential to advance therapeutic development. Approximately 15% of the protein database is comprised of complexes formed by interactions between multiple proteins.[26] Moreover, around 62% of these complexes exhibit a helical structure at their interface.

This data underscores the importance of alpha-helices in mediating protein-protein interactions. In addition, peptides have been designed that exhibit stability (conformational robustness) and specific secondary structures. Suitable conformational stability requires more than 15 amino acid residues. Recent interest has centred on the potential of stable α-turns and α-helices restricted by hydrogen bonds as alternative β-sheet-based methodologies for the management of various illnesses, including cancer and HIV.[26]
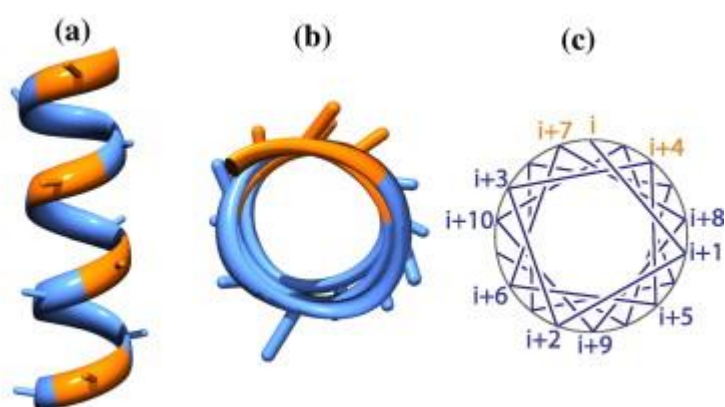
Figure 1.6 The arrangement of residues along a typical α-helix. The side-view shows the i, i + 4, i + 7, and i + 11 residues displayed on the same face (coloured orange). The top-down view shows the distribution of these residues, while the α-helical wheel shows the helix as a cylinder with the residues arranged around its circumference.

In cancer treatment, inhibiting protein-protein interactions is crucial. P53 is a tumour suppressor protein that plays a vital function in protecting cells from noxious alterations. HDM2 plays a crucial role in regulating the level and activity of the tumour suppressor protein P53. When HDM2 is overexpressed, it can interfere with the normal functioning of P53. The binding of P53 and HDM2 involves a helical conformation, where three hydrophobic amino acid residues (Phe19, Trp23, and Leu26) from P53 interact with a hydrophobic groove on HDM2. Disrupting this interaction could lead to the stabilization of P53, which is a promising avenue for developing a new therapeutic strategy for certain types of cancer (it would not be a suitable approach for all cancers).[27] Vassilev et al., have synthesized a small molecule inhibitor that triggers the activation of the P53 pathway in cancerous cells by binding to the specific P53 binding site on HDM2.

Studies involving these small molecule inhibitors targeting HDM2-P53 interactions have demonstrated their capability to induce cell arrest, promote apoptosis, and hinder the growth of human tumour xenografts in nude mice.[28] Investigations using X-ray crystallography have revealed that the binding pocket of HDM2 has a deep cavity loaded with side chains made up of hydrophobic amino acids from the peptide's helical region. Nutlins – a series of analogues of cis-imidazoline – were developed as small molecule antagonists, with Nutlin- being the most optimised compound. The latter was shown to inhibit HDM2-P53 complexes with an IC50 of 90 nM and exhibited activity against xenografts in vivo.[29]
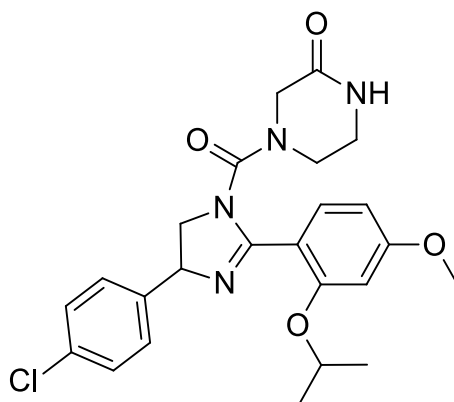
Figure 1.7 The schematic of Nutlins, a group of analogues derived from cis-imidazoline, designed as small molecule antagonists. Among them, Nutlin represents the most optimized compound in this series. It has been demonstrated to effectively inhibit HDM2-P53 complexes with an IC50 of 90 nM and has shown promising activity against xenografts in vivo.

Investigations into inhibiting the HDM2-P53 interaction have continued due to its potential for cancer therapy. Plante et al. (2009) designed a set of proteomimetic inhibitors, known as oligobenzamides, targeting the three critical residues (Phe19, Trp23, and Leu26) at the HDM2-P53 complex interface.[30] To create a successful imitation of the helical structure, it is crucial to design a framework that replicates the amino acid residues found at positions i, i+4, and i+7 of the P53 helix. By utilizing O-alkyl substituents on the amino-terminated tri-benzamide, the orientation of the i, i+4, and i+7 residues of the helix could be emulated. These findings indicate the feasibility of constructing a reliable mimic of the helical structure.[28]
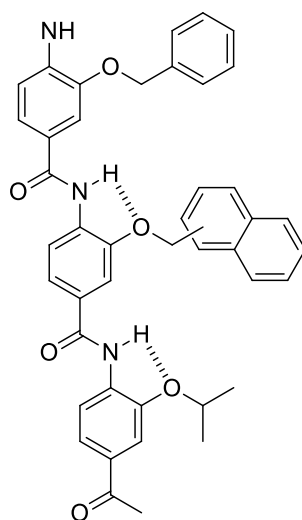
Figure 1.8 The schematic illustrates the molecular arrangement of a proteomimetic inhibitor—an oligobenzamide—showcasing its chemical structure. The inhibitor's structure was overlaid onto the P53 helix, revealing that the O-alkyl substituents of the amino-terminated tri-benzamide align consistently on one face, resembling the spatial orientation of the i, i+4, and i+7 residues of the α-helix. These findings demonstrate the successful creation of an effective mimic.

There has been significant interest in developing non-peptidic small molecule α-helical mimics for inhibiting protein-protein interactions. In 2011, reported the synthesis of an innovative pyrrolopyrimadine-based receptor and evaluated the potential of this scaffold to disrupt the P53-MDMX interaction and serve as an α-helical mimic. Initially, the scaffold underwent screening against a library of 900 compounds, with a focus on primary amines containing hydrophobic groups. These hydrophobic groups were crucial for emulating the side chains of the three amino acids found in P53. Notably, this specific scaffold demonstrated conformational rigidity, good aqueous solubility, and cell permeability. Furthermore, the synthetic route was relatively straightforward, enabling the construction of large libraries and facilitating high throughput screening. Consequently, this scaffold holds promise for discovering a range of inhibitors for protein-protein interactions of this nature.[31]
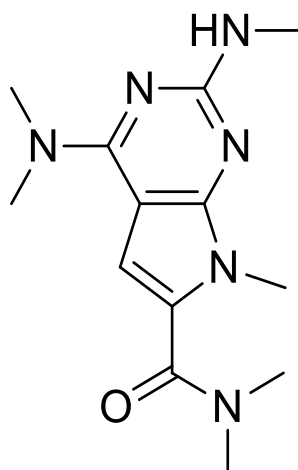
Figure 1.9 A summary of the focus on developing non-peptidic small molecule α-helical mimics for inhibiting protein-protein interactions. They describe the synthesis of a new pyrrolopyrimidine-based receptor and highlight its evaluation for disrupting the p53-MDMX interaction to assess its potential as an α-helical mimic.

1.6 Functionalized Scaffold Molecules as Large Ligands for Selective Protein Binding

The majority of studied molecules disrupt interactions by binding within active protein cavities. In contrast, synthetic molecules that affect protein function by binding to the protein's outer surface remain relatively unexplored. Exploring this uncharted territory not only has the potential to identify new drug candidates, but also contributes to our understanding of the periphery of proteins and the mechanisms of surface recognition. As far back as 1985, Fischer et al. presented evidence of a tetracarboxyphenyl porphyrin acting as a topographical mimic for cytochrome-c binding, with a binding affinity (Kd) of 5μM. Cytochrome-c, a well-studied protein found in horse heart, plays a crucial role in both electron transport and apoptosis – making it an attractive target. The surface of the heme edge of cytochrome-c features a pattern of cationic lysine residues and hydrophobic regions, highlighting its especially strong reliance on electrostatic interactions.[32,33]
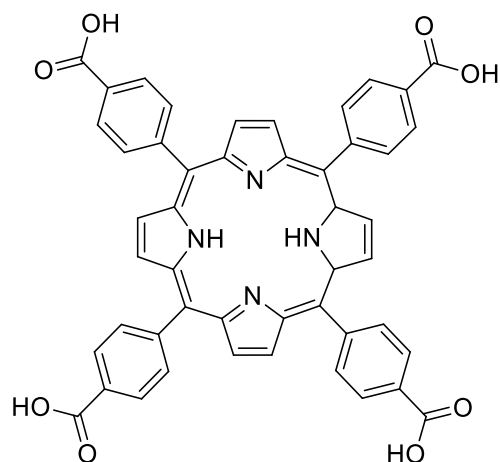
Figure 1.10 depicts the chemical structure of tetracarboxyphenyl porphyrin, which is highly desirable due to its critical involvement in electron transfer and apoptosis processes. The illustration also highlights the presence of cationic lysine residues and hydrophobic regions arranged along the heme edge's surface, underlining the significant reliance on electrostatic interactions, particularly in its functional role.

Hamilton et al. expanded the research in this area by exploring tetraphenyl porphyrin scaffolds and calix[4]arene scaffolds using various analytical techniques, including fluorescence spectroscopy. In 1997, they proposed a novel approach that involved utilizing a macrocyclic scaffold to which peptide loops could be covalently linked. They developed an antibody mimic utilizing calix [4] arene connected to four constrained peptide loops. Calix [4] arene was chosen due to its easy accessibility and ability to adopt a cone shape, which aligns the para substituents on the same edge of the ring, thus creating a binding domain.[32]
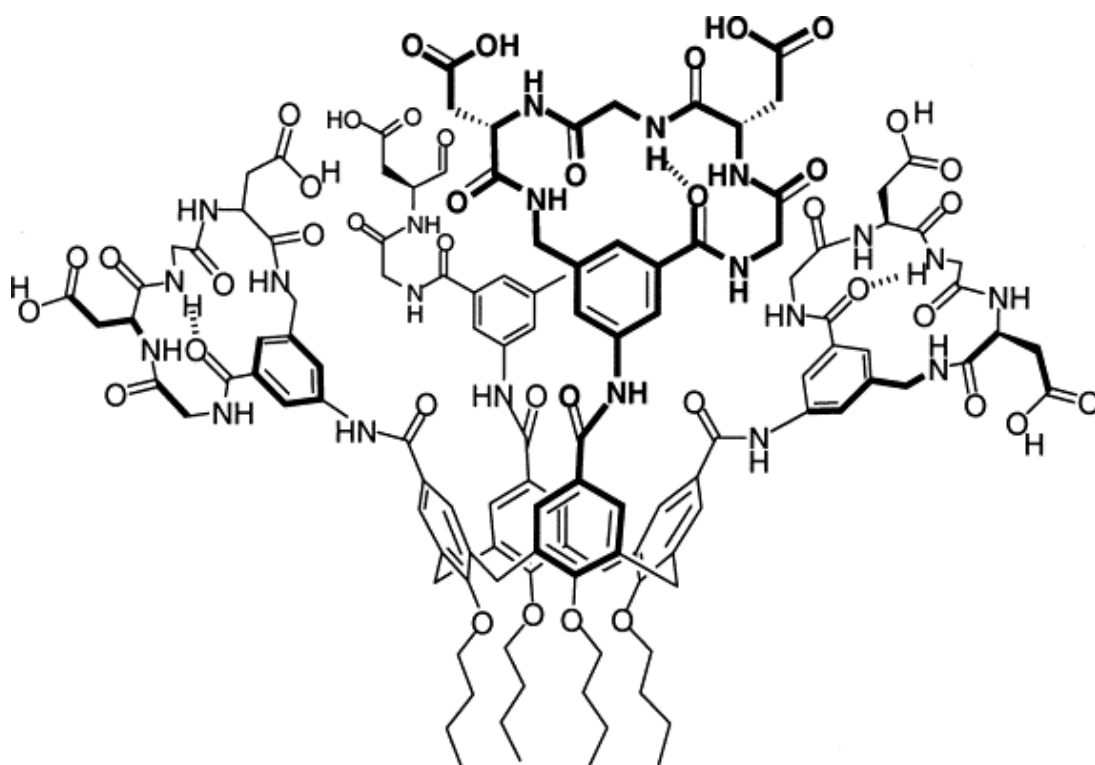
Figure 1.11 A diagram is presented to illustrate the chemical structure of an antibody mimic, constructed using a calix[4]arene scaffold and covalently linked to four peptide loops with the sequence Gly-Asp-Gly-Asp. This synthetic mimic was specifically designed by Hamilton and his colleagues for surface recognition of cytochrome-c. Reprinted with permission from [**Lin, Q.; Hamilton, A. D. C. R. Chim.** 2002, **5, 441-450**].

The initial protein of interest was cytochrome-c, an extensively researched and thoroughly characterized protein recognized for its positively charged surface. To achieve an effective interaction, the peptide loops were designed with the negatively charged sequence Gly-Asp-Gly-Asp. The choice of negatively charged peptide loops was deliberate to complement the positively charged surface of the target protein. From X-ray studies, it was observed that four peptide loops could bind to four lysine residues on the target protein, enabling the synthetic receptor to occupy a significant surface area. The presence of the receptor disrupted the formation of complexes between cytochrome-c and cytochrome-c peroxidase. In 2000, Hamilton demonstrated that receptors constructed on a tetraphenyl porphyrin framework, with various amino acid and peptide derivatives surrounding the outer edge, could recognize and interact with the surface of cytochrome-c.[32] The findings demonstrated that the number of hydrophobic and anionic groups

on a protein surface affected a receptor's relative affinity to that surface. These receptors had a high affinity to bond to the surface of cytochrome-c in an aqueous solution, with the greatest affinity at a Kd of 20 nM. Earlier studies showed that the apoptotic protease activating factor, APAF1 (apoptotic protease activating factor 1) and cytochrome-c can interact. The apoptosis may be activated because of the interaction between cytochrome-c and APAF -1, a highly regulated key process in the intrinsic apoptotic pathway aimed at eliminating damaged or unwanted cells. Dysregulation of this pathway can have implications for various diseases, including cancer, neurodegenerative disorders, and autoimmune diseases, where excessive or insufficient apoptosis may occur.[34]

(a) R= -COOH

(b) R=

(d) R=

(e) R=
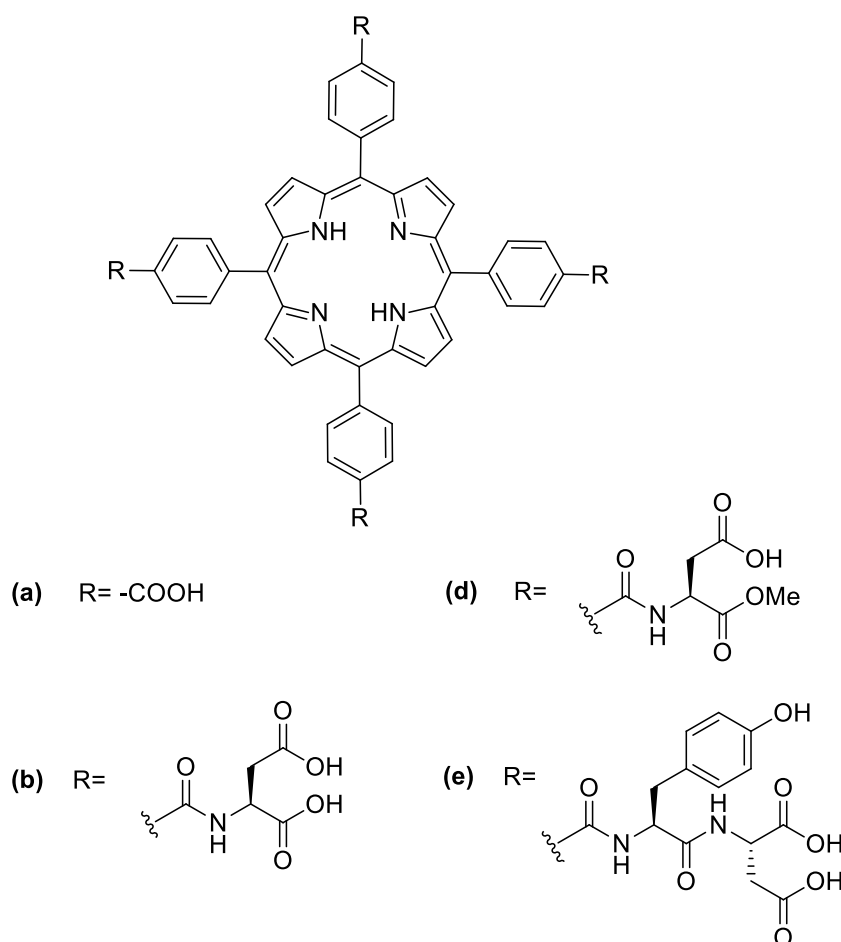
Figure 1.12 The figure illustrates the surface of cytochrome-c and how it can be targeted by receptors designed using a tetraphenyl porphyrin scaffold, incorporating various amino acid and peptide derivatives around its periphery. The study's findings reveal that the receptor's relative affinity for the protein surface is contingent on the number of hydrophobic and anionic groups

incorporated. Remarkably, these receptors show strong binding affinity in an aqueous environment, with receptor 19 having the highest affinity for the cytochrome-c surface, characterized by a Kd value of 20 nM.

The research described in this thesis makes use of a diverse set of large molecules. The next sections introduce and describe the properties that are vital for understanding their applications, which are discussed in later chapters. By providing a comprehensive overview of these properties, the research aims to establish a solid foundation for exploring the practical implications of these large molecules. Understanding their key characteristics is essential for uncovering their potential in various applications and elucidating their role in pharmaceutical sector.

1.7 Dendrimers

Dendrimers are highly branched, three-dimensional macromolecules with a well-defined and symmetric structure, and numerous arms extending from the centre.[35] The step for synthesising dendrimers produces highly branched molecules with a defined peripheral group. Consequently, dendrimers with defined branching molecules are the result of procedures which are simpler to synthesise. However, undefined polymers with unequal branching may be obtained using polymerisation synthesis. Recent investigations have emphasised the synthesis of dendrimers using chemical and biological means, [36] largely because of the potential they have in biological and medicinal applications.[37]

1.7.1 The Structure and Chemistry of Dendrimers

The chemistry of dendrimers is characterised by highly symmetric molecules that begin with a central group of atoms called the core.[38] Branches of other atoms extend from this core and are known as 'dendrons', which grow through diverse chemical reactions.[39] Dendrimers can be produced with a control not achievable with many linear polymers, leading to globular macromolecules with many branches on the peripheral group.
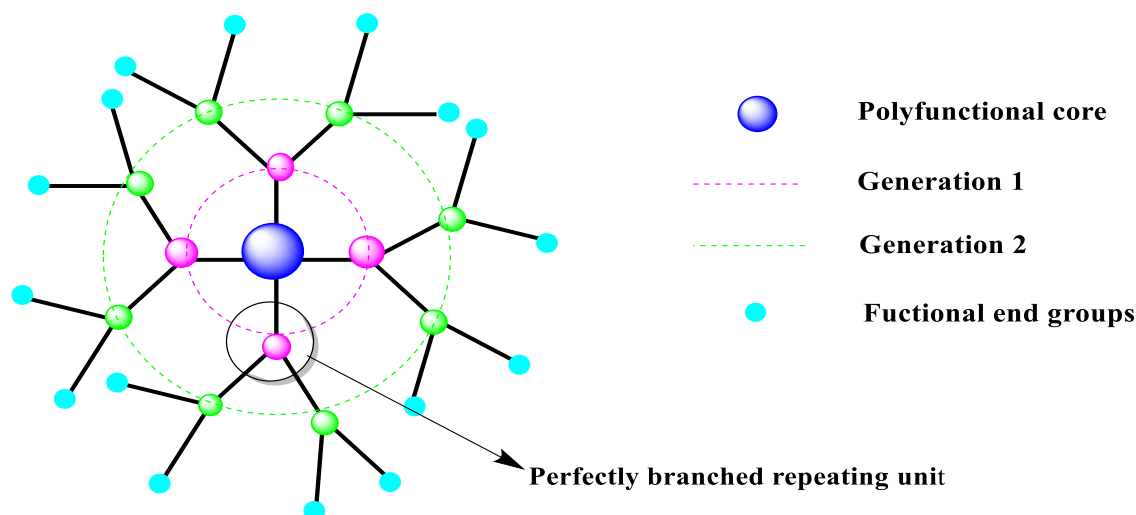
Figure 1.13 A visual representation of the fundamental architecture of dendrimers. Dendrimers are highly branched, tree-like macromolecules characterized by a central core from which multiple generations of repeating units radiate outward. These repeating units form a layered structure, with each generation containing a higher number of branches.

1.7.2 Synthesis Methods of Dendrimers

The controllable synthesis of dendrimers has allowed for the formation of structures with diverse backbones and surface functional groups. Two prominent methods for dendrimer synthesis are divergent synthesis and convergent synthesis. Divergent synthesis, developed by Donald Tomalia, involves the activation and curing of the dendrimer from a polyfunctional core to the surface, resulting in a radial growth.[40] On the other hand, Craig Hawker and Jean Fréchet introduced a convergent synthesis approach that constructs dendrimers by growing them outward from the surface towards focal points. Although both methods produce dendrimers of equal value, they have their respective advantages and limitations.[41]

27

Figure 1.14 There are two main methods for the synthesis of dendrimers: (A) the convergent method and (B) the divergent method.

Divergent synthesis is commonly utilized when scaling up the production of dendrimers, but can result in defects, such as absent arms or dimers, because of iterative reaction sequences and steric strain at the periphery. The process of synthesizing dendrimers can be challenging, particularly when it comes to purification. The conventional method often involves intricate purification procedures due to the complex branching and numerous functional groups present in dendrimers – challenges addressed by the alternative convergent method.[42] In the latter, independent molecular building blocks, or 'dendrons', are first synthesized and purified individually, ensuring their structural purity. Subsequently, these purified dendrons are combined or 'converged' with

a polyfunctional core molecule to form the dendrimer. This approach simplifies the purification process and results in well-defined dendrimers with fewer impurities, offering a more controlled and efficient means of dendrimer synthesis.[43]

Nevertheless, the divergent synthesis faces challenges in formulating high-generation (5G and 6G) dendrimers, due to steric overcrowding around the core. Importantly, both the divergent and convergent methods have limitations, as the dimensions, surface area, and backbone structure of dendrimers play a crucial role in their biological interactions. In the current research, PAMAM dendrimers will be produced through divergent synthesis as this method is adaptable and capable of producing modified and functionalised dendrimers.

1.8 Properties of Dendrimers

In contrast to linear polymers, dendrimers exhibit a consistent and uniform geometry. They are characterized by their non-dispersive nature, which is achieved through a well-defined polymerization process and meticulous control during synthesis. Their unique spherical structure and dimensions closely resemble several important biological polymers. Dendrimers' biological properties have considerable importance and extensive applications in the field of biomedicine.[44]

1.8.1 Solubility

Solubility plays a crucial role in achieving desired outcomes across a wide range of dendrimer applications. This characteristic hinges on the specific functional groups present on the surfaces of dendrimers.[45] One effective approach for enhancing solubility involves modifying the dendrimer's end groups with appropriate functional entities. The desired solubility in particular solvents can be attained by incorporating appropriate multiple modified functional groups on their surface, a modification which also enhances their reactivity and binding capacity. The spherical structure and internal cavities, especially of higher generation dendrimers, has made them attractive and versatile molecules for encapsulating hydrophobic drugs.[46]

1.8.2 Biocompatibility

Typically, any polymer-based carrier employed in biomedical contexts must be non-toxic and biodegradable. The cytotoxicity of dendrimers, in particular, depends largely on the composition of their external groups that come into direct contact with biological cells during interactions. While numerous published studies have examined dendrimer cytotoxicity in vitro, the number of published in vivo studies is limited. In PAMAM dendrimers, the positively charged surface can harm cell membranes and result in cell lysis. Cationic dendrimers exhibit higher cytotoxicity than anionic ones, with PAMAM–OH dendrimers showing the least.[47]

1.8.3 Distribution

Distribution is a fundamental pharmacokinetic characteristic that defines how substances disperse within body tissues and fluids and can be altered by manipulating polymer carrier size and conformation. To be suitable for in vivo applications, polymeric carriers like dendrimers must have a distribution pattern that inherently facilitates precise tissue targeting.[46]

1.9 Interactions Between Drug Molecules and Dendrimers

Research on dendrimers has expanded significantly since their discovery over a century ago, with particular attention being paid to their unique density distribution, including their highly dense peripheral functions and adaptable internal space around the focal core.[48] Their potential application in drug delivery has been explored for approximately 30 years, largely owing to their ability to covalently or non-covalently bind drug molecules to the periphery, thus facilitating drug delivery.
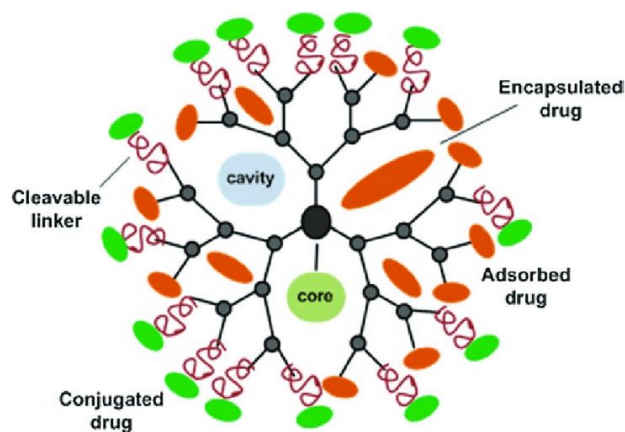
Figure 1.15 Dendrimers employ three drug binding mechanisms: encapsulation within their interior, surface functionalization for targeted delivery, and covalent conjugation. These versatile approaches enhance drug stability, solubility, and controlled release, improving drug delivery precision and efficacy.

1.9.1 Encapsulation of Drugs by Noncovalent Interactions

Due to their internal porous structure, dendrimers have been examined as potential drug delivery systems. They can encapsulate guest molecules through non-bonding interactions. Moreover, dendrimers can interact with poorly soluble medications due to their unique structure, which includes both hydrophobic and hydrophilic components. The hydrophobic interior of dendrimers can encapsulate hydrophobic drugs, thereby improving their solubility. Importantly, however, dendrimers can also be functionalized on their surface with hydrophilic groups, making them versatile carriers for a wide range of drugs, including those with varying solubility characteristics.[48] The presence of nitrogen and oxygen within these internal compartments enables them to create hydrogen bonds with drug molecules, indicating that dendrimers' ability to encapsulate substances relies on hydrophobic interactions, hydrogen bonding, and electrostatic interactions, including acid-base interactions. Early studies showed that the hydrophilic outer regions and flexible inner cores of unimolecular micelles can accommodate globular proteins. Meijer et al. made a significant discovery in this regard, which allowed for the creation of a dendritic structure protected by amino acids at the 64-amine terminal of PPI dendrimers.[43] Based

31

on their research findings, it was observed that the dendrimer can bind four larger guest molecules, such as Rose Bengal, and up to ten smaller guest molecules, such as p-nitrobenzoic acid. Fréchet further investigated the hydrophobic interaction between the carboxylic acid surface of a poly (benzyl ether) dendrimer and a hydrophobic chromophore. The investigation concluded that dendrimers could enhance the water solubility of hydrophobic substances like pyrene, thereby facilitating their interactions. In this case the assistance was between aromatic guest molecules and benzyl ether building blocks. The results have potential for application with the many medications that are hydrophobic.[49]

Kojima et al. investigated the water solubility of methotrexate (MTX) and Adriamycin (ADR), which are both practically insoluble in isolation.[50] Their study revealed that hydrophobic drugs can be effectively enclosed within the hydrophobic core of MPEG-PAMAM dendrimers. ADR was solubilized on the surface of MPEG chains, while MTX molecules were solubilized through their increased encapsulation from the electrostatic interactions resulting from an acid-base reaction with the dendrimer. In addition to acid-base interactions and hydrogen bonding, the study revealed that the formation of host-guest complexes was facilitated by the interactions' stabilizing effect on the complex and often resulted in specific recognition and binding of the guest by the host. Host-guest complexes have applications in various fields, including drug delivery, supramolecular chemistry, and molecular recognition. The researchers demonstrated that PPI dendrimers, modified with adamantyl urea and adamantyl thiourea, could act as carriers for (butyloxycarbonyl)-protected peptides. The peptide was observed to bind to the dendrimer through ionic interactions and hydrogen bonding, and it could be easily released under mildly acidic conditions.[50]

Due to the size of proteins around 6,000 Da, large molecules like dendrimers are often required for effective protein interactions. Proteins are macromolecules composed of folded chains of amino acids, forming intricate three-dimensional structures. They exhibit a wide range of sizes,

ranging from small peptides to massive multi-subunit complexes. The size and shape of a protein has a significant influence on its properties and functions, enabling different sized dendrimers to be utilized to target specific regions of a protein. Smaller dendrimers with lower generation numbers are suitable for binding to smaller protein regions, such as active sites or specific binding pockets. These dendrimers can interact with critical residues involved in protein function or recognition by penetrating the cracks and crevices of proteins.

1.10 Graphene Oxide and its Structure

The exploration of graphene and other advanced materials has attracted substantial attention within the scientific community. This surge in interest is primarily driven by the pursuit of innovative implantable and wearable electrochemical sensors tailored for medical applications. Graphene, in particular, stands out as a remarkable carbon-based nanomaterial characterized by its unique structural attributes. Comprising a two-dimensional honeycomb lattice of sp2 carbon atoms, graphene's atomic arrangement gives it exceptional electrical, thermal, and mechanical properties.[51] These properties, combined with its biocompatibility and chemical versatility, render graphene an ideal candidate for the development of cutting-edge sensor technologies in the medical field. The pursuit of graphene-based electrochemical sensors holds significant promise for revolutionizing healthcare by enabling real-time, non-invasive monitoring of physiological parameters and biomarkers, thereby advancing diagnostics and patient care. In 2004, Andre Geim and Konstantin Novoselov successfully isolated and characterized graphene, a two-dimensional material. Their ground-breaking achievement led to them being awarded the Nobel Prize in Physics in 2010.[51] Subsequent to its discovery, graphene has garnered significant attention due to its distinctive physical and chemical properties, as well as its potential application in fields such as electronics, energy storage, and biomedicine.[52] The Hummers method is commonly used to produce graphene oxide, which is a low-cost and straightforward chemical process used to produce graphene oxide (GO), a versatile precursor material to graphene. It

involves the oxidation and exfoliation of natural graphite to form GO sheets with oxygen-containing functional groups. Graphene oxide has garnered significant attention in the field of nanomaterials due to its high conductivity following reduction, selectivity after functionalization, and sensitivity. GO can be characterized quantitatively through parameters such as degree of oxidation, layer thickness, specific surface area, electrical conductivity, and functionalization density. These measures enable precise assessment and tailoring of GO's properties for diverse applications in nanomaterials and beyond. Graphene oxide is composed of a single-layer sheet of graphene, with oxygen functional groups covalently bonded to the edge of the sheet. These functional groups can be hydroxyl, epoxy, carboxyl, and phenol. Due to the strong π-π bonds between graphene layers, pure graphene sheets have limited solubility in water. This makes GO more suitable for protein applications, as its oxygenated functional groups make it hydrophilic and water-soluble, properties essential for chemical derivatization and processing.[53]
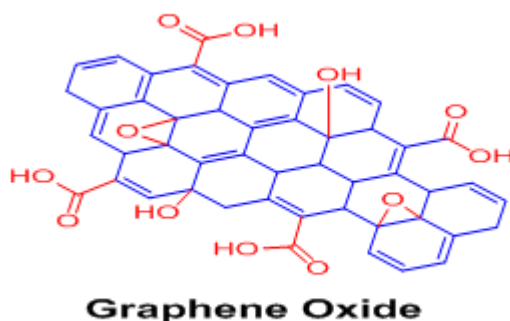
Graphene Oxide

Figure 1.16 The structure of graphene oxide, which involves the oxidation of graphite through a process termed 'Hummers' method', graphene oxide, possesses oxygen functional groups and its versatility has made it valuable for applications in many fields. Chemically modifying GO is a simple and effective technique that has been widely utilized to develop sensors for biomedical, electrochemical, and diagnostic applications. Oxygenated functional groups on GO can be modified with various electroactive molecules through covalent functionalization, which reduces the non-specific binding that is often observed with plain graphene sensors.

To enhance the properties of graphene various quantitative methods have been developed, such as covalently bonding precise quantities of chemical linkers to GO, enabling fine tuning of its

surface and properties. By judiciously controlling the degree of modification, it is possible to enhance GO's electrical conductivity, stability, selectivity, and sensitivity, particularly useful in electrochemical sensing applications. These quantitative adjustments enable GO-based sensors to be optimized to have improved performance metrics, including enhanced sensitivity with lower detection limits, improved temporal stability, and precise control of selectivity, all of which are vital in the development of advanced sensing technologies and diagnostics.[48]

1.10.1 Application of Graphene Oxide in Binding Molecules

The exceptional characteristics of graphene oxide (GO) have shown immense promise in applications involving selective protein recognition and binding. GO has many oxygen-containing functional groups on its surface which can bind to proteins and peptides based on their size and charge.[49] GO can specifically bind to proteins like bovine serum albumin (BSA), cytochrome c, and lysozyme, which is useful in protein purification and biosensing. GO's large surface area also makes it possible to immobilise many proteins, including antibodies, enzymes, and DNA strands, which facilitates processes such as enzyme immobilization and the construction of protein microarrays. GO can be functionalized with different chemical groups, including amino and carboxyl groups, which can be used to covalently attach proteins to its surface. Due to its high sensitivity and selectivity, GO has been investigated as a potentially useful material for protein detection. GO-based biosensors offer a versatile platform for the detection of a broad spectrum of proteins, enabling early diagnosis and monitoring of disease, and research within many areas of medicine, biology, and environmental science. Their high specificity and sensitivity make them valuable tools for improving healthcare and analytical capabilities.[50]

1.10.2 Application of Graphene Oxide in Protein Binding

Graphene oxide has emerged as a versatile platform for protein binding applications in diverse scientific and technological domains. GO has been shown to bind the enzyme lactate

dehydrogenase (LDH), with a binding strength that increases with the number of carboxyl groups on the GO surface. However, it is important to note that the use of GO as a ligand for protein binding has limitations and challenges.[27] For example, the binding interactions can be affected by factors such as pH, salt concentration, and the specific functional groups on GO and the protein.[29] Additionally, the potential cytotoxicity and immunogenicity of GO need to be carefully considered when using it for biomedical applications. Overall, while GO has shown promise as a ligand for protein binding, further research is needed to fully understand and optimise its binding properties for specific applications. Two important remaining challenges include maximising binding and improving selectivity through functionalization - primarily through the addition of amino acids.[51,52]

1.11 References

1   S. Jones and J. M. Thornton, *Proc. Natl. Acad. Sci. U.S.A.*, 1996, **93**, 13-20.

2   M. J. Cloninger, *Curr. Opin. Chem. Biol.*, 2002, **6**, 742–748.

3   G. Parati, S. Kjeldsen, A. Coca, W. C. Cushman and J. Wang, *Hypertension*, 2021, **77**, 692–705.

4   I. Capila and R. J. Linhardt, *Angew. Chem., Int. Ed. Engl*, 2002, **41**, 390–412.

5   M. A. Gregory and S. R. Hann, *Mol. Cell. Biol.*, 2000, **20**, 2423-2435.

6   J. D. Chavez, A. Keller, B. Zhou, R. Tian and J. E. Bruce, *Cell Rep*. 2019, **29**, 2371–2383.

7   I. M. Nooren and J. M. Thornton, *EMBO J.*, 2003, **22**, 3486-3492.

8   O. Keskin, A. Gursoy, B. Ma and R. Nussinov, *Chem. Rev.,* 2008, **108**, 1225–1244.

9   J. Janin, *Biochimie*, 1995, **77**, 497-505.

10   C. S. Goh, D. Milburn and M. Gerstein, *Curr. Opin. Struct. Biol.*, 2004, **14**, 104–109.

11   D. Reichmann, O. Rahat, M. Cohen, H. Neuvirth and G. Schreiber, *Curr. Opin. Struct. Biol.*, 2007, **17**, 67–76.

12   A. A. Bogan and K. S. Thorn, *J. Mol. Biol.*, 1998, **280**, 1-9.

13   W. E. Stites, *Chem. Rev.*, 1997, **97**, 1233-1250.

14   H. Yin and A. D. Hamilton, *Angew. Chem., Int. Ed. Engl*, 2005, **44**, 4130–4163.

15   I. S. Moreira, P. A. Fernandes and M. J. Ramos, *Proteins: Struct., Funct., Genet.*, 2007, **68**, 803–812.

16   B. Schuster-Bockler and A. Bateman, *Genome Biol.,* 2008, **9**, R9.

17   T. Clackson, and J. A. Wells, *Science*, 1995, **267**, 383-386.

18   A. M. Asberry, X. Cai, X. Deng, U. Santiago, S. Liu, H. S. Sims, W. Liang, X. Xu, J. Wan, W. Jiang, C. J. Camacho, M. Dai and C. D. Hu, *J. Med. Chem.*, 2022, **65**, 13793–13812.

19   J. A. Wells and C. L. McClendon, *Nature*, 2007, **450**, 1001–1009.

20   R. M. Scarborough and D. D. Gretler, *J. Med. Chem.*, 2000, **43**, 3453–3473.

21   B. Ma, Y. Pan, K. Gunasekaran, O. Keskin, R. B. Venkataraghavan, A. J. Levine and R. Nussinov, *Phys. Biol.*, 2005, **2**, S56.

22   Y. Wakayama, *Jpn. J. Appl. Phys.*, 2016, **55**, 1102AA.

23   S. A. Qureshi, R. M. Kim, Z. Konteatis, D. E. Biazzo, H. Motamedi, R. Rodrigues, and D. F. Mark, *Proc. Natl. Acad. Sci.*, 1999, **96**, 12156-1216.

24   McMillan, K.; Adler, M.; Auld, D. S.; Baldwin, J. J.; Blasko, E.; Browne, L. J.; Devlin, J. J., Proc. Natl. Acad. Sci., 2000, 97, 1506-1511.

25   He, M. M.; Smith, A. S.; Oslob, J. D.; Flanagan, W. M.; Braisted, A. C.; Whitty, A.; Cunningham, B. C., Science, 2005, 310, 1022-1025.

26   P. Restorp and J. Rebek, *Bioorg. Med. Chem. Lett.*, 2008, **18**, 5909–5911.

27   M. R. Arkin, Y. Tang and J. A. Wells, *Chem. Biol.*, 2014, **21**, 1102–1114.

28   J. P. Plante, T. Burnley, B. Malkova, M. E. Webb, S. L. Warriner, T. A. Edwards and A. J. Wilson, *Chem. Commun.*, 2009, 5091–5093.

29   L.T. Vassilev, B.T. Vu, B. Graves, D.Carvajal, F. Podlaski, Z. Filipovic, and E. A. Liu, *Science,* 2004, **303**, 844-848.

30   B. Klajnert and M. Bryszewska, *Acta Biochim. Pol.*, 2001, **48**, 199-208,

31   J. H. Lee, Q. Zhang, S.Jo, S. C. Chai, M.. Oh, W. Im, H. Lu and H.-S.Lim, *J. Am. Chem. Soc.*, 2011, **133**, 676-679.

32   R. K. Jain and A. D. Hamilton, *Org. Lett.*, 2000, **2**, 1721–1723.

33   J. P. Collman, R. Boulatov, C. J. Sunderland and L. Fu, *Chem. Rev.*, 2004, **104**, 561–588.

34   E. Abbasi, S. F. Aval, A. Akbarzadeh, M. Milani, H. T. Nasrabadi, S. W. Joo, Y. Hanifehpour, K. Nejati-Koshki and R. Pashaei-Asl, *Nanoscale Res. Lett.*, 2014, **9**, 1–10.

35   B. Klajnert and M. Bryszewska, M., *Acta Biochim. Pol.*, 2001, **48**, 199-208.

36   M. E. Giorgi, R. Agusti and R. M. De Lederkremer, *Beilstein J. Org. Chem.*, 2014, **10**, 1433–1444.

37   F. Zeng and S. C. Zimmerman, *Chem. Rev.*, 1997, **97**, 1681–1712.

38   M. Fischer and F. Vogtle, *Angew. Chem., Int. Ed. Engl.,* 1999, **38**, 884–905.

39   C. J. Hawker and J. M., Frechet, *J. Am. Chem. Soc.*, 1990, **112**, 7638-7647.

40   D. A. Tomalia, H. Baker, J. Dewald, M. Hall, G. Kallos, S. Martin, J. Roeck, J. Ryder and P. Smith, *Polym. J. (Tokyo, Jpn.),* 1985, **17**, 117–132.

41   C. J. Hawker, J. M. Frechet, *Macromolecules*, 1990, **23**, 4726-4729.

42   F. Chiba, T. C. Hu, L. J. Twyman and M. Wagstaff, *Macromol. Symp.,* 2010, **287**, 37–41.

43   M. A. Van Dongen, C. A. Dougherty and M. M. Banaszak Holl, *Biomacromolecules*, 2014, **15**, 3215–3234.

44   U. Boas, J. B. Christensen and P. M. H. Heegaard, *J. Mat. Chem.*, 2006, **16**, 3785-3798.

45   A. S. Saxena and S. A. Singh, *Int. J. Res. Pharm. Sci. (Jaipur, India)*, 2012, **1**, 44-52.

46   A. Z. Wilczewska, K. Niemirowicz, K. H. Markiewicz, and H. Car, *Pharmacol. Rep.*, 2012, **64**, 1020-1037.

47   N. Malik, R. Wiwattanapatapee, R. Klopsch, K. Lorenz, H. Frey, J. W. Weener, E.W. Meijer, W. Paulus, and R. Duncan, *J. Controlled Release*, 2000, **65**, 133-148

48   F. Najafi, M. Salami-Kalajahi and H. Roghani-Mamaqani, *J. Mol. Liq.*, 2022, **347**.

49   C. C. Lee, J. A. MacKay, J. M. J. Fréchet and F. C. Szoka, *Nat. Biotechnol.*, 2005, **23**, 1517–1526.

50   J. Planas-Iglesias, J. Bonet, J. García-García, M. A. Marín-López, E. Feliu and B. Oliva, *J. Mol. Biol.*, 2013, **425**, 1210–1224.

51   A.K. Geim, *Science*, 2009, **324**, 1530-1534, DOI: 10.1126/science.1158877

52   D. C. Marcano, D. V. Kosynkin, J. M. Berlin, A. Sinitskii, Z. Sun, A. Slesarev, L. B. Alemany, W. Lu and J. M. Tour, *ACS Nano*, 2010, **4**, 4806–4814.

53   K. I. Bolotin, K. J. Sikes, Z. Jiang, M. Klima, G. Fudenberg, J. Hone and H. L.Stormer, *Solid State Commun.*, 2008, **146**, 351-355.

Chapter 2

Functionalization of GO with oligo amino acids and its applications as enzyme inhibitors by using α-chymotrypsin

2.1 The new carbon-based materials:

Essentially, graphene, which consists of 2D sheets composed of sp2 hybridized carbon atoms, was initially isolated in 2004.[1] This material was swiftly harnessed for diverse applications in protein binding. Geim and Novoselov's seminal discovery of graphene involved its production using the 'Scotch tape' method, a process in which single sheets of graphene were carefully exfoliated from the bulk graphite.[2] Graphene in its purest form, devoid of any defects, exhibits impermeability to all molecules, including the smallest, such as helium. This remarkable property arises from the tightly packed arrangement of carbon atoms within its lattice.[2] Conversely, graphene oxide (GO), a derivative of graphene, holds significant potential for protein binding. This is because GO features a diverse chemistry with various oxygen functional groups, leading to distinct interactions between ions and GO. The abundance of oxygen-rich functional groups in GO arises from the oxidation process employed during its synthesis, wherein graphite serves as the primary raw material. These intriguing attributes present exciting possibilities for investigating GO as a substitute material capable of achieving high performance and protein binding. Furthermore, GO nanosheets can be organized into a layered structure through filtration or coating techniques, creating rapid and selective 2D nanochannels that enhance molecular filtration.[3]
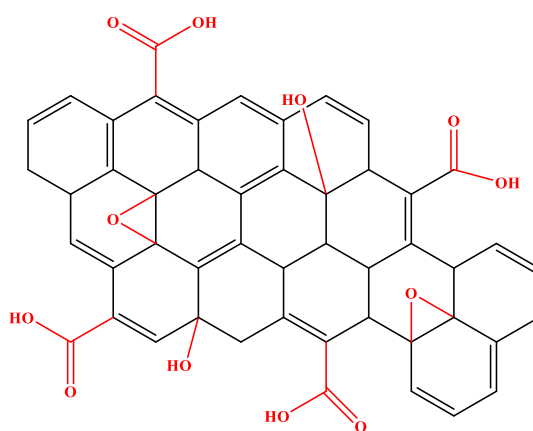

Figure 2.1 Shows the structure of Graphene oxide.

The history of GO traces back to an unintended discovery made by Brodie. In 1859, Brodie, a professor at the University of Oxford, was in pursuit of determining the molecular weight of graphite.[4] He observed that graphite exhibited markedly distinct properties from other carbon forms, such as diamond or charcoal. With the belief that graphite represented a unique element, he theorized that the most suitable approach to conduct elemental analysis on graphite was through its oxidation. Although Brodie had the knowledge of the molecular weights of hydrogen and oxygen, graphite remained the missing piece of the puzzle.[5] Brodie's discovery had a significant drawback—the use of hazardous chemicals. Subsequently, in 1898, Staudenmaier introduced modifications in response to Brodie's work to enhance the graphite oxidation process.[6] A century later, in 1957, Hummer and Offeman developed a safer oxidation method.[7] Today, GO holds the potential to enable a myriad of diverse applications. Despite its discovery nearly 160 years ago, it has only garnered widespread attention from the scientific community in the past decade, primarily because it is considered as a precursor to graphene. However, GO itself possesses considerable scientific significance as a fundamental form of oxidized carbon, boasting a range of intriguing properties that can be harnessed across various applications.

2.2 Simplified synthesis method

One of the primary benefits of employing GO for protein binding is the convenience of its synthesis method. Utilizing a straightforward approach, such as the modified Hummer's method and Tour's method, allows for a large-scale production of GO. Overtime, there has been a dedicated effort to refine and simplify these methods, enhancing their safety and practicality while simultaneously increasing the yield of GO. In the following sections, we will provide a brief chronological overview of GO synthesis methods, beginning with the methods by Brodie, Staudenmaier, Hummer, modified Hummer, and Tour.

2.2.1 Brodie's method

As aforementioned, during the 19th century, Brodie initiated the first synthesis of GO while exploring the chemistry of graphite. In his research, recognizing that graphite exhibited little reactivity towards potent oxidizing agents, he employed potassium chlorate (KClO3) and nitric acid (HNO3) as the oxidizing agents. The introduction of KClO3 into a graphite slurry, combined with fuming HNO3, yielded a novel compound that was subsequently discovered to contain carbon, oxygen, and hydrogen. In the subsequent stage, the batch, which is devoid of salts, was generated during the reaction and underwent a process of washing before subsequently dried at 100°C. It was subsequently exposed to an oxidizing environment once more. After three such sequential treatments, the appearance of the substances transformed into a light-yellow colour, which remained consistent even with additional rounds of oxidation. When Brodie measured the weight of these substances, there was an increase compared to the original graphite, confirming the occurrence of oxidation. In his experiment, he emphasized that achieving the product through a single extended treatment was challenging. To maintain the substance's original condition, the oxidation process had to be introduced each time. Based on his elemental analysis, he proposed the molecular formula of the final product to be $C_{11}H_4O_5$ and named it graphitic acid. Furthermore, the resulting substances were characterized by their small size, limited thickness, and an imperfect structure, which he described as resembling a crystal. However, it's important to note that his observations and conclusions were constrained not only by theoretical considerations but also by the limitations of the characterization techniques available during his research, leaving ample room for further improvement and exploration.[7]

2.2.2 Hummer's method and modified Hummer's method

Hummer and Offeman introduced an alternative method for synthesizing GO. These two chemists, affiliated with the Mellon Institution of Industrial Research, devised an oxidation

process for graphite involving a mixture of concentrated sulfuric acid (H_2SO_4), sodium nitrate ($NaNO_3$), and potassium permanganate ($KMnO_4$) at a temperature of 45°C.[7] They asserted that the entire oxidation process could be accomplished in just 2 hours, resulting in a greater degree of oxidation in the final product compared to the Staudenmaier method. However, subsequent research revealed that the product of the Hummer's method resulted from an incomplete oxidation of graphite. A pre-expansion process was found to be advantageous in enhancing the degree of oxidation. This pre-treatment of graphite involved using a mixture of H_2SO_4, $K_2S_2O_8$, and P_2O_5 at 80°C for several hours, a procedure initially introduced by Kovtyukhova in 1999.[8] Before subjecting the pre-treated mixture to oxidation using the Hummer's method, it underwent a series of steps, including dilution, filtration, washing, and drying. It was later determined that if the graphite flakes were either expanded or reduced in size, some of these intricate pre-treatments could be omitted. Numerous adaptations to the Hummer's method have been explored, such as augmenting the quantity of potassium permanganate, introducing phosphoric acid in precise proportions, omitting sodium nitrate, and extending the reaction time. These adjustments are intended to enhance the level of oxidation and enhance the final production of GO. GO produced via the modified approach typically consists of thin flakes measuring around 1 nm in thickness and averaging approximately 1 µm in lateral dimension. These modifications have substantially improved both the degree of oxidation and the yield of GO compared to the original results obtained through Brodie's method. Nevertheless, the process of separating and purifying GO using the modified Hummer's method remains somewhat intricate and time-consuming.

2.2.3 Tour method

The Hummer's method, also known as the Tour method, made its debut in 2010 courtesy of the Tour Group at Rice University. This innovative approach dispensed with the use of sodium nitrate and instead increased the quantity of potassium permanganate. Additionally, they introduced a new acid, phosphoric acid, into the reaction vessel. By conducting the reaction with a 9:1 ratio of H2SO4 to H3PO4 in the presence of six equivalents of KMnO4, the group not only improved the

overall reaction efficiency but also demonstrated that the addition of extra KMnO4 yielded a larger quantity of hydrophilic oxidized GO materials.[9] The most significant advantage of implementing this method lies in the elimination of sodium nitrate, thereby avoiding the generation of toxic gases such as NO2, rendering it a more environmentally friendly process.

Synthetic protein ligands may be able to prevent the unwanted protein aggregations that can cause several illnesses, including thromboembolism, diabetes, and Alzheimer's disease.[10] A synthetic inhibitor's ability to bind a protein is primarily due to specific interaction from functional groups and charge position at precise locations across a 3-dimensional surface.[11]
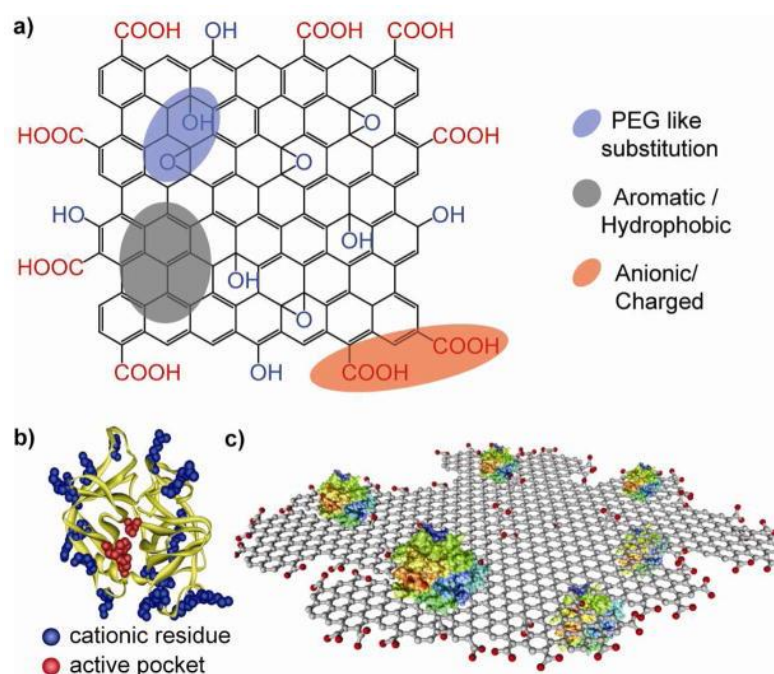
Figure 2.2 The diagram illustrates the composition of graphene oxide (GO) (a) and α-chymotrypsin (ChT) (b), as well as the schematic representation of the interaction between graphene oxide and the protein (c). It elucidates the process of graphene oxide's binding to α-chymotrypsin and its subsequent impact on ChT activity and secondary structure. These investigations provide insights into the potential of GO as a protein receptor for further evaluation.

This example uses an unfunctionalized GO and the interaction strength is simply related to the strength of charge interactions. As a result, unfunctionalized GO will bind all proteins with a cationic surface.[12] In the natural systems, proteins also bind using the functionality provided by

the amino acids, which are positioned precisely on their 3-dimensional surface.[13] It is these amino acids, and their position on the surface that give the proteins their selectivity when binding other biomolecules - including other proteins.[14] Certain amino acids are known to be particularly important with respect to protein-protein interactions. For example, tyrosine is a relatively rare amino acid that has a low level of incorporation within many proteins.[15] However, when present, it does so within the binding domain. As such, it is generally accepted that it has a significant role in protein recognition and selectivity. While several studies have described the functionalization of GO with amino acids, relatively few studies focused on protein binding.[16] The most prevalent approach to functionalization involves the employment of a coupling agent and an excess of unprotected amino acid. The consequence of this approach is an oligomeric addition of the amino acid as the initial coupling of the first amino acid, which generates a monomeric functionalized surface with a reactive carboxylic acid that is free to react with a second amino acid, and this may react with a third amino acid.[16] May be advantageous in terms of flexibility and increased functionality, and may result in establishing high-affinity and robust binding interactions. In a previous study, our group proposed the use of oligomeric tyrosine to produce a functionalized GO that would exhibit significantly stronger binding to a protein than GO, or a GO with a simple monomeric layer of tyrosine, as shown in Scheme 2.2. However, the aromatic groups of the tyrosine simply adsorb tightly to the GO surface due to a very strong and unhelpful π-π interactions. The nature of the oligomer interactions means that the overall interactions with the surface of GO are cooperative and outcompete the potential GO-protein interaction.[17]
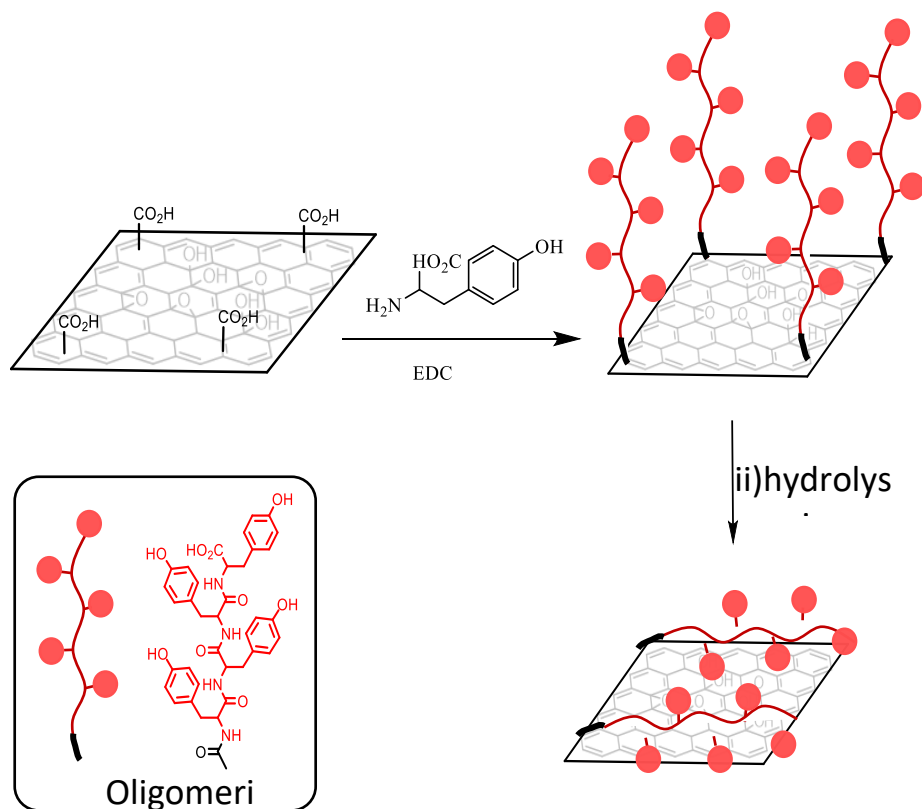
Figure 2.3 illustrates the initial step, which involves functionalization with an oligomeric layer of amino acids. The oligomeric system was created by combining EDC and non-protected tyrosine with a suspension of GO in water and stirring it at 70°C for 24 hours.

In the case of the monomeric system, the single tyrosine is able to bind the protein much more strongly than the oligomer or unfunctionalized GO. Despite the initially unexpected result, it did confirm the importance of functionalization with respect to binding. Although the monomeric system is an excellent ligand, it could still form π-π interactions with the GO surface.[18] Hence, these individual monomeric interactions are expected to be notably weaker compared to the cooperative interactions seen in the oligomeric system with the GO surface. Consequently, it should be relatively easier for the monomeric amino acid system to engage with a protein surface. However, the proximity between the GO surface and the target protein in the monomeric system may give rise to steric hindrances that weaken the binding. Moreover, the rigidity of the monomeric system could potentially enhance selectivity. It is also plausible that neither system will exhibit strong binding affinity, and unfunctionalized GO might, in fact, serve as the most

47

effective ligand. As a result, each system possesses its own set of advantages and disadvantages, making a case for or against protein binding.[19]

2.2 Aims and objectives.

The main goal of this project is to study various functionalized GOs with respect to improved binding. The objective is to revisit the concept that oligomeric functionalization may result in enhanced binding.[13] This will be followed up by studying a series of amino acids that are known to be effective /ineffective with respect to binding. If this is successful, a combination of these two approaches may result in a methodology for the synthesis of GO based ligands selective for different proteins. Kinetic binding was assessed indirectly by measuring rates of enzyme hydrolysis in the presence and absence of various GO ligands.   As the active site entrance is in the middle of the enzyme's binding site, binding strength will be directly proportional to the inhibition efficiency. The method was briefly described in the introduction above and is based on the one described by De et al. The first aim is to functionalize GO with an oligomeric amino acid.[20] Although our group's previous experiments with oligo tyrosine did not improve the binding, it is our belief that we may have success with glutamic acid, which cannot form π-π interactions with the GO surface.[17] As such, the oligomeric chains will be free to extend from the surface and present an increased number of carboxylic acid groups at the surface, and therefore increase binding affinity. Additionally, monomeric chain was synthesized by using a protection, coupling and deprotection method. Although the primary function of the monomeric system is to control thus allowing comparison with the oligo, it is likely to be a strong ligand (stronger than unfunctionalized GO). The increase in the number of carboxylates on the surface of GO can be attributed to the unique molecular structure of glutamic acid. Glutamic acid, which is an amino acid, possesses two carboxylic acid groups within its chemical composition. When glutamic acid is introduced to the surface of GO, each molecule of glutamic acid contributes two of these carboxylic acid groups, effectively doubling the total number of carboxylates present on the GO

surface. This chemical modification has significant implications, as it enhances the functionalization of GO.[21] The idea is represented schematically in Figure 2.4

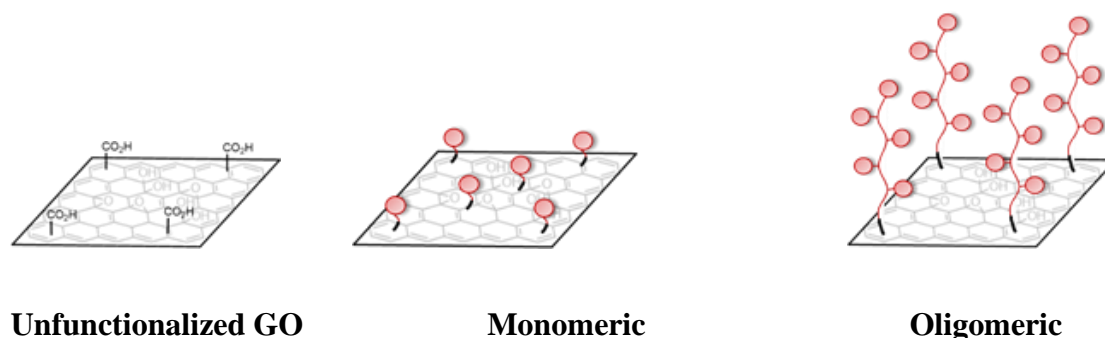**Unfunctionalized GO**   **Monomeric**   **Oligomeric**

Figure 2.4 The diagram illustrates the utilization of two distinct methods to modify GO with glutamic acid. In the initial approach, glutamic acid is covalently linked to GO, and subsequent hydrolysis of the methyl ester results in the formation of carboxylic acid groups. This process yields GO with a thin layer of glutamic acid, incorporating a fixed spacer. Conversely, the second approach seeks to simplify the synthesis by directly reacting unprotected tyrosine (possessing both -NH2 and COOH groups) with GO. This approach results in a GO surface adorned with a thicker layer of glutamic acid, creating an oligomeric system.

Having established the success or otherwise of an oligomeric methodology based on the number of charge-charge interactions, we subsequently planned to study the effect of an amino acid's specific functionality on binding. The objective was to determine whether interactions are dominated by the charge-charge interactions, or whether the amino acid functionality can have a significant effect on the binding affinity (positive or negative).[22] If tjos was the case, it can be determined that the methodology should be applicable to the development of GO based ligands that are selective for specific proteins. For these experiments, all amino acids would be added as protected acids for the purpose of providing a layer of monomeric amino acids after deprotection. The selected amino acids are known to be important/unimportant with respect to protein-protein binding. Once synthesised, all products will be analysed using FT-IR, elemental Analysis (EA), thermogravimetric Analysis (TGA), and Raman Spectroscopy, Additionally, techniques such as X-ray diffraction (XRD), X-ray photoelectron spectroscopy (XPS), and scanning electron microscopy (SEM) have been employed to analyse and characterize graphene and its properties.
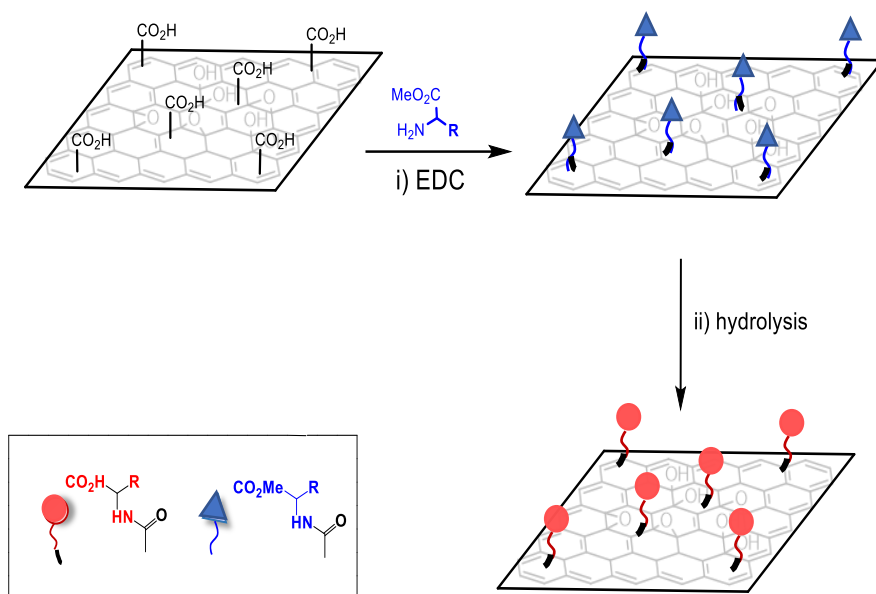
Figure 2.5 The monomeric system was synthesized using the same initial step, except that the methoxy ester of glutamic was used. After isolation, the functionalized GO was resuspended in water and the ester group hydrolysed using sodium hydroxide.

2.3 Results and Discussion

GO can be synthesised using well-established methods. However, one of the disadvantages of GO in dispersing agents by using surfactants to stabilize the dispersion, and its bulk structure is that it is difficult to conduct analyses using liquid-phase NMR or other standard methods. As a result, the evaluation of the structure and attributes of GO uses solid phase techniques such as FT-IR, XPS, elemental analysis, and various microscopic techniques.[23]

2.3.1 Unfunctionalized Graphene Oxide Synthesis

This makes the synthesis of GO safer for researchers and laboratory personnel. Additionally, it simplifies the procedure, making it more user-friendly while maintaining the effectiveness of producing high-quality GO. Thus, the Tour method is considered an improvement in terms of both safety and practicality compared to the original Hummers' method. Therefore, GO

was synthesised using a Tour method as illustrated in the Figure 2.6. Graphite powder was added to the 9:1 mixture of cool concentrated H_2SO_4/H_3PO_4 and $KMnO_4$ was mixed (in droplets) to limit the potential hazards of exothermic reaction. In addition to the graphite source, the choice of oxidation reagents plays a crucial role in determining the degree of oxidation of the flakes. The most frequently employed oxidation agents in the synthesis of GO are a combination of KMnO4 and H2SO4. The permanganate ion, found in $KMnO_4$, is a well-known oxidation reagent. Its reactivity, however, can only be initiated in an acidic environment, which is primarily established through the formation of Di manganese heptoxide when KMnO4 interacts with a strong acid.[9]
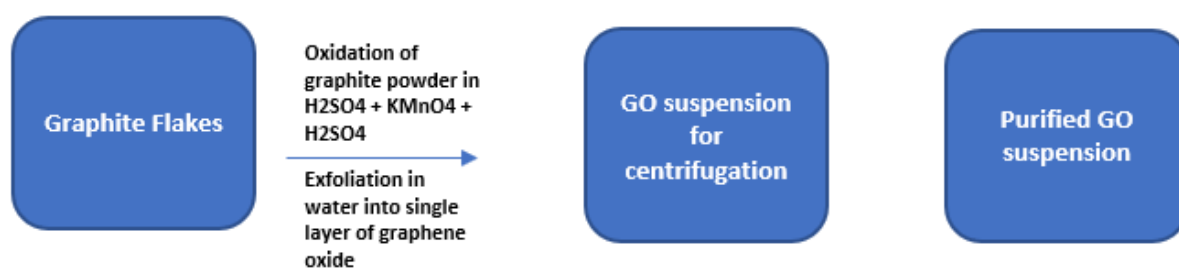
Figure 2.6 The diagram depicts the step-by-step process for synthesizing GO through the modified Tour method. These key stages encompass the creation of a graphite oxide suspension, oxidation facilitated by potassium permanganate, subsequent dilution with deionized water, purification via centrifugation and washing, and the final phases of exfoliation and stabilization.

The GO's structure is determined by comparing its characterization data with previously published data.[17] The initial approach was FT-IR. During the FT-IR analysis, several peaks were identified. This confirmed the existence of functional groups containing oxygen. A broad band was observed at 3350 cm^{-1}, indicating the presence of hydroxyl groups (OH), and there is a small shoulder at 3500 cm^{-1} which corresponding to water. Additionally, the peaks were at 1732 cm^{-1} carbonyl and carboxyl C=O, 1228 cm^{-1} (epoxy C–O), 1622 cm^{-1}

aromatic C=C, and 1041 cm^{-1} (skeletal C=O or C-C) were detected, which corresponded to

carboxylic and epoxy groups.
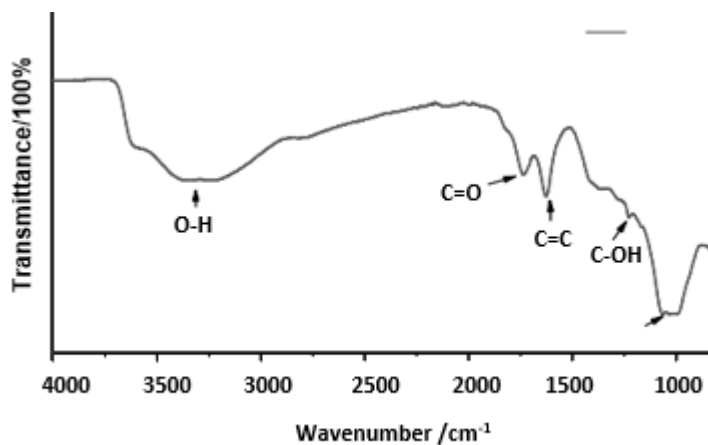
Figure 2.7 provides confirmation of the presence of oxygen-containing functional groups within the sample. A broad band was observed at 3350 cm^{-1}, indicating the presence of hydroxyl groups (OH). Additionally, peaks at 1732 cm^{-1} carbonyl and carboxyl C=O, 1228 cm^{-1}(epoxy-C–O),1622cm^{-1}aromaticC=C.
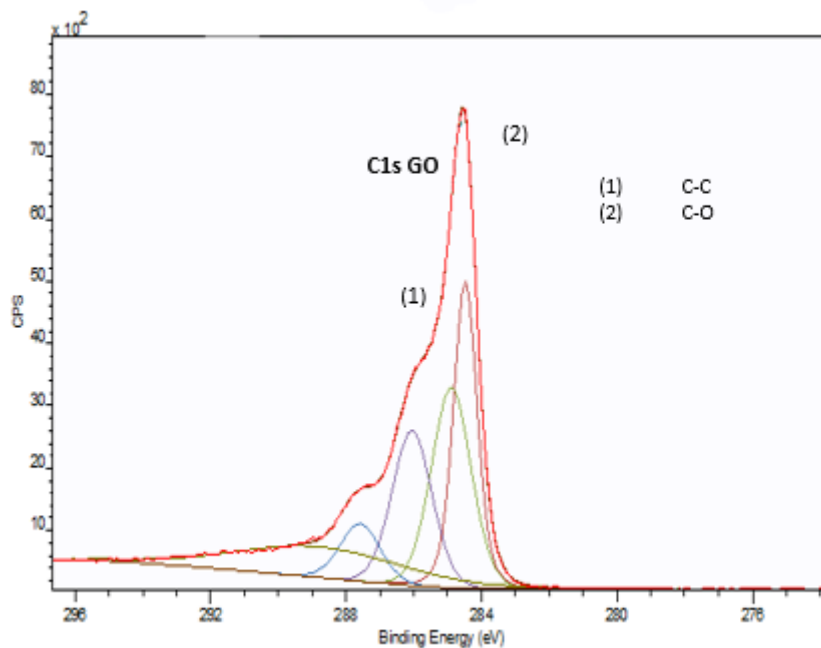
Figure 2.8 Deconvolution and Identification of Carbon Functional Groups in the C1s and XPS Spectra of GO

Further analysis on oxygen functional group of GO can be analysed using X-ray photoelectron spectroscopy (Thermo Fisher, K-Alpha spectrophotometer). The XPS scans utilised monochromatic Al-Kα X-ray source with energy of 1486.69 eV. Figure 2.8. shows C1s spectrum of GO. Typical GO comprises of four typical peaks approximately located at 284.44 eV for C-C (graphitic) group, 285.3 eV for C-O (ether, alcohol and epoxy) group, 287.76 eV for C=O (carbonyl) group, and 288.1 eV for O=C-OH (carboxyl) group respectively.
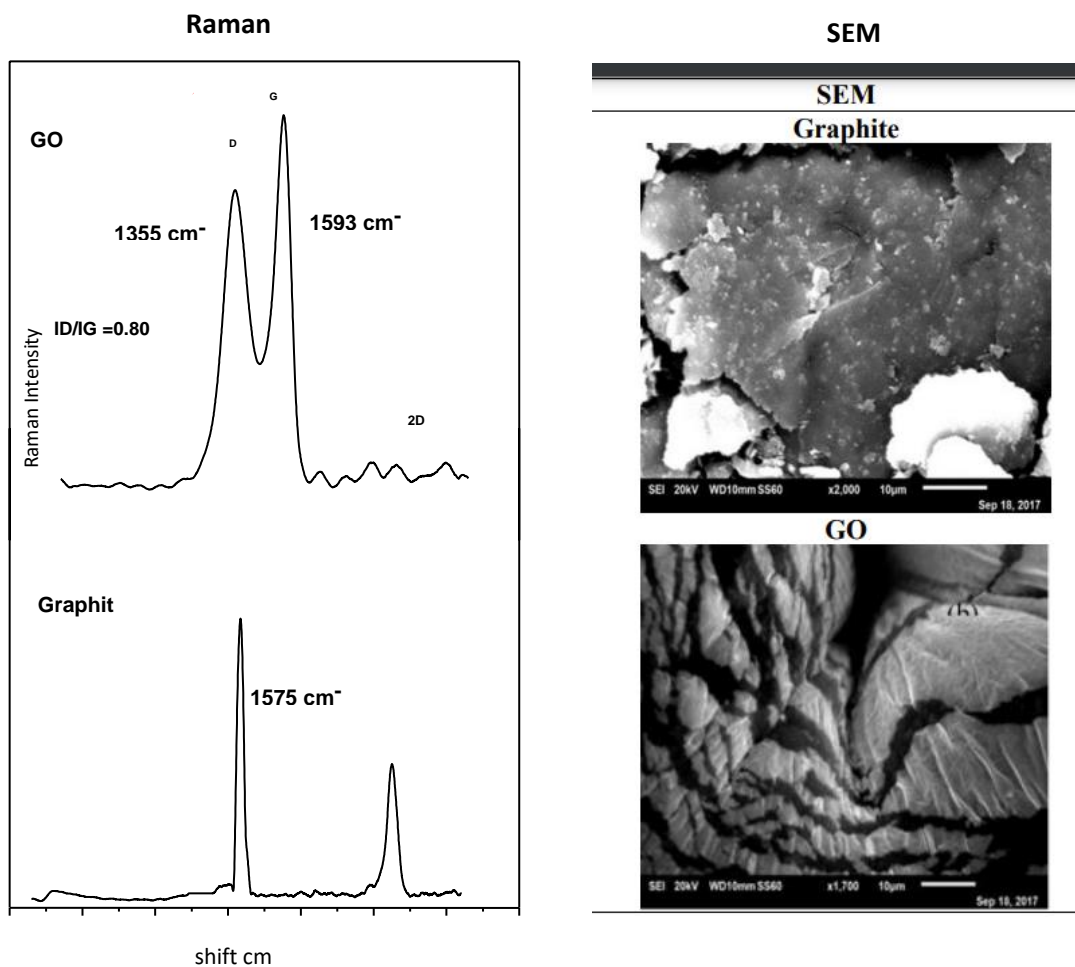
Figure 2.9 Raman spectra (left) showing the ID/IG and SEM images of graphite and GO (right)

Raman was used to determine the type of carbon forms on elements. Two significant peaks at 1355 cm-1 and 1593 cm-1 provide evidence of the GO's structure. In line with the D and G-bands at 1575 cm-1, the graphite displays a single, strong peak. The ID/IG intensity ration of GO is 0.80, indicating that the attachment of functional groups containing oxygen caused the sp2 of a carbon bond to be changed or modified to the sp3-hybridised carbon on the surface of GO. The I2D/IG ratio reveals a multilayer (less than five layers) of GO sheets produced, as shown by the observation of a wider and symmetrical 2D band at 2500-3200 cm1. The presence of oxygen-containing functional groups in GO can be investigated using X-ray diffraction (XRD) analysis. In this study, XRD analysis was performed using Cu-Kα radiation as the source, and scans were conducted over a 2θ range from 5° to 100°. The XRD equipment was operated at a voltage of 40 kV and a current of 40 mA. Typical XRD spectrum obtained from the

GO sample prepared for this study. Notably, when comparing the XRD patterns of graphite powder and GO, some significant differences become apparent. Graphite powder exhibits a sharp diffraction peak at 2θ=26.7°, corresponding to an interlayer spacing of 0.33 nm. In contrast, GO displays a peak at approximately 10°, indicative of an interlayer spacing of 0.83 nm. This increase in interlayer spacing in GO results from the introduction of oxygen functional groups during the synthesis process, where graphite is oxidized to form GO. Furthermore, the absence of a peak within the 2θ=25~30° range indicates the complete conversion of graphite into GO. It's worth noting that the interlayer spacing between the GO sheets can vary depending on the ambient relative humidity.24

The interlayer space (d) of graphite and graphene oxide can be calculated from Bragg law:

$$\text{equation: } n\lambda = 2d\sin\theta$$

where n is the diffraction series and λ is the X-ray wavelength in this case 0.154 nm.

2.3.2 Chemical Functionalisation of GO

The next step involved functionalising the GO with a layer of different amino acids. As previously stated, it is essential to determine the well-characterised structural characteristics of the synthesised materials and the successful functionalisation of GO.

2.3.3 Synthesis of monomeric glutamic acid functionalized GO

Our first target was a monomeric glutamic system, a monomeric glutamic acid system, containing two carboxylic acid (COOH) groups. These groups can change their charge states depending on the pH of the solution, transitioning between protonated (COOH, positively charged) and deprotonated (COO-, negatively charged) forms. This pH-dependent behaviour leads to varying charge densities within the molecule. Additionally, having two carboxylic acid groups in the glutamic acid system increases the number of potential charge-charge interactions, influencing its chemical reactivity in different pH environments. Therefore, this increasing the binding affinity. For the purpose of accomplishing this, single layer of diester-protected glutamic acid was added. The functionalised

GO material was dispersed in water, and the ester groups were hydrolysed using NaOH to produce the targeted GO-Glu mono system as shown in Scheme 2.10. The C=O peak for the diester-protected system began at approximately 1600 cm^1 and continued to 1750 cm^1. In addition, no peaks corresponding to the OH stretching of carboxylic acids for the GO or the glutamic acid could be observed between 3000 –3500 cm^1. Nevertheless, upon deprotection, the OH peak could be observed, and the carbonyl peak was simpler and no longer reaching the ester region (1750cm^1). These data confirm the addition of the protected glutamic acid and its hydrolysis to remove the ester protecting groups.[25]
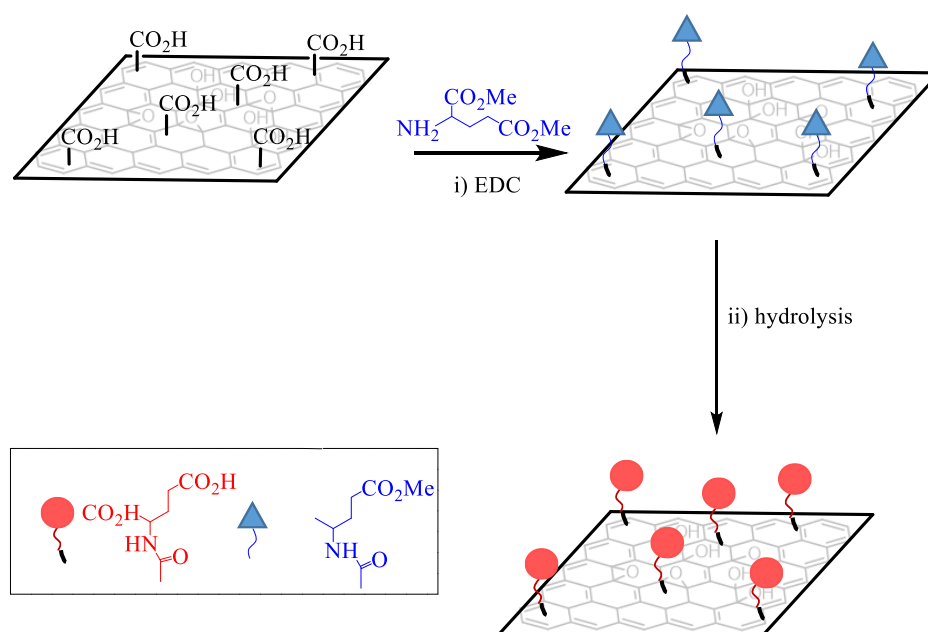
Figure 2.10. demonstrates a straightforward process in which a monomeric system of diester-protected glutamic acid was introduced. The functionalized graphene oxide (GO) material was subsequently dispersed in water, and the ester groups were hydrolyzed using sodium hydroxide (NaOH) to yield the desired GO-Glu monomeric system.

2.3.4 L-Synthesis of Oligomeric Glutamic Acid Functionalised GO

Non-protected glutamic acid (-NH$_2$ and CO$_2$H) were employed to synthesise an oligomeric functionalised GO. The intention was to generate a reaction between the amine groups with the carboxylate groups on GO and subsequently resulting in a reaction on the new carboxylic acid groups (from the unprotected glutamic acid) with a second and third of glutamic acid (s). The amino

56

acid and coupling agents were added in excess to create the functionalised GO. It is highly probable for the FT-IR spectroscopy to be used qualitatively rather than quantitatively, and was employed to determine the successful introduction of the amino acids onto the surface of GO. The incorporation of amino acids on the surface of GO was validated by FT-IR spectroscopy. Similar peaks were found for GO-functionalised glutamic acid and their commercial amino acid. After successfully attaching amine to GO sheets, we analysed the elemental content of the compounds using SEM-EDX. Due to the varied surface, bulk chemical compositions of the sample, and the method used, we anticipated that these techniques would provide diverse results and we expect large error in the repeated experiment. As a result of the fact that the results provided here were not sufficient for characterisation by itself, we combined it with additional approaches. Therefore, the assessments between methodologies are still credible. The findings reveal that nitrogen can only be produced from an amino acid, and this confirms the addition of the glutamic acid. The FT-IR spectra were obtained, revealing the vibrational stretching frequencies of the $-OH$ and $-NH$ functional groups in the range of 3210-3550 cm^{-1}. Furthermore, a peak was observed in the 2300-2950 cm^{-1} region, which can be attributed to the vibrational modes of the hydrophobic portion of glutamic acid that was incorporated into the functionalized GO structure. The XRD pattern of the reactant L-Glu also demonstrated its high crystallisation, and the diffraction peak at 10° indicates a layered structure in GO. In the pattern of L-Glu/GO, the peak of GO was no longer visible, and the peaks present at 28.4^o, 40.6^o, 45.2^o were different from those of the glutamic acid starting material. These results again indicate that the reaction had been successful.[26]
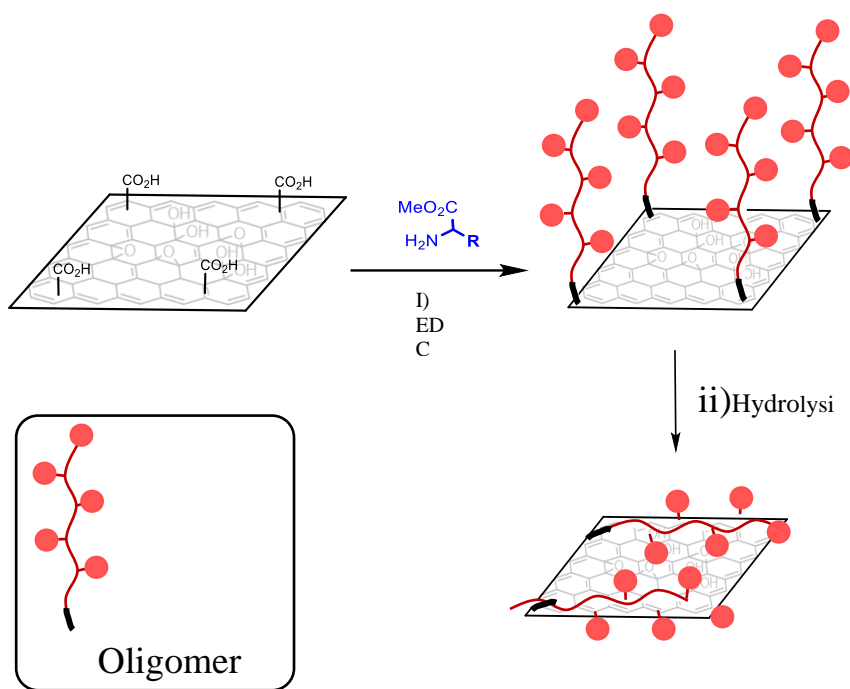
Scheme 2.11 Production of oligomeric layer on the surface of GO, and potential binding on the surface of GO

2.3.5 Characterisation of the Monomeric and Oligomeric GO Systems

Oligomeric and monomeric GO-Glu were thoroughly examined in terms of flexibility in the space produced on the surface of GO. It was crucial to compare their elemental composition and amine concentration as we investigated the influence of these structures on protein binding. Carbon content increased from around 44% for GO to 50% and 60% for the monomeric and oligomeric systems respectively, which aligned with the expected improvement in carbon content. However, SEM-EDX of glutamic acid compared to carbon content rose from around the conversion rates for GO, which observed to be increased from 40% to 45% and 48% for the monomeric and oligomeric systems respectively. The increase in carbon content was as expected because the addition of glutamic acid introduced more carbon relative to oxygen and nitrogen. As such, it was also expected that the oligomeric system to possess the highest level of carbon compared to the monomeric system, which has more than the unfunctionalized GO. This correlation between carbon concentration and functionalisation level is consistent with the earlier group research.[17]

The carbon-to-nitrogen mass ratio can be used as a qualitative indicator to measure the various degrees of functionalisation. A lower ratio suggests a greater percentage of nitrogen in comparison to carbon. Only carbon and oxygen were found on the GO surface, according to SEM-EDX mapping, although nitrogen was also visible in the pictures of the monomeric and oligomeric samples. Moreover, SEM-EDX analysis reveals that the monomer and oligomer had carbon to nitrogen ratios respectively, as shown in Table 1.

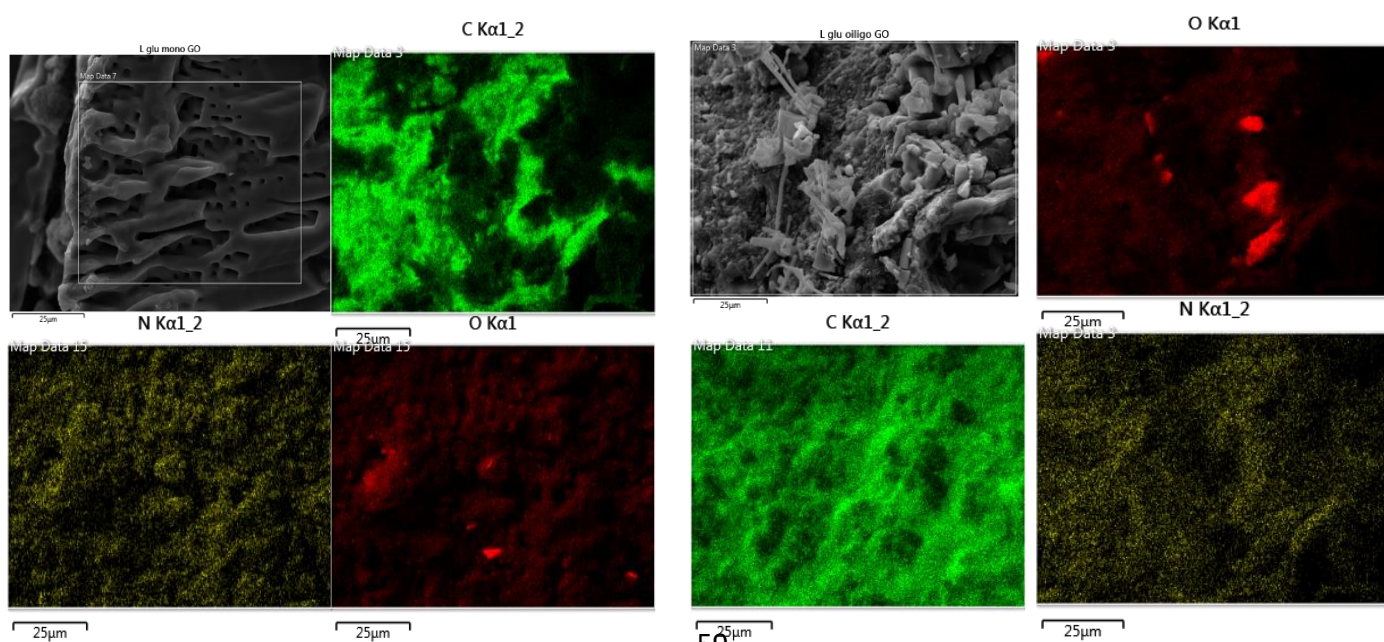| SEM-EDX			
Compound	C (mass %)	N (mass %)	O (mass %)
GO	**54.95 %**	**/**	**44.8 %**
GO-Tyr (Mono)	**58**	**6**	**33.90**
GO-Ph-Ala (Mono)	**60**	**14**	**25**
GO-Glutamic (Mono)	**51**	**15**	**27**
GO-Glutamic (Oligo)	**61**	**13**	**26**
GO-Valine	**74**	**2**	**24**

Table 1. SEM-EDX data for GO

Figure 2.12 SEM-EDX element mapping of GO-Glu a) Mono and (b) Oligo of all elementals. The scale bar is 20 μm and SEM-EDX mapping, although nitrogen was also visible in pictures of the monomeric and oligomeric samples. Moreover, SEM-EDX analysis reveals that the monomer and oligomer had carbon to nitrogen ratios respectively.

X-ray photoelectron spectroscopy (XPS) was employed to analyze surface materials and assess changes in the carbon-to-heteroatoms (N and O) ratio resulting from functionalization. It provides accurate information about surface elemental composition and chemical states. However, XPS primarily probes the top few nanometers of a sample, limiting its insight into bulk composition. Additionally, it may not be suitable for very thin or highly insulating materials. According to XPS data, Glu oligo has prominent peaks in their C 1s spectra with C-C bond energies of 284.5 and 286.5 eV. There are other notable peaks in the spectra, upon considering the bond energies of C=O, C-O, C=N, and C-N as 532.38, 531.28, 401.55, and 399 eV, respectively, the deconvoluted spectra of N 1s and O 1s exhibited clear signals corresponding to C-N-C, N-H, O-C=O, and O-H. These signals are significant enough to warrant further investigation and analysis. The oligomer's amide to amine peak ratio was 1:0.33. Nevertheless, a ratio of 1:1.35 can be seen in the monomeric system, where more amide linkages were formed. The mismatch that occurred in the results was due to the different synthetic processes. During the formation process of oligomeric and monomeric systems, the amino acids N-terminus has the capability to undergo a reaction with the carboxylate groups present on the surface, resulting in the formation of amide bonds. This reaction occurs in both oligomeric and monomeric production processes. In the case of the oligomeric technique, where an unprotected Glu is utilized, it is possible for the N-terminus to react with the C-terminus of another amino acid or a growing oligomer. Assuming those are the same number of monomer or oligomer connected to GO, this will result in significant increase of the presence of amides present in the oligomer and additional amide bonds are formed. This leads to a more pronounced amide peak for XPS for the oligomeric.[27]
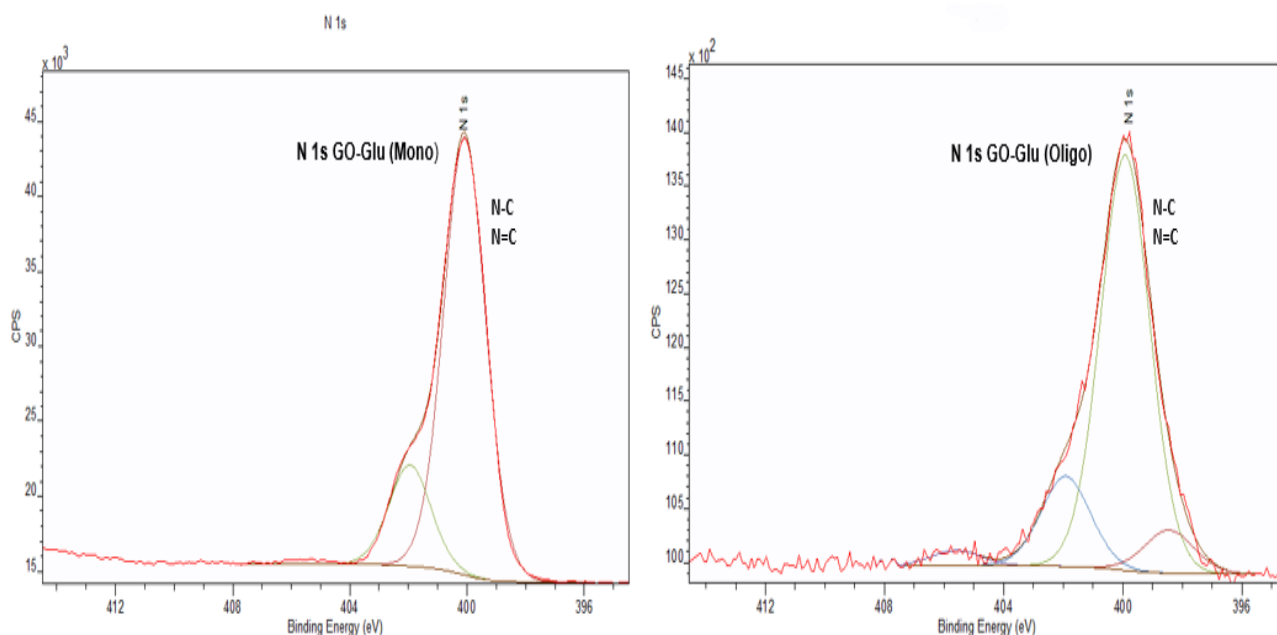
Figure 2.13. Functionalisation to present the deconvoluted XPS spectra of the N1s of (b) GO-Glu (Mono) and (c) GO-Glu (Oligo)

XRD can also provide information regarding the functionalisation from the d spacing. After functionalisation, the space between GO layers should increase as the amino acids occupy additional space on the surface. In addition, the oligomeric system should provide the largest spacing, as the GO surface has multiple layers of amino acid, XRD spectra demonstrated broad diffraction peaks at 26°. This broadening could be attributed to the insertion of carboxylic groups from Glutamic Acid on the surface of GO. The d-spacing increased due to the insertion of oligomeric system, resulting in a thicker layer. Furthermore, a significant difference was observed between the oligomeric and monomeric methods in terms of the layer being produced (0.86 nm for monomeric and 1.0 nm for oligomeric).
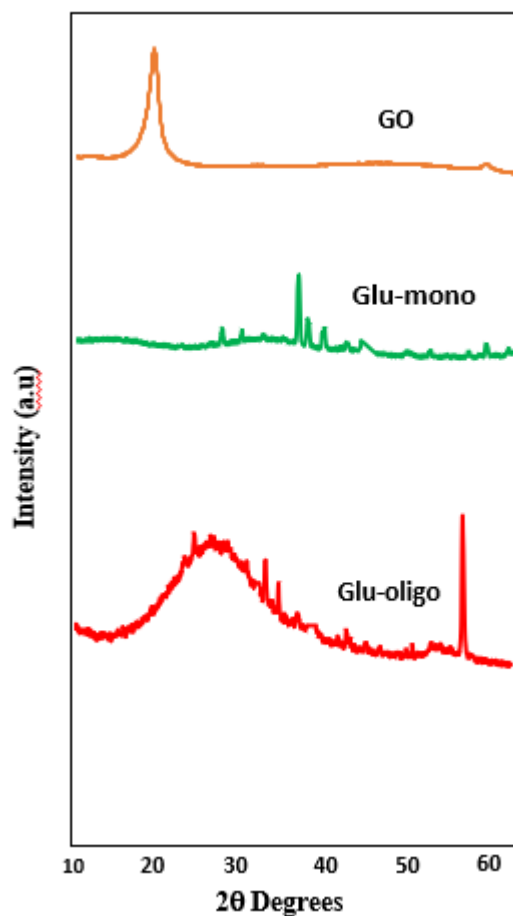
Figure 2.14 XRD patterns are functionalized of GO-Glu (Mono) and GO-Glu (Oligo) showing the d- space.

The thermal gravimetric analysis (TGA) conducted on GO exhibited similar results to our previous findings and those reported in published reserach.[17] In the published research, a significant weight loss was observed when the temperature ranges from 150°C to 300°C, while detailed data highlighted a gradual decrease in mass between 400°C and 950°C, which was attributed to the removal of more stable oxygen functionalities. The degradation process of GO occurred in three distinct stages. Initially, there was a weight loss of approximately 30% in the temperature ranging from 60–120°C, primarily attributed to water evaporation. The second stage occurred between 130°C and 400°C, leading to the elimination of oxygen-containing groups, resulting in a 30% reduction in mass. The third and final phase, which took place between 400°C and 750°C (at which point the measurements were halted), involved the pyrolysis of oxygen and unstable carbon species, generating CO and CO_2. It is expected that the functionalised systems will behave very differently during the first and second phase. This is due to the

layers of functionalisation, which have the bulk of the oxygen containing groups and are easily degraded. In addition, as the functionalisation contributes significantly to the overall weight, we expect greater reductions in the mass percentages (greatest for the oligomeric system). The data does indeed demonstrate that the monomeric and oligomeric systems degraded much more rapidly, with both exhibiting a rapid early degradation correlating to water loss. Subsequently, in the case of the monomer, a rapid decomposition took place when the temperature was between 100 to 600 °C, leading to a significant weight loss of approximately 55%. Similarly, the oligomeric system demonstrated a consistent and rapid decomposition when temperature was between 120 to 450 °C, resulting in a substantial weight loss of around 85%. This was succeeded by a final pyrolysis stage occurring between 600 and 800 °C. for both systems. As predicted, the faster decomposition of the functionalised systems was due to the degradation of amino acids and oligomers, which is reflected in the proportionate increases in weight loss.
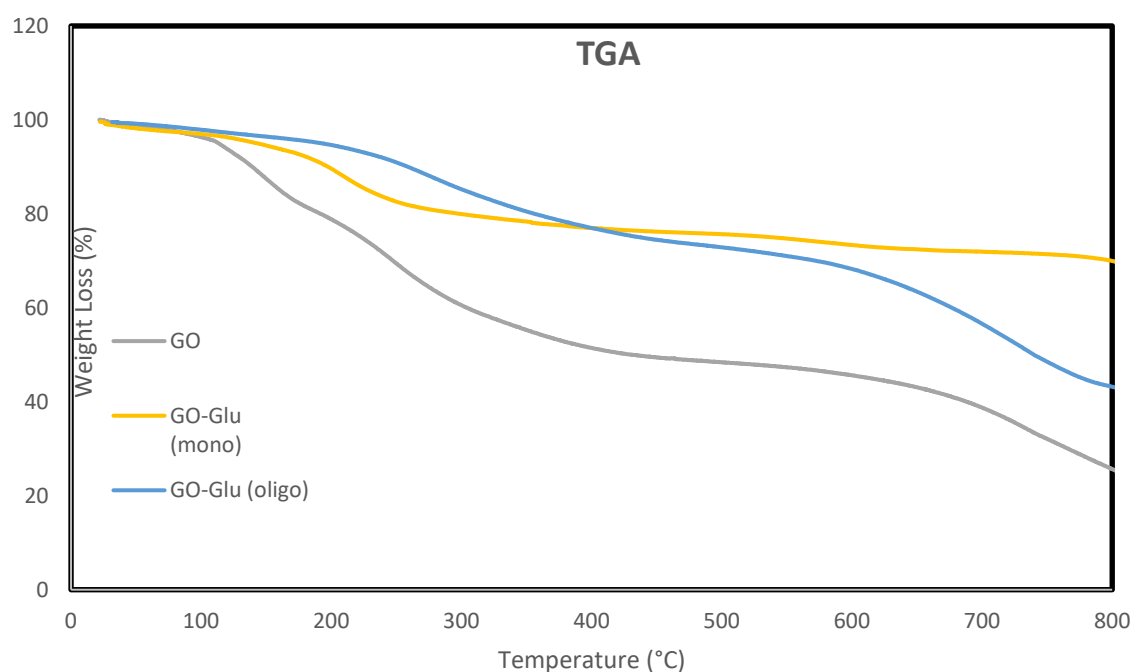

Figure 2.15. TGA of GO-Glu (Mono) and GO-Glu (Oligo)

When considering all the characterisation data, the synthesis of the required monomeric and oligomeric functionalised GO was successful. As such, we were able to test our hypothesis that an

oligomeric system would bind proteins significantly stronger than the equivalent monomeric system or an unfunctionalized GO.

2.3.6 Inhibition assay to determine binding between the GO systems and α-chymotrypsin

Given its remarkable physicochemical characteristics, GO has been extensively investigated as a possible ligand for protein binding. The presence of carboxyl (-COOH) and hydroxyl (-OH) functional groups on GO enables the binding of proteins through various types of interactions including electrostatic, hydrophobic, and hydrogen bonding interactions. These functional groups serve as binding sites for proteins, facilitating their attachment to the GO surface.[28,29] Glutamic acid is an amino acid with two carboxylic acid functionalities, which reacts with the carboxylic acids on GO and the number of possible carboxylate groups, thereby increasing the potential for ionic interactions with a protein.[30] However, as aforementioned, these carboxylic acid groups can also interact with the surface of GO and potentially limit the binding to the proteins. One approach to address this issue is to protect the carboxylic acid groups of glutamic acid before adding it to GO. This can be achieved by temporarily adding a protecting group to the carboxylic acid functionalities. After the glutamic acid is attached to GO, the protective groups can be eliminated, or deprotected to expose the carboxylic acid groups and potentially enhance the binding to the proteins.[17]

The choice of whether to adopt protecting group and deprotection method will depend on the specific system and application. Some common deprotection methods include acid or base hydrolysis, hydrogenation, or photolysis.[31] It is important to carefully optimise the protecting group and deprotection conditions to ensure that the glutamic acid is attached to GO, and the carboxylic acid groups are exposed in a controlled and efficient manner. The addition of non-protected glutamic acid is simpler than other alternatives and it is advantageous to use oligomeric glutamic acid due to this method's ability to add even more carboxylates. Additionally, using oligomeric glutamic acid instead of oligomeric tyrosine can overcome limitations in protein binding caused by interactions of aromatic side chains with the GO surface. This is because oligomeric glutamic acid lacks functional groups that can interact with

the surface of GO, effectively avoiding π-π stacking interactions. There are several protocols to measure binding between proteins and macromolecular ligands. Our experiments adopted enzyme inhibition to assess *relative binding*. We have used this method previously and found it to be an excellent method to compare the binding ability of a series of related systems. Although direct binding affinities cannot be obtained, a relative level of binding can be determined and used to compare binding efficiencies for a range of related systems. Specifically, the level of any inhibition is directly related to the extent of the binding.The reaction used is shown in Figure 2.17 below.The by-product is p-nitroaniline, which is yellow in colour and can be followed using UV-Vis spectroscopy.Concentration vs time plots were used to obtain the rate data, and a linear region was used to obtain an initial rate. The concentration of the by-product p-nitroaniline was calculated using the extinction coefficient (15960 M^{-1} at 400 nm), which can be determined from a simple Beer Lambert analysis.[32] Our first experiment was a control using only α-chymotrypsin and BTNA substrate. The experiment was carried out with a pH level of 7.46, 0.01 M phosphate buffer containing 0.56 mM BTNA, 1mM Chy, with data collected every 30 seconds over a period of 300 seconds. The gradient from the linear region of the plots determined the initial rate, which was then used to estimate relative binding abilities.[32] During the analysis of the control sample's results, it was expected that the chymotrypsin alone would demonstrate its full enzymatic activity without inhibition, resulting in a 0% inhibition of its activity. Having carried out the controlled experiments, we then investigated the binding potential of GO, GO-Glu-mono and GO-Glu-oligo.These experiments were carried out using the same procedure as the control but with GO inhibitors at a concentration of 25 μg/mL.
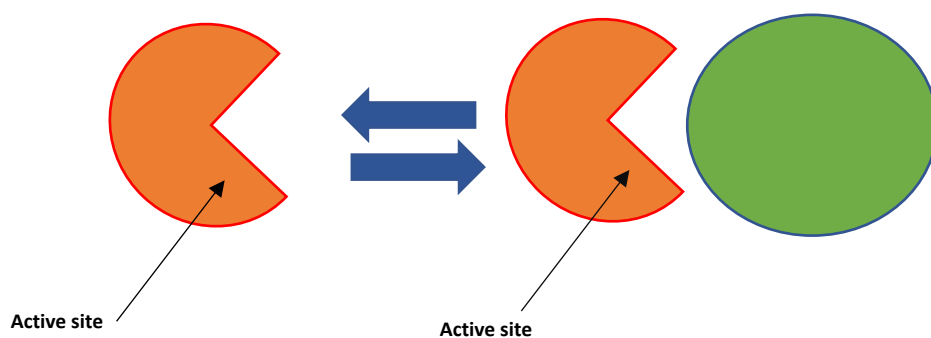

Active site   Active site

Figure 2.16 In the surface-bound inhibitor assay, the left side of the image represents the enzyme's active site, where substrates are freely able to enter and participate in catalytic reactions. However, the right image shows the introduction of a surface-binding inhibitor, which effectively obstructs substrate access to the active site, thereby impeding catalysis and demonstrating the inhibitory action of the inhibitor in this assay.

N-benzoyltyrosine-p-nitroanilide (BTNA)

Yellow
UV active nitroaniline
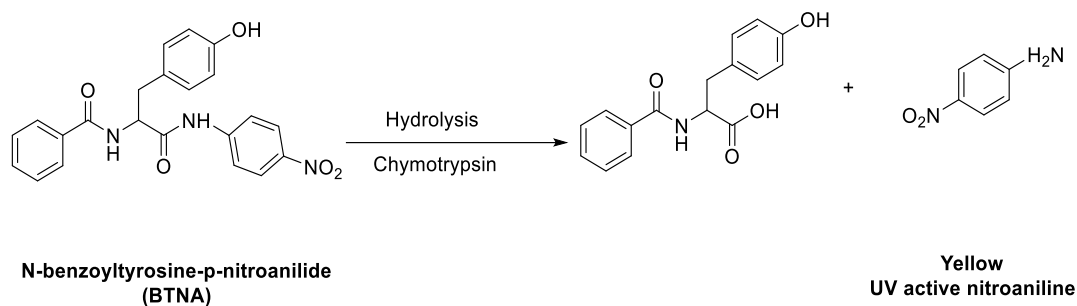
2.17 The figure shows the hydrolysis reaction for the enzyme substrate N-benzoyl tyrosine p-nitroanilide (BTNA) by α-chymotrypsin. The extent of hydrolysis is directly related to the binding of GO to Chy or Inhibition.

The initial rate plots and rate data are presented in Table 1 and 2, with all the data expressed relative to Chy. The extent of the reaction of Chy minus the extent of the reaction of inhibition is shown. The numerical data is displayed in Table 1. It is evident that both GO-Glu mono and GO-Glu oligo exhibit stronger inhibitory effects compared to GO alone. This heightened inhibitory activity can be attributed to the higher concentration of carboxylic acids in both GO-Glu mono and GO-Glu oligo, resulting in an increased potential for negative charges. Consequently, the binding affinity is enhanced, leading to greater levels of inhibition. To illustrate at the given concentrations, GO-Glu mono can bind up to 50% of the protein, while GO-Glu oligo can bind more than 60%. These substantial inhibition levels underscore the significantly enhanced binding capabilities of the functionalized GO systems in comparison to GO alone, which can only bind 20% of the protein.

Changes in the concentration of nitroaniline over time

[sec]	Chy	GO	GO-Glu oligo	GO-Glu mono
0	0.00	0.00	0.00	0.00
30	6.43	4.12	1.99	3.95
60	11.52	8.27	4.64	6.86
90	16.36	12.57	6.70	9.27
120	21.55	16.94	7.82	12.57
150	28.52	21.38	10.16	14.83
180	33.02	25.79	12.35	17.36
210	38.38	30.28	13.83	19.91
240	43.23	34.96	16.87	21.81
270	48.88	39.82	19.25	23.76
300	55.23	45.40	20.43	26.31
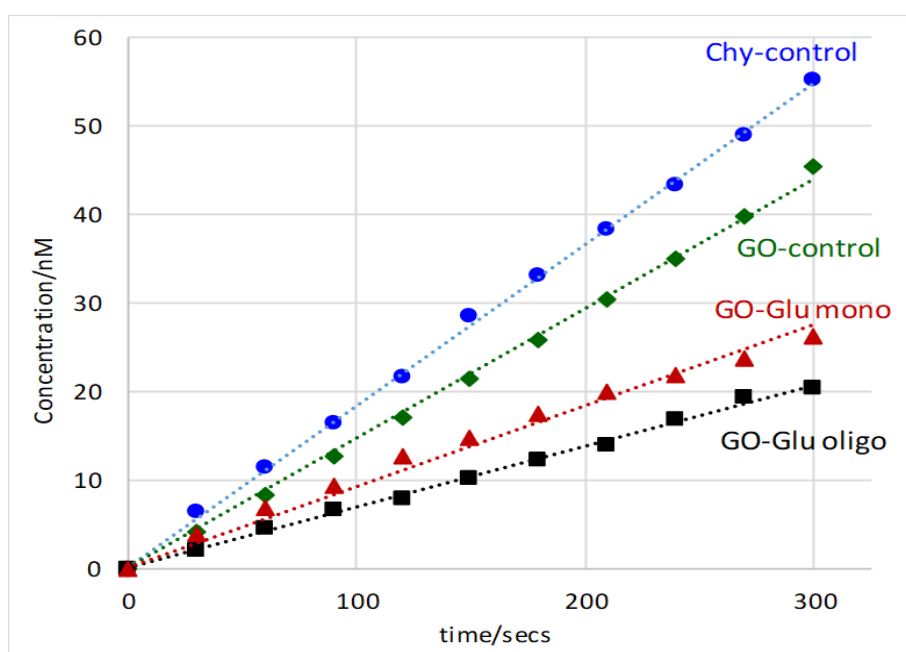
Figure 2.18 Rate plot for control - GO - GO Glu-mono and GO Glu-oligo

0.56 mM BTNA, 1mM Chy and 25 mg/mL inhibitor			
Experiment	Initial rate- $x10^{-7}$ M	Extent of reaction-%	Relative binding-%
Chy	1.8	100	0
GO	1.51	84	16

GO-Val	1.25	69	31
GO-Ph	1.32	73	27
GO-Tyr	1.01	56	44
GO-Glu-mono	0.87	48	52
GO-Glu-oligo	0.68	38	62

Table 3. The data indicates that relative binding is directly proportional to the inhibition percentage, which is calculated as a straightforward. The extent of reaction of chy % minus the extent of reaction of Inhibition.
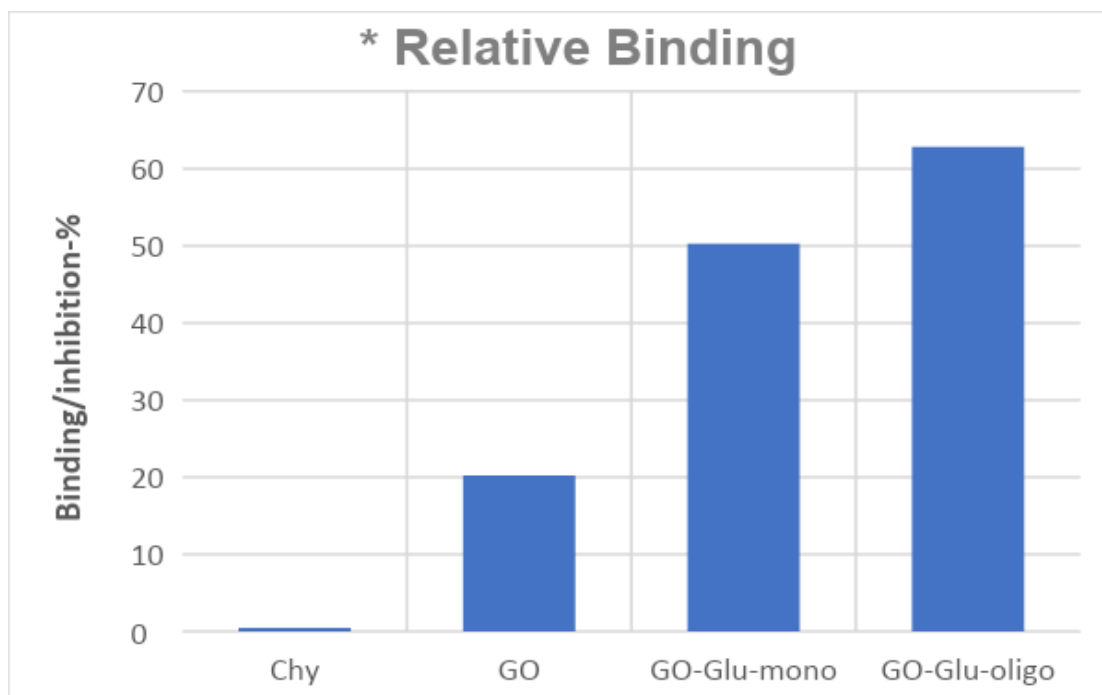
Figure 2.19 relative binding. The data clearly indicates that the GO-Glu oligo binds strongest and calculated as the extent of reaction of chy % minus the extent of reaction of inhibition.

In enzyme kinetics, relative binding is expressed as a percentage and calculated by subtracting the extent of reaction with an inhibitor from the extent of the reaction with chymotrypsin, which is set as the reference (100%). This measurement assesses the strength of the inhibitor that competes with the substrate for binding towards chymotrypsin. A higher relative binding percentage indicates an increasingly potent inhibitor in terms of its ability to interfere with the enzyme's activity.

From the graphs shown in the figure 2.19, it is evident that the GO-Glu oligo had higher inhibition rates. Initial rates were calculated at pH 7.46 for all experiments, and in all cases, the fit was good, with R2 values greater than 0.98. The data demonstrate that functionalised GO systems has higher performance compared to GO alone as inhibitors. Since inhibition is dependent on binding, also it is possible to conclude that functionalised GO systems bind to the protein surface more powerfully than unfunctionalized GO, resulting in increased inhibition. The most potent inhibitor is GO-Glu (oligo), and has greater binding strength in comparison to both the monomeric system and GO alone, with the oligo system having four times the binding strength than GO alone. In summary, the data validates that a GO surface with an oligomeric layer of glutamic acid is the most effective in inhibiting chymotrypsin activity.

2.3.7 Investigation selectivity through the functionalization of GO with diverse amino acids

When proteins bind, selectivity is influenced by the shape of the binding surface, type, and functionality of the amino acids. As previously shown, GO Glu-oligo demonstrates high binding strength to chymotrypsin (at the concentrations used, more than 60% of the enzyme was bound). However, the fact that a ligand has strong bind does not mean that it can offer any level of selectivity when binding other proteins. For this purpose, a protein's binding surface was simulated by introducing several different amino acids that can present different types of functional groups. In order to study the simulated protein, we selected a series of different amino acids with various functional groups as shown in Scheme 2.20. Tyrosine was chosen due to its aromatic group properties that can provide additional π-π interactions, as well as a phenolic OH group that can provide an additional negative charge (after deprotonation to the phenolate) and provide secondary H-bonding interactions. In these respects, we would expect to see some significant binding when using tyrosine. For similar reasons, we have also decided to investigate phenylaniline, which is similar to tyrosine, but lacking in the phenolic OH group. Therefore, when we compare the binding of tyrosine with phenylalanine, any differences can be ascribed to the role of the OH group and the extent to which it influences the binding affinity. We also compared and studied the

69

glutamic acid system, which as discussed above, can contribute to a second carboxylic acid to the binding process. Finally, we considered valine, as this amino acid does not have any additional functional groups that can contribute to the binding in a positive way. In fact, the hydrophobic iso-propyl group may inhibit and reduce binding affinities. The aim here is to compare the relative binding with respect to the functional groups. If predictable changes in the binding occur, then it should be possible to introduce some element of selectivity through functionalisation. As such, we predicted that either glutamic acid or tyrosine have the highest binding strength, as these amino acids have functional groups that should enhance binding. At this stage, we expected that the binding performance of glutamic acid functionalised GO is slightly better than the tyrosine derivative. Due to the lack of additional OH group present in Tyrosine, we expected the phenylalanine system to bind with a measurably smaller affinity than either the glutamic or tyrosine functionalised GO, but better than the Valine system. The predicted series is therefore, Glu $\gtrsim$ Tyr > Phe > GO > Val.
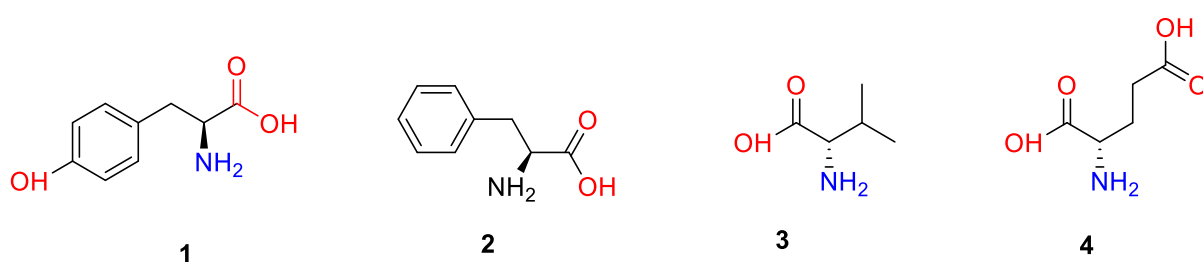
Figure 2.20. The proposed amino acids that will be used to functionalize GO to determine whether some level of selectivity can be introduced

The binding was assessed using the same inhibition assay described above. The rate plots are shown in Figure 12.
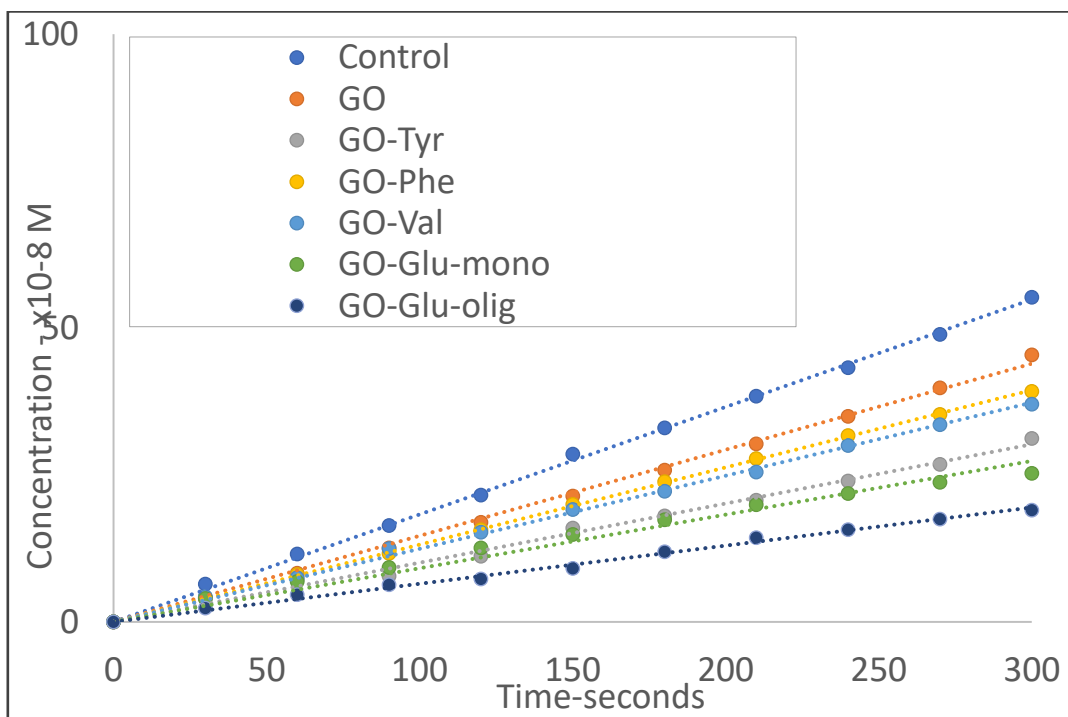
Figure 2.21 Initial rate plots (concentration vs time) for GO, Control and Amino acids
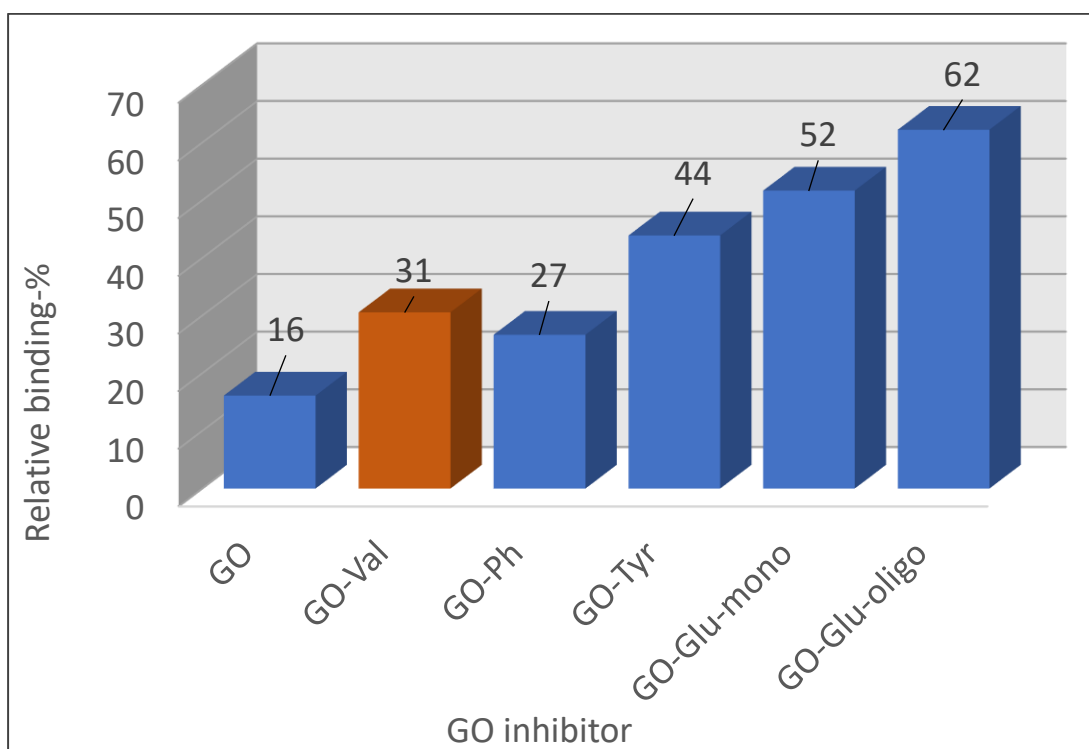
Figure 2.22. Relative binding was assessed using the same inhibition assay. The binding proceeded as expected, except for Valine, which did not behave as predicted. (Relative Binding = [(Extent of Reaction with Chymotrypsin - Extent of Reaction with Inhibition) / Extent of Reaction with Chymotrypsin] * 100%)

Table 4. Experiment Initial Rate-Abs/sec Initial rate Conc/time Extent of reaction-% Relative binding-% Chy

Experiment	Initial rate-Abs/sec	Initial rate Conc/time M/s	Extent of reaction-%	Relative binding-%
Chy	29	1.8×10^{-2}	100	0
GO	23	1.4×10^{-2}	78	22
GO-Val	19	1.2×10^{-2}	66	34
GO-Ph	18	1.1×10^{-2}	62	38
GO-Tyr	16	1.0×10^{-2}	55	45
GO-Glu-mono	15	0.9×10^{-2}	52	48
GO-Glu-oligo	11	0.8×10^{-2}	38	62

The present study initially hypothesized that valine would exhibit a weak interaction with GO because valine is hydrophobic in nature that would lead to only weak or limited interactions with GO due to the potential mismatch in the chemical affinities of the two entities. However, the experimental results yielded unexpected findings, where it has demonstrated a strong interaction between valine and GO. This stark contrast can be attributed to poor adsorption of valine onto the GO surface. The poor loading observed between the valine and GO could be attributed to the chemical properties of valine, such as its hydrophobic nature, which may have impeded interactions with the hydrophilic functional groups present on GO. The results obtained through SEM-EDX analysis revealed an unexpected observation regarding the nitrogen content in two amino acids, glutamic acid, and valine. It was observed that the nitrogen content in the glutamic acid was significantly higher than anticipated at a ratio of 13. In contrast, valine exhibited a considerably lower nitrogen ratio of only 2 rather than the 13 as shown in Table 1.

Due to its ability to establish electrostatic interactions with the GO surface, the presence of carboxyl groups in glutamic acid makes it a promising candidate for binding to GO. This interaction arises from

the attraction between negatively charged carboxyl groups and the positively charged GO surface. This electrostatic interaction contributes to the strong binding affinity between glutamic acid and GO. In contrast, phenylalanine (Phe) possesses an aromatic side chain that enables additional binding interactions with the GO surface. Specifically, the aromatic ring of in Phe can interact with the graphene layers of GO through π-π stacking. These π-π stacking interactions contribute to the overall binding affinity between Phe and GO. However, it is important to emphasize that the strength of these interactions may be weaker compared to the electrostatic interactions exhibited by glutamic acid. Oligomeric Glu acids has a higher binding affinity compared to the monomeric amino acids. This increased affinity arises from the presence of multiple carboxylate groups, which can participate in electrostatic interactions with substrates or proteins for the monomeric systems. The binding properties depend upon the specific chemical structures and functional groups. Electrostatic interactions, aromatic stacking interactions, and the presence of charged or polar groups play crucial roles in determining the binding strength.

2.4 Conclusion:

Our objective was to determine if functionalized GO is more effective in binding proteins than unmodified GO, which is known to have great binding strength on protein surfaces. By introducing functional groups, such as glutamic acid, it was expected that the binding strength would enhance and potentially accomplish selectivity. Glutamic acid was selected due to its significance in protein-protein and protein-surface binding. In addition, we investigated whether the extent of functionalization, including surface thickness and the effect of any spacers provided by the oligomer, played a crucial role in protein binding. Using unprotected glutamic acid and an EDC coupling technique, we successfully synthesised GO with an oligomeric layer of glutamic acid in a single synthetic step. We also synthesised monomeric functionalized GO via a subtle variation of the same method involving two steps, which are EDC-mediated addition of C-protected glutamic acid and hydrolysis to remove the protecting group. All GO systems, including the monomeric and oligomeric layers, were capable of inhibiting chymotrypsin activity, which indicates efficient protein binding. Based on the initial rate data, the oligomeric system exhibited the strongest inhibition and, consequently, the strongest binding, which was nearly four times superior to unfunctionalized GO. The conclusion is that the monomeric system is less effective at inhibiting compared to the oligomeric functionalized GO. This is, due to several factors that account for the decreased efficacy of the monomeric system in inhibiting compared to the oligomeric system including: (i) lower binding affinity: typically, monomeric systems have fewer functional groups accessible for interaction and binding with target molecules or processes. (ii) The limited number of binding sites, which may result in interactions that are weaker or less stable, thereby reducing inhibition; and (iii) in the monomeric system, functional groups may operate independently, thus lacking the cooperative or synergistic effects observed in the oligomeric system.

In addition, (iv) this is different to the Tyr system which could bind cooperatively to the protein surface. As for Glu, there was no competition between protein binding and GO binding. In summary, our study has shown that functionalized GO can strongly bind to chymotrypsin, and the degree of oligomerization

can influence the binding affinity. Our goal is to exploit these findings to develop novel protein ligands and enzyme inhibitors with improved selectivity for their binding. We are currently using this methodology and the obtained results to design and create new GO inhibitors.

2.5 References

1   A. K. Geim, K.S. Novoselov, *The rise of graphene.*, 2007, **6**, 183-191.

2   V. C. Tung, M. J. Allen, Y, Yang, R.B. Kaner, *Nature Nanotechnology*, 2009, **4**, 25-29.

3   De, M., Chou, S. S., Dravid, V. P., J. Am. *Chem. Soc.*, 2011, **133**, 17524-17527.

4   Qiu, Z., Hu, J., Li, Z., Yang, X., Hu, J., You, Q.,Yin, J., *Colloids Surf. A: Physicochem. Eng. Aspects*, 2020, **593**, 124-135.

5   S. Garaj, W. Hubbard, A. Reina, J. Kong, D. Branton, J. A. Golovchenko, *Nature*, 2010, **467**, 190-193.

6   C. Kotlowski, M., Larisika, P. M. Guerin, C. Kleber, T., Mastrogiacomo, W.Knoll, *Sens. Actuators B*: *Chem.*, 2018, **256**, 564-572.

7   Ali, M. A., Hu, C., Jahan, S., Yuan, B., Saleh, M. S., Ju, E., Panat, R., *Adv. Mater.*, 2021, **33**, 2006647.

8   A. L. Hopkins, *Nat. Biotechnol.*, 2007, **25**, 1110-1111.

9   You, C. C., De, M., Han, G., Rotello, V. M., J. *Am. Chem. Soc.*, 2005, **127**, 12873-12881.

10 A. A. Aziz, L. J. Twyman, *ACS Appl. Mater. Interfaces*, 2019, **11**, 44941-44948.

11 H. S. Park, Q. Lin, A. D. Hamilton, *Proc. Natl. Acad. Sci.*, 2002, **99**, 5105-5109.

12 F. Chiba, L. J.Twyman, *Bioconjugate Chem.*, 2017, **28**, 2046-2050.

13 Li, S., Aphale, A. N., Macwan, I. G. Patra, P. K. Gonzalez, W. G. Miksovska, J. Leblanc, R. M., *ACS Appl. Mater. Interfaces*, 2012, **4**, 7069-7075.

14 W. Park, Na, K., *Wiley Interdiscip. Rev.: Nanomed. Nanobiotechnol.*, 2015, **7**, 494-508.

15 Yan, M., Liang, Q., Wan, W., Han, Q., Tan, S., Ding, M, *RSC Adv.*, 2017, **7**, 30109-30117.

16 A. A. Bogan, K. S. Thorn, *J. Mol. Biol.,* 1998, **280**, 1-9.

17 D. C. Marcano, D. V. Kosynkin, J. M. Berlin, A. Sinitskii, Sun, Z., A. Slesarev, J. M. Tour, ACS *Nano*, 2010, **4**, 4806-481.

18 Y. Nishina, S. Eigler, *Nanoscale*, 2020, **12**, 12731-12740.

19 J. M. Gutierrez, F. A. Hernández-Ferrer, J. Ansón-Casaos, A., Rubianes, M. D. Rivas, G. Martinez, M. T.J. *Mater. Chem.* B, 2015, **3**, 3870-3884.

20 D. Graf, F. Molitor, K. Ensslin, C. Stampfer, A. Jungen, C. Hierold, L. Wirtz, *Nano Lett.,* 2007, **7**, 238-242.

21 R. A. Copeland, *Enzymes: a practical introduction to structure, mechanism, and data analysis,* John Wiley & Sons, 2023, **5**, 456-473.

22 S. Mallakpour, A. Abdolmaleki, and S.J. Borandeh, *Thermoplastic Composite Mater.,* 2017, **30**, 358-380.

23 H. Meng, G. X. Sui, P. F. Fang, and R. Yang, Polymer*,* 2008, **49**, 610-620.

24 M. S. Dresselhaus, A. Jorio, M. Hofmann, G. Dresselhaus, R. Saito, *Nano Lett.,* 2010, **10**, 751-758.

25 A. M. Dimiev, J. M. Tour, ACS *Nano*, 2014, **8**, 3060-3068.

26 T. Yamada, S. Shinoda, K. Kikawa, A. Ichimura, J. Teraoka,T. Takui, and H.Tsukube, *Inorg. Chem.*, 2000, **39**, 3049-3056.

27 W. Gao, *Graphene Oxide: Reduction Recipes, Spectroscopy, and Applications.,* 2015, **33**. 61-95.

28 N. O. Fischer, C. M. McIntosh, J. M. Simard, and V. M. Rotello, Proc. *Natl. Acad. Sci*., 2002, **99**, 5018-5023.

29 K. S. Thorn, A. A. Bogan, *Bioinformatics*, 2001, **17**, 284-285.

30 S. Hartwig, M. M. Nguyen, S. Hecht, Polym. *Chem.*, 2010, **1**, 69-71.

31 K. Bose, K. K. Kundu, Can. *J. Chem.*, 1977, **55**, 3961-3966.

32 R. Lumry, S. Rajender, Biopolymers, 1970, **9**, 1125-1227.

33 S. J. Wodak, J. Janin, in *Advances in Protein Chemistry*, 2002, **61**, 9-73.

34 J. Tsai, R. Taylor, C. Chothia, and M. Gerstein, J. *Mol. Biol.,* 1999, **290**, 253-266.

Chapter 3

A Strategy Utilizing Dynamic Combinatorial Methods for the Synthesis of Macromolecular Based Protein Ligands.

3.1 Introduction

Dynamic combinatorial chemistry (DCC) offers a method for the reversible assembly of molecular building blocks either through covalent or non-covalent bonding, allowing for diverse combinations.[1] As a result, dynamic combinatorial libraries (DCLs) can encompass a wide range of compounds, and are not limited to any specific field. DCLs have applications across various scientific disciplines, including chemistry, materials science, and drug discovery. They are valuable for exploring molecular diversity and screening for potential candidates in areas beyond pharmaceuticals, such as nanomaterials, catalysis, and the development of new functional materials. The flexibility and adaptability of DCLs make them a versatile tool for generating and screening compound libraries in diverse research fields.[2] The distribution of these products is governed by their thermodynamic stability, as the reactions among the building blocks are reversible. DCLs offer an advantage over traditional combinatorial libraries where they may respond to external stimuli, such as the introduction of a target molecule.[3] Consequently, the library composition is re-equilibrated, favouring the selection and binding of the members with the highest affinity for the target.[4] This approach leverages dynamic combinatorial libraries, where molecules interchange and the most effective binders self-select without requiring individual synthesis and characterization, streamlining the discovery of potent binding compounds.[5] Protein-template DCC, which emerged in the late 1990s, demonstrated its potential for discovering inhibitors specific to the template protein. This method proves to be a powerful strategy for accelerating the discovery and the development of novel ligands for biological targets through iterative optimization processes, making it highly promising for drug development. In this discussion, we will explore recent applications of DCC for identifying protein ligands based on the type of reversible reaction employed over the past decade.[6]

Supramolecular chemistry benefits from DCLs by exploring the self-assembly of complex molecular structures. In chemical sensing, DCLs assist in discovering ligands with high selectivity for target

analytes, which are beneficial in chemical and biosensor development. They also contribute to materials design and catalysis research, optimizing catalysts and reaction conditions.

DCLs offer insights into molecular recognition, impacting host-guest chemistry and drug-receptor interactions. In biotechnology, they aid in discovering biomimetic molecules for applications such as drug delivery and tissue engineering. Overall, DCLs are versatile tools for exploring chemical space, generating diverse molecular structures, and advancing various scientific fields.
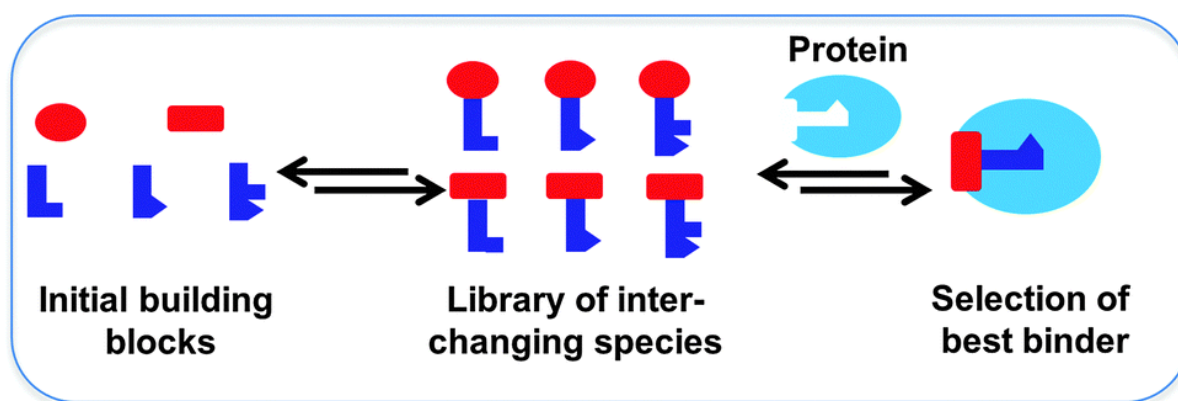

Figure 3.1. The concept of protein-templated dynamic combinatorial chemistry (DCC) involves utilizing proteins as templates to guide the formation of dynamic combinatorial libraries, enabling the rapid exploration of diverse chemical space for potential ligands or inhibitors. Reprinted with permission from M. Mondal, A. K. Hirsch.2015, 44, 2455–2488.

3.2 Dendrimers

As described in chapter 1, dendrimers are spherical, hyperbranched globular macromolecules possessing 3D topologies resembling the size and shape of a range of biological macromolecules.[7] They are synthesised via a controlled stepwise branching methodology, yielding dendrimers with fixed (quantized) sizes and an increasing number of terminal groups (known as generations or G). Specifically, dendrimers with precise diameters ranging from just a few angstroms to well over 100 Å can be made easily (the G 1.5 PAMAM dendrimer with 16 terminal acid groups can be seen in the top left of Scheme 2 below). The maximum addressable area that each dendrimer can theoretically bind, can be estimated from their diameters. For this proposal, we will study dendrimers up to generation 4.5, (possessing 64 terminal groups) and maximum addressable areas that range from 100 Å2 to around 4000

Å2. It transpires that this range in maximum addressable areas matches the range of interfacial binding areas of most proteins.

3.1.2 Thioester Exchange

There are several possible reactions that can be used for DCC. The essential aspect is that they must be reversible, be atom efficient (which means negating or minimising too many unwanted by-products), and high yielding.[13] Suitable reactions include imine formation, esterification, and cycloadditions. For the work described in this chapter, we selected the reversible thioester exchange reaction involving a thioester and a thiol. Thioester DCLs (dynamic combinatorial libraries) are a subcategory of combinatorial chemistry libraries based on thioester exchange reactions. [14]These libraries are a combination of building blocks with thioester functional groups that can endure reversible exchange reactions to generate a dynamic mixture of compounds. In addition to the discovery of novel ligands for receptors and catalysts for organic reactions, thioester DCLs are utilised in a vast array of applications. The production of thioester DCLs involves combining a set of thioester-containing building blocks, typically with two distinct functional groups at the molecule's extremities that can participate in thioester exchange reactions.[15] The thiol/thioester exchange reaction is a rapid and reversible process that can take place in aqueous environments, with a half-life (t1/2) of approximately 20 minutes in a neutral solution as shown in the scheme 1. Existing research related to DCC has adopted this technique, with Ramström & colleagues reporting how a library of acetylcholinesterase inhibitors was produced under neutral aqueous media via the thiol/thioester exchange process. [16,17]
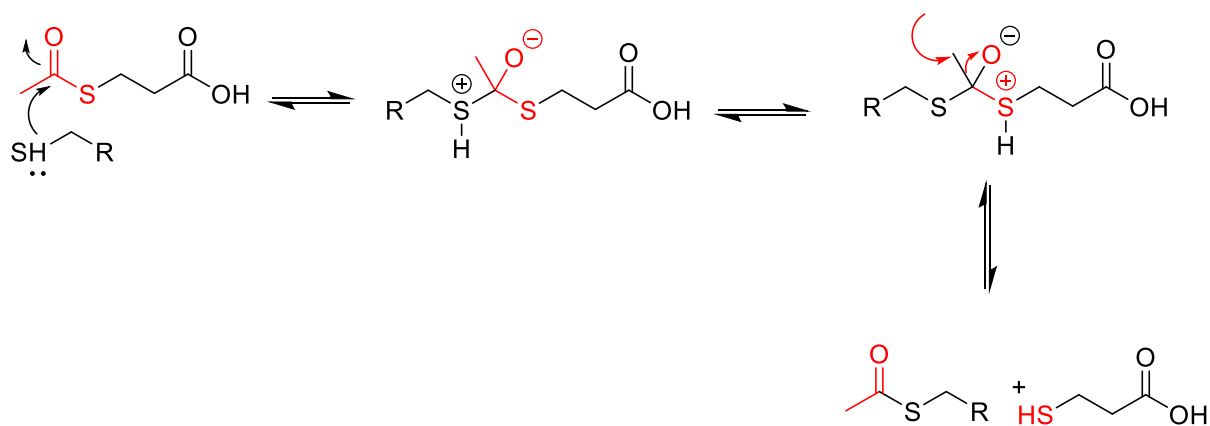
Figure 3.2 Exploring the Dynamics of Thiol and Thioester Exchange Reactions: Investigating a Rapid, Reversible Process in Aqueous Environments (with a half-life of approximately 20 minutes in neutral solution

For instance, thioester DCLs were to discover new ligands for the dopamine receptor and new catalysts for the aldol reaction. Thioester Dynamic Combinatorial Libraries (DCLs) are versatile tools for discovering novel chemical entities and optimizing reactions due to their adaptability and diversity. Their rapid and reversible transformations enable the exploration of uncharted chemical space, fostering the discovery of unique compounds. Thioester DCLs are valuable for developing ligands, catalysts, and functional materials, offering selective amplification of desired properties. Additionally, their adaptability to external stimuli makes them crucial in applications such as drug discovery for optimal binding affinity.

3.2 Specific work leading up to this project.

Dendrimers for protein binding - We postulated that prior knowledge to the size of a protein's interfacial area would allow us to predict the dendrimer with the strongest binding to a specific protein. Our preliminary studies used negatively charged carboxylate dendrimers and proteins with positively charged interfacial areas. The results revealed that selective binding could be achieved by matching a dendrimer's maximum addressable area with a protein's interfacial area. For instance, the interfacial area of the protein chymotrypsin (2400 A2) is more than twice as large as that of the smaller protein cytochrome-c (1000 A2). For cytochrome-c, the best binding was predicted to occur using the dendrimer with a maximum accessible area of 1200 Å2. On the other hand, chymotrypsin, which has a greater

interfacial area (2400 Å2), has optimum interaction with a larger dendrimer with an addressable area of 2250 Å2. For these experiments, it's crucial to remember that binding was independent of the number and density of charges. Circular dichroism (CD) experiments were instrumental in assessing the impact of dendrimers on protein structure and interactions. These experiments provided crucial insights into the influences of dendrimers upon the protein's conformation and binding affinity. Essentially, CD spectroscopy measures the differential absorption of left and right circularly polarized light by chiral molecules, offering a window into the structural characteristics of biomolecules.[15] CD experiments demonstrated that the protein's structure remained intact and was not denatured during the complexation with the dendrimers. This finding indicates that dendrimers did not disrupt the overall folding and stability of the protein. Our group have investigated the impact of terminal group functionality upon binding affinity. Dendrimers are either functionalized with an amino acid (tyrosine) known to be crucial for protein binding and an amino acid known to be of little utility for protein binding (valine). The dendrimer's size was held constant for these tests. According to our investigation the results of these investigations revealed a notable correlation between terminal group functionality and binding affinity. The dendrimer functionalized with tyrosine, a group known to enhance protein binding, exhibited a 30% higher affinity for chymotrypsin compared to an equivalent-sized non-functionalized dendrimer. In contrast, the binding affinity's strength of the valine dendrimer was around 24% less than that of the non-functionalized dendrimer. We are now recommend taking advantage of the variations in dendrimer size and the possibility of virtually endless terminal group functionaliation (via DCC) to produce explicit dendrimer ligands. To explore similar but non-clinical topics (such as protein purification and protein characterization), the same methods can be applied.

3.3 Proposed methodology DCC Approach for protein templated dendrimers functionalization

A two-step methodology will be used to select the optimum dendrimer for a given protein. The dendrimers and thioester terminated amino acids will be created in the first step. This means that the target protein will be added to a solution containing a library of differently sized dendrimers and a library

of functionalised amino acids. The target protein will act as a template thus allowing the optimum dendrimer to be assembled and selected. Subsequently, the selected dendrimer will be isolated and characterised to determine its size, as well as the type and proportion of amino acids on the surface. This information can then be fed into subsequent synthesis and selection rounds for the purpose of optimising the selectivity of the dendrimer ligand. The process is shown schematically in Figure 3.3

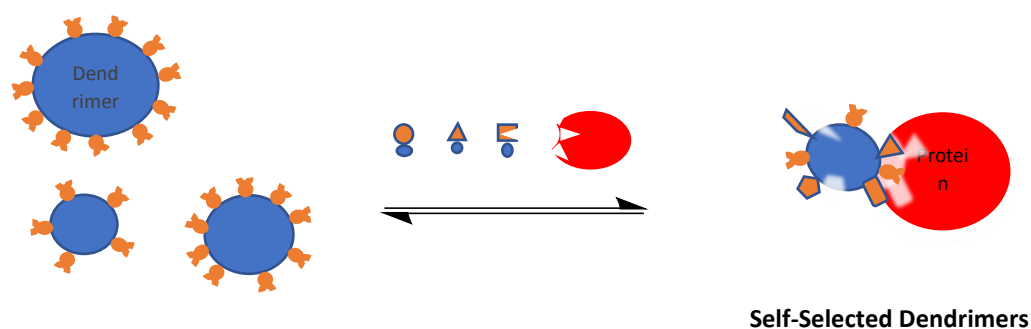

Self-Selected Dendrimers

Figure 3.3 The Dynamic Combinatorial Chemistry (DCC) approach for customizing protein-templated dendrimers. Selected dendrimers are isolated and characterized to determine the size and surface amino acid composition. This data informs subsequent synthesis and selection rounds, enabling the optimization of dendrimer ligand selectivity.

3.4 Proteins to be studied:

Our first targets will be the serine protease protein family, which is extensively studied and characterised. The serine protease family of proteins all possess the same catalytic and specificity is accomplished by the presence of additional binding regions.[19] However, due to the similarity of their action/mechanism, it is difficult to identify specific inhibitors for each protein/enzyme. Consequently, an active site inhibitor for one protein will frequently inhibit other serine protease family members. Therefore, the development of enzyme-specific inhibitors has been hampered by a lack of specificity. Despite the similarity of their active sites, their active site entrances and interfacial regions differ greatly in topology, size, amino acid composition, and distribution.[20] In view of these considerations, this family of proteins is an ideal test system for evaluating and validating our protein-binding methodology. We

will specifically target chymotrypsin, elastase, cathepsin-D, carboxypeptidase, and trypsin, as these proteases have similar activity but vastly distinct surface chemistry. In addition to aiding in the development of our methodology, this family of proteins represents a difficult and medically significant target. This family of proteins is extensively recognised, characterised, and investigated, thus allowing us to concentrate on devising the techniques necessary to demonstrate the validity of this " proof of concept".

3.5 Result and discussion

Our initial protein targets consist of positively charged interfacial regions. Through a DCC approach, we plan to generate negatively charged PAMAM dendrimers with terminal amino acids (carboxylate-ended). In order achieve this goal, it is necessary to have a single dendrimer with terminal thiol groups and a library of amino acids possessing a thioester. The generation of a collection of thiol ester-functionalised amino acids for the dynamic combinatorial selection process[21] necessitate a library of thioester amino acids. The protocol involves the use of EDC as a coupling agent to react a N-protected amino acid with a dihydroxy thiol, followed by the removal of the C-BOC protecting group to provide water-soluble thiol ester as shown in Scheme 3.4. The library can then be generated by repeating this process with various amino acids, and through this method, a diverse library of thiol ester-functionalized amino acids could be generated.[22]
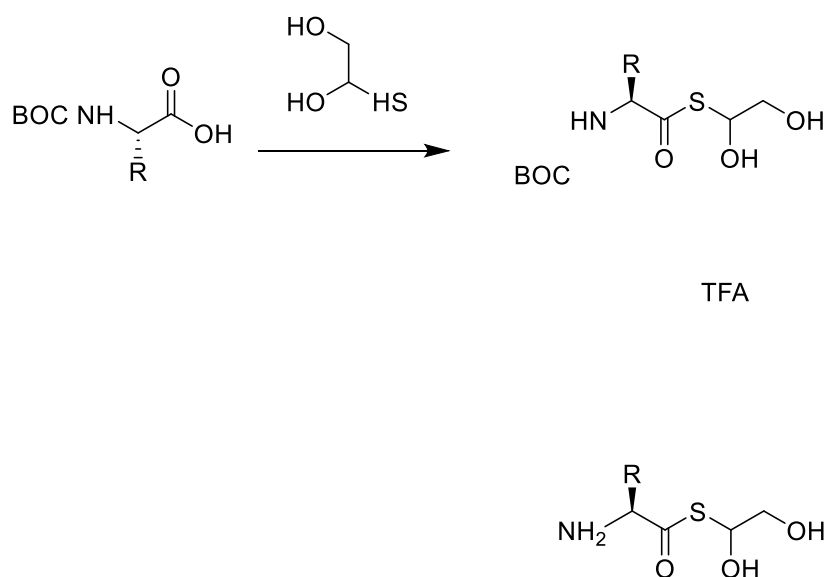
Figure 3.4 illustrates the synthesis of the thioester using EDC as a coupling agent to chemically bind a protected amino acid with a dihydroxy thiol. Subsequently, the removal of C-BOC protecting group results in the yield of a water-soluble thiol ester. This method enables the construction of a diverse library of thiol ester-functionalized amino acids through the repetition of the process with various amino acids, providing versatility in compound generation.

The synthesis of the thiol-terminated dendrimer involves adding a protected thiol to an amine-ended dendrimer via an amide linkage.[22] This can be achieved by using an excess amount of an acid-functionalised thiol and EDC as the coupling agent. The thiol can then be generated after removing the protecting group (see Scheme 3.5). This is a well-known method for functionalising dendrimers via amide links and is dependable.[23,26]
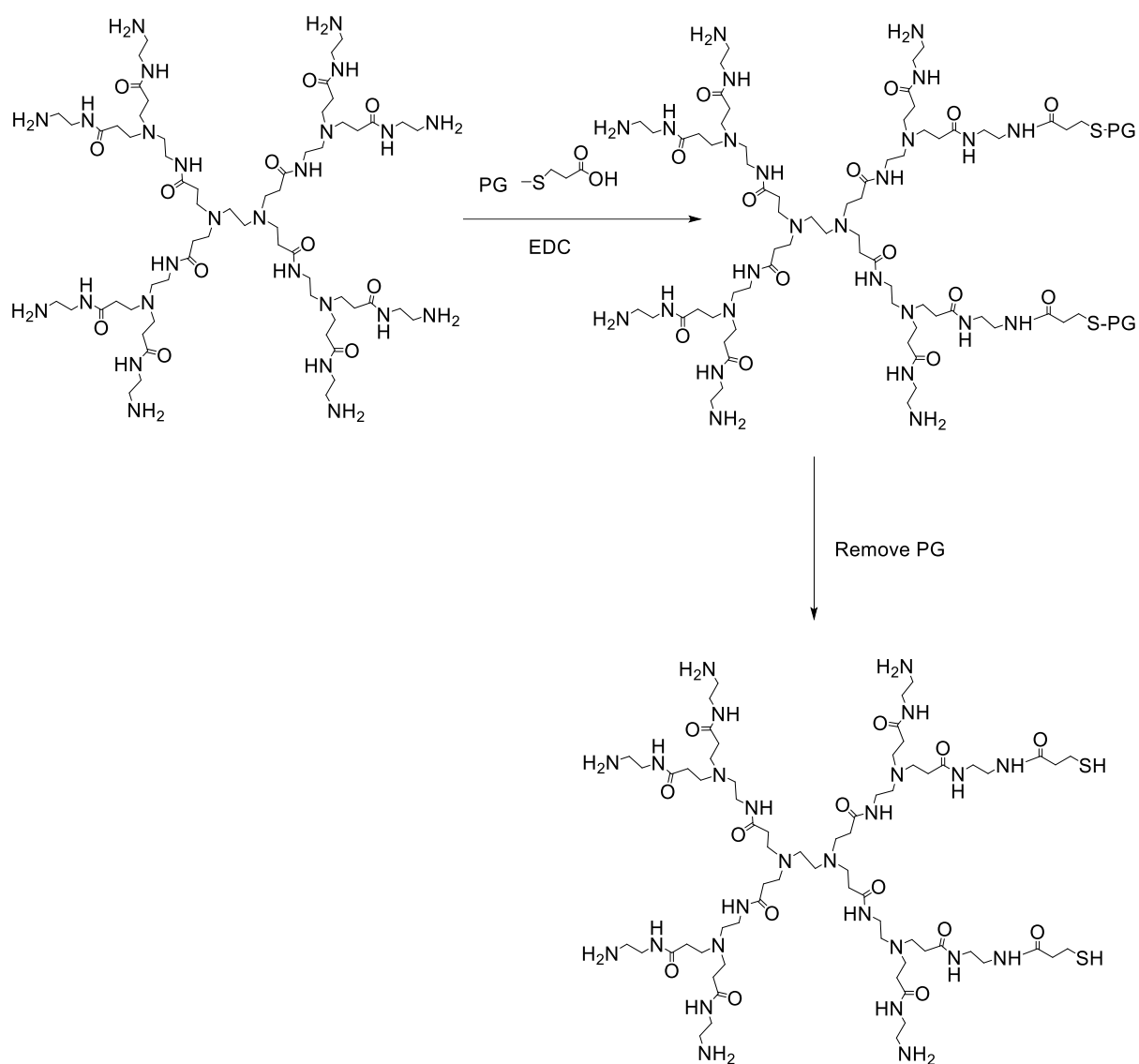
Figure 3.5 Proposed synthesis of thiol-terminated dendrimers by adding a protected thiol to an amine-ended dendrimer via an amide linkage - PG = protecting group

Prior to working with the dendrimers, we decided that it would be prudent to develop the methodology using a model compound. Specifically, a compound that represents the terminal functionality of a single dendritic arm. A mono-acetylated ethylene diamine was able to fulfil this aim, as it contains the amine-ended functionality of the dendrimer as well as a methyl amide that stimulates the amide connectivity to the dendrimer.[25] The synthesis is shown in Scheme 3.6 and involved the synthesis of a protected thiol and its addition to acetyl ethylene diamine, followed by deprotection.[24]

Figure 3.6 Proposed synthesis of model thiol dendrimers involved the synthesis of a protected thiol and its addition to acetyl ethylene diamine, followed by deprotection.

3.5.1 The synthesis of 3-trityl sulfanyl propanoic acid: The first step in the synthesis necessitates the generation of a pr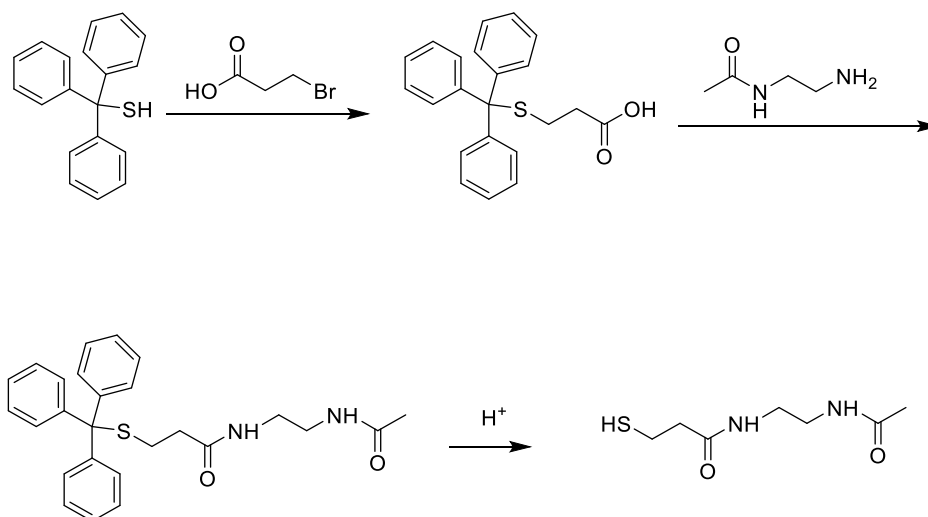otected thiol acid that could react with the amine of acetyl-ethylenediamine. Various protecting groups were considered, but the trityl group was selected as it is stable to neutral and basic conditions. but very sensitive to acid.[24] As such, it can be easily removed from a dendrimer. 3-trityl sulfanyl propanoic acid was synthesised by adding trithylthiol to the 3-bromopropionic acid and stirred in THF at 23 °C. Following the completion of the reaction, the resultant mixture was subjected to extraction using DCM (dichloromethane) to separate and isolate the product. The organic layer was subjected to brine washing to eliminate any remaining acid or base. Next, the organic layer was dried using magnesium sulphate to remove the water, and the solvent was evaporated using a rotary evaporator. This process yielded a crude product. To obtain a purified product, column chromatography was employed, resulting in a yield of 1.3 g (50%) of the protected thiol. The appearance of the product can vary from a white to a pale-yellow solid.
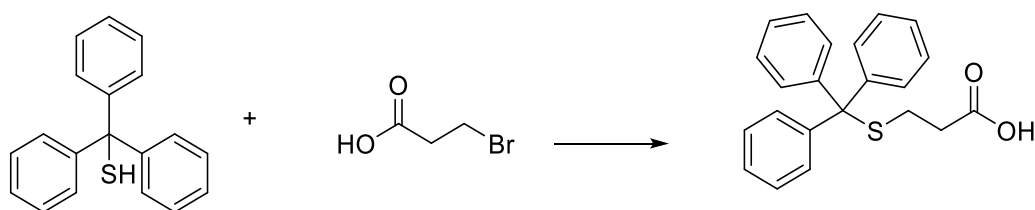
Figure 3.7 Synthesis of 3-trityl sulfanyl propanoic acid
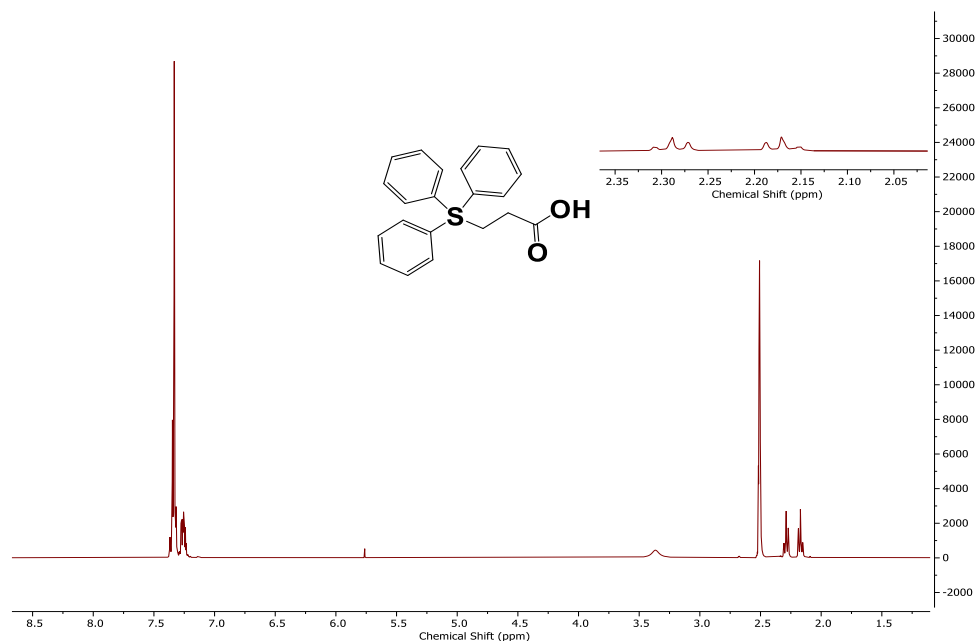
Figure 3.8. ^{1}NMR of 3-trityl sulfanyl propanoic acid shows a peak at 2.14 ppm (2H, t, CH$_2$) and a multiple between 7.12-7.24 ppm (15H, m, PH-H)

Initial characterisation of 3-trityl sulfanyl propanoic acid was carried out ^{1}H and ^{13C} NMR. For the ^{1}H NMR, a peak at 2.14 ppm (2H, t, CH$_2$) was observed and assigned to the two hydrogens on the methylene group. A second triplet, corresponding to the second methylene, was observed at 2.39 ppm. Finally, a multiplet between 7.12-7.24 ppm (15H, m, PH-H) could be observed, and this corresponds to the 15 protons of the three phenyl groups. The infrared spectrum revealed a broad peak at 3320–3480 cm^{-1} corresponding to the O-H stretching of the carboxylic acid group, a peak at 2900–3000 cm^{-1} corresponding to the C-H stretching of the aliphatic chain, and a peak in 1700–1750 cm^{-1} corresponding to the C=O stretch of the carboxylic acid group.

Figure 3.9 IR of 3-trityl sulfanyl propanoic acid showing the O-H AND C-H and C=O groups

The molecular ion peak appears at a mass-to-charge ratio of 348 (MH$^+$). The peak was observed at 275 (MH$^+$). which is corresponding to the starting material.

Figure 3.10 Synthesis of N-(2-Acetamidomethyl)-3-(Triphenyl 4-Sulfanyl)

The synthesis of N-(2-Acetamidomethyl)-3-(Triphenyl 4-Sulfanyl) Propanamide was initially attempted. 3-Tritylthio propionic acid was reacted with N-(2-Aminoethyl) Acet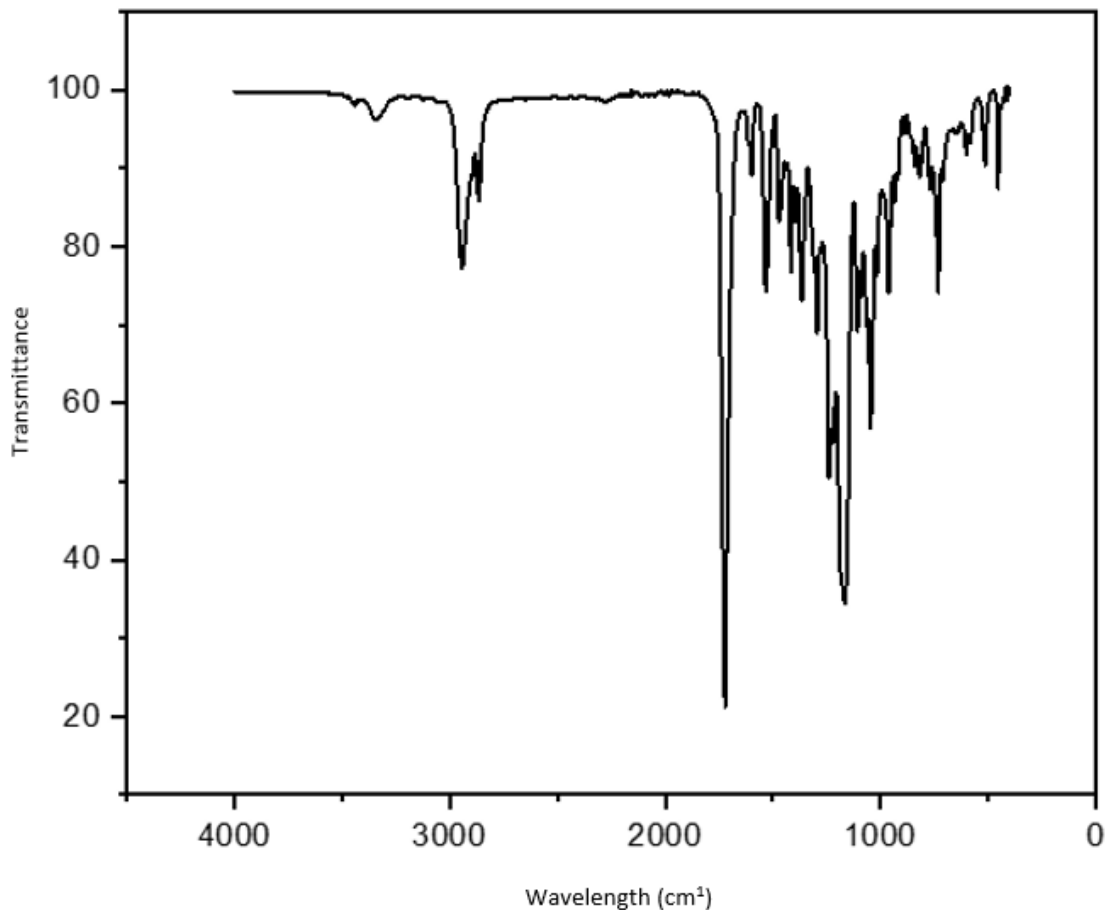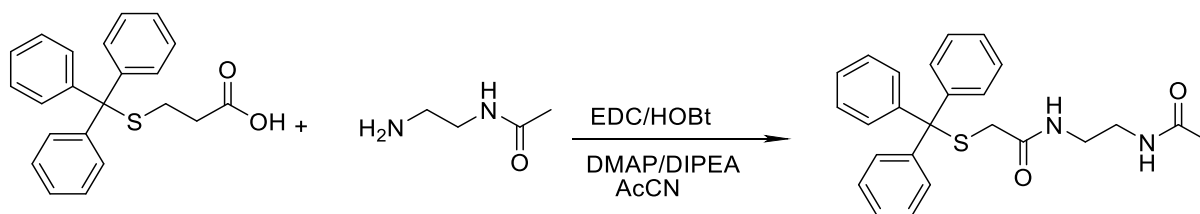amide in acetonitrile and EDC (as a coupling agent). After the completion of a chemical reaction, the reaction mixture is typically quenched or treated to prevent further chemical reactions. This is usually achieved by adding a suitable quenching agent, followed by concentrating the reaction mixture to remove any excess reagents or solvents. The concentration step can be performed using a rotary evaporator under reduced pressure." The ^{1}HNMR spectrum of the product peaks at 1.4 ppm and 3.1 ppm which are not related to the target compound. However, we were able to observe an aromatic peak corresponding to 15 hydrogens and two peaks that integrated as 4 and 2 for the NCH_2 and SCH_2 respectively. The product's mass spectrum demonstrated an m/z+ of 348, indicating that we had simply recovered our starting material. The IR spectrum showed broad peaks around 3250-3480 cm^{-1}, corresponding to the stretching of the O-H group stretching and carboxylic acid groups. Additionally, a peak was observed around 2955-3000 cm^{-1}, corresponding to the C-H stretch of the aliphatic chain.

The expected product was thus not obtained. However, there could be three reasons for the failed reaction. These could be: (i) Firstly, reaction may not have completed, resulting in a mixture of starting material and product; (ii) side reactions may have occurred, which would have interfered with the desired reaction, such as hydrolysis or elimination reactions. And (iii) finally, the starting materials or DMAP might have impurities, which affect the outcome of the reaction. Despite the multiple attempts, all previous efforts to obtain a pure product were unsuccessful. In order to address the issue related to side reaction, various reagents were changed numerous times, and repeated reactions were carried out. However, none resulted in the formation of the desired products. To overcome these challenges, a two-step process was devised, incorporating the introduction of an intermediate acyl chloride (scheme 3.11). The procedure involves utilizing oxalyl chloride to generate the acid chloride. Subsequently, this intermediate is directly reacted with the amine of acetyl ethylene diamine without any isolation or purification steps in between.
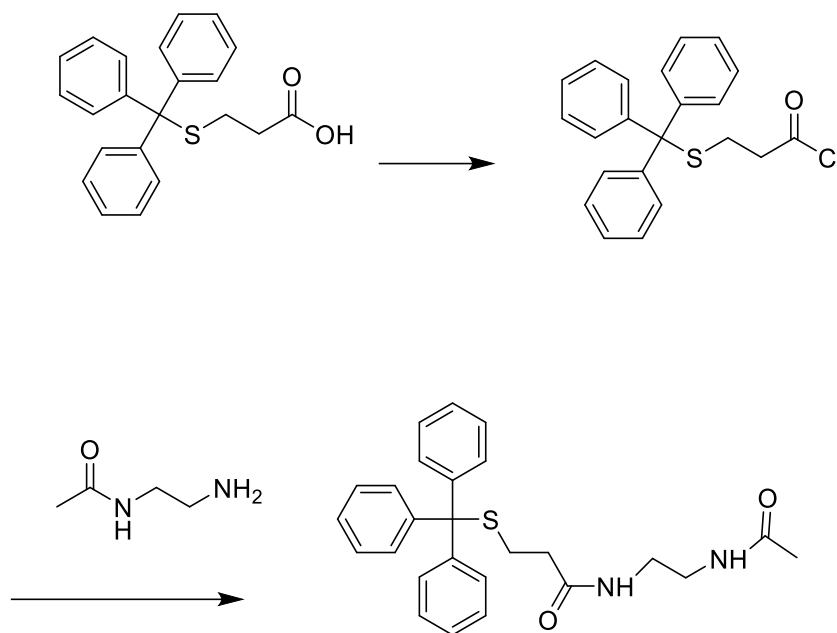
Figure 3.11 The proposed two-step process to synthesise model thiol.

3.5.2 Synthesis of N-(2-acetamidoethyl)-3-(triphenyl 4-sulfanyl) propanamide by using oxalyl chloride

Oxalyl chloride is commonly utilised in organic synthesis, with N, N-dimethylformamide serving as a catalyst to create acyl chlorides from carboxylic acids. Similar to thionyl chloride, this reagent breaks down into volatile by-products during the reaction, simplifying the workup process. The synthesis of 3-(tritylthio) propanoyl chloride was carried out through a stepwise process. First, tetrahydrofuran (THF) was mixed with a solution of 3-(tritylthio) propanoic acid at room temperature. After adding oxalyl chloride to the solution, N, N-dimethylformamide (DMF) was introduced as a catalyst. The mixture was stirred to create the reaction to ensure complete mixing and proper reaction conditions After a reaction time of 17 hours, a solution of acetyl ethylene diamine was added to the flask. The reaction mixture was maintained at a temperature of 23°C for a duration of 24 hours. The spectra of the crude product only demonstrated peaks for the starting material. This could be due to errors in the synthetic approach, and/or instability of the intermediate acid chloride was the main reason for the difficulty in obtaining the product. At this point, we were out of time and forced to stop. If additional time was available, we could

repeat the reaction and quenched with the amine. This would avoid any problems due to the hydrolysis of the intermediate acid chloride. Alternatively, we could try one of the many amides coupling methods.

3.6 Conclusion

The synthesis of 3-trityl sulfanyl propanoic acid was successfully achieved. This was made possible through combining trithylthiol with 3-bromopropionic acid in THF (tetrahydrofuran) at room temperature. A range of spectroscopic methods were adopted for the purpose of characterising the synthesized compound. Specifically, the methods that were adopted were ^{1}HNMR and ^{13}CNMR, which is a nuclear magnetic resonance spectroscopy as well as IR spectroscopy. The spectroscopic analysis confirmed the presence of CH_2 and phenyl groups within the molecular structure of the synthesized compound.

We have attempted to synthesize N-(2-acetamidomethyl)-3-(triphenyl 4-sulfanyl) propenamide. During the early stages of the experiment, we were adopting a one-step approach. This was done by employing EDC (ethyl(dimethylaminopropyl) carbodiimide) as the coupling agent. However, this method has resulted in unexpected and formidable challenges during our experiments. After the completion of the attempt, we were not able to yield the desired product in a pure form. This does not stop us from repeating our endeavours to yield the desired product in order to ensure the experiment was carried out accordingly without any unknown missteps or anomalous occurrences that may be unknown to us. Unfortunately, the subsequent attempts have also failed. Not only we were unable to achieve the desired purity, but we were also unable to yield the product in itself. The resulting product does not meet the necessary level of purity.

Due to the aforementioned failed attempts and with the challenges still present, we have changed our strategy. The new strategy was a two-step procedure. It started with the synthesis of an acid chloride intermediate. Subsequently, a reaction was made to occur between the acid chloride and the corresponding amine. Unfortunately, this approach has also failed to yield the desired results. We simply failed to isolate the target product. We have made further attempts using the same approach to ensure we did not make any unforeseen mistakes, missteps, anomalous reactions or any other unknown issues to try to achieve the desired product. Despite the efforts and the numerous attempts, they all were subsequently failed to yield the desired product.

The efforts being poured into synthesising this compound have been extensive. It is now proven that there are vast challenges that need to be addressed. Furthermore, it is possible that we may have underestimated the complexity of organic synthesis. This means that further studies will be needed to extensively and methodically explore the issues surrounding the failures. Therefore, future research is recommended for the purpose of continuously explore and innovate the approach in order to successfully yield not only the desired product, but also at the desired level of purity. We also recommend that sufficient time allocation may be needed and also to examine our attempts in detail to not only validate our attempts, but also not to underestimate the complexity of this task.

3.7 References

1- P. Frei, R. Hevey, B. Ernst, *Chem. Eur. J*., 2019, 25, 60–73.

2- S. Otto, R. L. Furlan, J. K. Sanders, *Curr. Opin. Chem. Biol.*, 2002, 6, 321–327.

3- B. Le Droumaguet, K. Velonia, *Macromol. Rapid Commun*., 2008, 29, 1073–1089.

4- R. Huang, I. K. Leung, *Molecules*, 2016, 21, 910.

5- J. Xu, S. Zhao, S. Zhang, J. Pei, Y. Li, Y. Zhang, L. Hu, et al., *Int. J. Biol. Macromol*., 2020, 150, 1184–1191

6- S. Y. Yang, *Drug Discovery Today*, 2010, 15, 444–450.

7- M. Mondal, A. K. Hirsch, *Chem. Soc. Rev*., 2015, 44, 2455–2488.

8- R. A. Hunt, S. Otto, *Chem. Commun*., 2011, 47, 847–858.

9- O. Astrom, J. M. Lehn, Nat. Rev. *Drug Discov*., 2002, 1, 26–36.

10- J. Li, P. Nowak, S. Otto, J. Am. *Chem. Soc.,* 2013, 135, 9222–9239.

11- D. A. Tomalia, H. Baker, J. Dewald, M. Hall, G. Kallos, S. Martin, P. Smith, *Macromolecules*, 1986, 19, 2466–2468.

12- S. Svenson, D. A. Tomalia, Adv. *Drug Deliv. Rev*., 2012, 64, 102-115.

13- P. J. Bracher, P. W. Snyder, B. R. Bohall, G. M. Whitesides, *Origins of Life and Evolution of Biospheres*, 2011, 41, 399-412.

14- C. Hobril, K. Charoen, E. K. Rodriguez, A. Nazarian, M. W. Grinstaff, Angew. *Chem. Int. Ed*., 2013, 52, 14070-14074.

15- Y. Folikumah, M. Behl, A. Lendlein, *Biomacromolecules*, 2021, 22(5), 1875- 1884.

16- A. K. Hubbell, G. W. Coates, J. *Org. Chem.,* 2020, 85(21), 13391-13414.

17- S. Zhao, Y. Wu, L. Hu, *Bioorg. Chem*., 2022, 119, 105520.

18- J. M. Rae, B. Jachimska, *Nanoscale*, 2021, 13(4), 2703-2713.

19- K. C. Honselmann, C. Antoine, L. Frohneberg, S. Deichmann, L. Bolm, R. Braun, D. Bausch, *Langenbeck's Arch. Surg.,* 2021, 406(7), 2343-2355.

20- P. Wijesinghe, H. W. M. Steinbusch, S. K. Shankar, T. C. Yasha, K. R. D. De Silva, J. *Chem. Neuroanat*., 2020, 106, 101772.

21- A. K. Hubbell, G. W. Coates, J. *Org. Chem*., 2020, 85, 13391-13414.

22- X. Sun, M. Chwatko, D. H. Lee, J. L. Bachman, J. F. Reuther, N. A. Lynd, E. V. Anslyn, J. Am. *Chem. Soc*., 2020, 142, 3913-3922.

23- J. E. Moses, A. D. Moorhouse, *Chem. Soc. Rev*., 2007, 36, 1249-1262.

24- R. J. Smith, C. Gorman, S. Menegatti, J. Polym. Sci., 2021, 59(1), 10-28.

25- Z. Z. Nori, A. Landarani-Isfahani, M. Bahadori, M. Moghadam, V. Mirkhani, S, *RSC Adv*., 2020, 10(55), 33137-33147.

26- V. Chechik, R. M. Crooks, *Langmuir*, 1999, 15(19), 6364-6369.

27- H. J. Johnston, A. N. Hulme, *Synlett,* 2013, 24(05), 591-594.

28- H. J. Johnston, A. N. Hulme, *Synlett*, 2013, 24(5), 591-594.

29-F. Chiba, G. Mann, L. J. Twyman, *Org. Biomol. Chem*., 2010, 8(22), 5056-5058.

30-J. Hu, K. Hu, Y. Cheng, *Acta Biomater*., 2016, 35, 1-11.

Chapter 4

A comparison between PAMAM dendrimers and HPAMAM for drug delivery

4.1 The need for drug delivery

All drug molecules are poisons. As such, and to avoid killing the patient, they must be given at a dosage below any toxic level. Often this is very low, the specific quantity of a medication or substance will depend on various factors, including the drug's potency, the patient's weight, age, and overall health, and the desired therapeutic effect. This need to balance a therapeutic effect with severe side effects (due to toxic levels of drug) can be made worse by the drugs poor bioavailability after administration.[1] The bioavailability can be perturbed by several factors. These include a poor solubility in the body's aqueous environment, a fast degradation as the drug moves around the body and rapid excretion.[2] In addition, most drugs are not exclusively taken up at the site of action and end up being administered to the entire body.[3] As a result, some excellent lead compounds fail to make it to market, as they would require very high dosages to elicit a beneficial therapeutic effect.[4] All these problems related to poor bioavailability can be resolved if a suitable drug delivery system (DDS) is used.[5]

A drug delivery system (DDS) refers to a formulation or device that regulates the release of drugs in terms of rate, timing, and location to ensure effective and safe delivery of therapeutic substances in the body.[6] This process involves administering a medicinal agent, releasing its active compounds, and transporting them across biological membranes to the desired target site. Among the various methods of drug administration, oral administration is the most common and convenient approach. It is easily administered, well-received by patients, cost-effective, and has less stringent sterility requirements as the presence of such impurities may further affect the overall bioavailability, reducing the amount of the active compound available for therapeutic purposes. Therefore, understanding and addressing these factors is essential for optimizing drug efficacy and patient outcomes.[7] Furthermore, oral dosage forms can be manufactured using diverse techniques, making them particularly appealing for generic drug manufacturers.[8] However, for drugs with poor water solubility, the required oral dosage to attain therapeutic blood levels can vary significantly based on the specific drug and its properties. In general, these drugs may require doses that are notably higher than those with good water solubility. However,

the exact range of required doses can vary widely and depends on factors such as the drug's pharmacokinetics, intended therapeutic effect, and individual patient characteristics. Dosing can range from two to ten times or more compared to drugs with high water solubility, making it essential to determine optimal dosing through careful testing and clinical evaluation. For most other routes of administration, medicinal liquids must be formulated with water as the solvent. Most pharmaceuticals are organic molecules and have low aqueous solubility, resulting in poor absorption and bioavailability.[9] To enhance a medication's solubility and protect against degradation, several methods are employed. These methods include physical modifications like thermal techniques and pH adjustments, chemical alterations such as prodrug formation and salt formation, and environmental protection against oxidation, light, and moisture. Additional methods involve lipid-based formulations, co-solvents, and polymer nanoparticles. The choice of method depends on the drug's properties and intended therapeutic use, with regulatory and safety considerations guiding the selection.[10] The dispersion of drugs within carriers can be achieved through different methods, including the use of eutectic mixtures, solid dispersions, solid solutions, and cryogenic techniques. enables enhanced drug delivery. Modifying the crystal structure of drugs, employing methods like polymorphs, amorphous forms, and co-crystallization, plays a pivotal role in enhancing their properties and effectiveness. These structural alterations influence the solubility of the drug and can be particularly significant when choosing between tablet and capsule formulations. Tablets and capsules may benefit differently from specific crystal structures, with the goal of optimizing drug performance, solubility, and overall therapeutic outcomes.[11]

When addressing the actions and side effects of a medicine, pharmacokinetics (PK) and pharmacodynamics (PD) are the two most important factors to examine. PD provides information about drug dose, delivery route, and frequency. PD allows us to increase the likelihood of successful treatment while reducing the risk of negative side effects. Pharmacokinetics plays a crucial role in determining the journey of a drug within the body, starting from its administration, and continuing until its elimination.[12] The process of transporting a drug to the intended location of action and releasing it there via either local (environmental) or peripheral control mechanisms is referred to as targeted drug delivery,

and Failure to achieve targeted drug delivery can result in reduced drug efficacy, systemic side effects, resource wastage, patient discomfort, and increased healthcare costs. Precise drug delivery is essential to optimize treatment outcomes, minimize side effects, conserve resources, and enhance patient well-being, playing a key role in advancing precision medicine. For targeting, drugs are often covalently or noncovalently joined to a targeting moiety, and then either passively or actively guided to the target area.[13] This is most often achieved by nanotechnology-based systems that can mediate targeted drug delivery. Aqueous soluble nano molecules can also facilitate the absorption of poorly soluble medicines via encapsulation,[14] as demonstrated by targeted delivery of several medications, including anti-HIV medicines and anti-cancer medicines (including doxorubicin, paclitaxel, and 5-fluorouracil).[15] One particularly useful property of nano molecules is towards the delivery of anticancer medications, where site specific delivery can be achieved simply by virtue of the nano molecules' large size. Simple targeting such as this means that significantly lower dosages of particularly toxic drugs can be achieved. This limits unpleasant side effects and can improve therapeutic outcomes. Nanocarriers have also been studied for their ability to carry DNA molecules for application to various gene therapies. In these examples, the nanocarrier can envelop the DNA in a pocket of water and protect it from degradation, significantly improving its half-life in the circulatory system and therefore dramatically improving bioavailability.[16]

The enhanced permeability and retention (EPR) effect was initially observed by Maeda and colleagues in hard mouse tumors.[17] They administered polymer-drug conjugates intravenously and achieved 10-to-100-fold higher concentrations compared to free drug administration. The first EPR-based drug to reach the clinic was DOXIL, a PEGylated liposomal drug, which was approved approximately 30 years ago.[18] Nanocarriers have a propensity to accumulate in tumors via passive targeting owing to the presence of leaky blood vessels and impaired lymphatic drainage in solid tumors.[19] The EPR effect allows for the permeability and retention of macromolecules in the tumour microenvironment by up to 70-fold. The tumor vasculature is characterized by leakiness, irregular diameter, shape, and density, resulting in heterogeneous perfusion, elevated interstitial fluid pressure, hypoxia, and an acidic environment. The

effectiveness of EPR-based drug delivery is influenced by several factors, including circulation time, targeting ability, and the capability to overcome barriers. Particle size, shape, and surface properties are crucial considerations. Research indicates that nanoparticle sizes ranging from approximately 40 to 400 nm are optimal for prolonged circulation and enhanced tumor accumulation while minimizing renal clearance.[20] Rigid, spherical particles in the size range of 50 to 200 nm are generally preferred to avoid liver and spleen uptake while remaining large enough to evade kidney clearance.[21] Surface properties also impact the internalization process, and surface modification techniques like PEGylation can prevent subsequent clearance by the reticuloendothelial system (RES). Therefore, the modulation of nanoparticle size, shape, and surface properties can significantly impact EPR-based drug delivery.[22] Several nanomaterials that have been utilised in the field of drug delivery are shown in Figure 4.1. For this study, we plan to investigate a class of branched and globular nanomaterials known as "dendritic macromolecules".[23] Specifically, we will compare and investigate dendrimers, which are perfectly branched monodispersed systems, with a polydisperse and imperfectly branched hyperbranched polymer. The structure and properties of these molecules will be discussed in the next section.
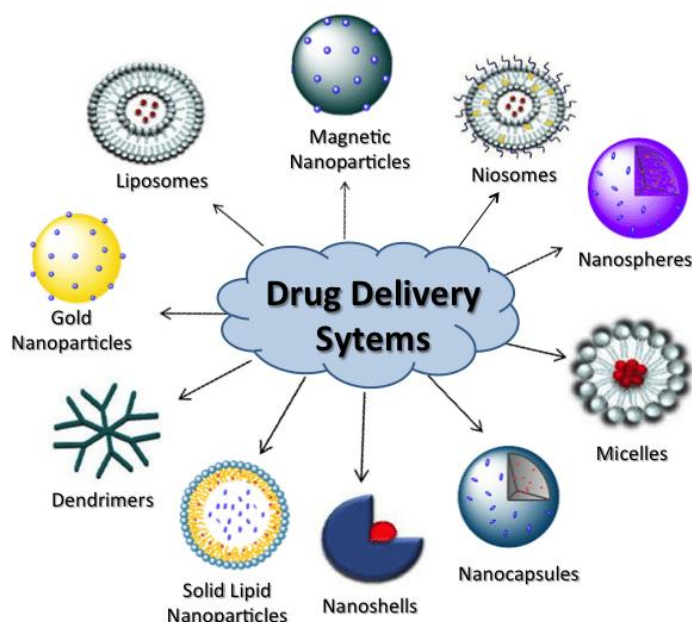

Figure 4.1 The examples of polymeric, lipid, and inorganic nanocarriers. Reprinted with permission from Conniot, J, Silva, J. M. 2014, 2,105

4.2 Nanoparticles in pharmaceutical formulations and their properties:

Before determining the optimal composition of a nanoparticle-based medication delivery system, it is necessary to comprehend how the body processes foreign particles. Three main entry points for nanoparticles into the human body are oral ingestion, direct injection, and inhalation.[24] The lymphatic system can disseminate and remove the particles further after absorption from the blood capillaries. The ability to disseminate particle size explains the capability of nanoparticles to cross the blood-brain barrier (BBB).[25] This is crucial since it allows for prolonged drug delivery for previously difficult-to-treat disorders. Certainly, the capacity to control drug distribution and reach new targets through methods like reducing particle size is indeed a driving force behind research on dendrimers, especially at a fundamental level. As particles become smaller, their surface area-to-volume ratio increases, enabling drugs encapsulated within dendrimers to be positioned closer to the particle's surface. This feature offers the potential for more precise drug delivery and enhanced therapeutic outcomes, which motivates fundamental research in the field of dendrimers and nanoscale drug delivery systems. Size' effects on the efficacy of nanoparticle-based medication formulations have been established; however, surface features can also be manipulated to create the optimal system.[26]

Size effects on the efficacy of nanoparticle-based medication formulations have been established; however, surface features can also be manipulated to create the optimal system.[27] To construct an optimal nanoparticle drug delivery system, it is essential to incorporate appropriate targeting ligands, control surface curvature, and manage reactivity in order to prevent aggregation, maintain stability, and ensure receptor binding for desired pharmacological effects.[28] Clearing the nano system is a crucial consideration since nanoparticles can be recognized by the lymphatic system, triggering the body's natural immune response to foreign substances. The hydrophobicity of nanoparticles influences their likelihood of elimination as they have a stronger affinity for binding to blood components.[23] Consequently, modifying the surface of hydrophobic nanoparticles to be hydrophilic can prolong their circulation time by reducing their tendency for rapid removal from circulation.[29]

4.2.1 Dendrimers in drug delivery

To improve therapeutic outcomes, dendrimers have developed as unique and effective materials that can be used as therapeutic agents or medications or as carriers for the transport of drugs. To use them and reach their full potential, molecular dendrimer interactions are essential. Enhancing the performance of dendrimers depends on their molecular interactions with pharmaceuticals or other substances in drug delivery systems or drug conjugates. A thorough review of the literature on dendrimer interactions with various materials revealed that both atomistic and mesoscale considerations of its interactions with medicines and polymers have been made.[30]

4.2.2 Dendrimers as promising carriers in the field of drug delivery

In addition to the qualities, dendrimers possess the following dendritic characteristics that make them appropriate for drug delivery: properties such as water solubility, encapsulation, and biological membrane permeability, a lot of peripheral function groups and being able to do more than one thing.[31] Numerous studies have employed dendrimers as carriers in various applications about cancer treatment. For example, drugs for photodynamic therapy and anticancer drugs have been tested on them. To deliver drugs, poly(amidoamines), poly(esters), poly(ethers), and poly(amide)-containing amphiphilic dendrimers with different interiors have been used. These large molecules can take drugs that don't dissolve in water.[32] Dendrimers have been called both "static covalent micelles" and "unimolecular micelles." There are two ways that dendrimers and drugs that don't like water can work together:

 (A) Drugs and dendrimers interact non-covalently (Host-Guest) by surface interactions or encapsulation (through hydrophobic interactions, physical entrapment, or hydrogen bonding) (electrostatic interactions).[33]

(B) The drug can be covalently linked to a dendrimer using spacers or cleavable linkages. For instance, cisplatin was conjugated to a sodium carboxyl-terminated PAMAM dendrimer called G-3.5, which enhanced its tumor-targeting capability compared to free cisplatin. This approach utilized passive

targeting in vivo. Both non-covalent and covalent systems can leverage the enhanced permeability and retention (EPR) effect.[34] The growth of nanomedicine to treat many ailments has made dendrimers an essential class of nanostructured carriers. Due to their precisely controllable size, low polydispersity, and multiple surface functionalities, dendrimers are particularly well-suited candidates for the delivery of antitumor drugs. They also have the potential to deliver drugs and optimise drug properties like pharmacokinetics in a manner like typical colloidal or macromolecular delivery systems.[34] Studies have shown that the cytotoxicity of dendrimers is influenced by their generation and surface composition, particularly the terminal functional groups. The cytotoxicity of cationic amine dendrimers, such as poly(amidoamine) (PAMAM) and poly (propylene imine) (PPI), has been well-documented. is inversely correlated with their concentration and production, according to studies. Because main amine terminal zones are present. Due to their structural uniqueness, dendrimers become ideal partners for active medicinal substances and permit the following:

(a) incorporation inside the cavity, (b) Binding of pharmacological molecules or biologically active substances to the functional groups around the dendrimer, and (c) offering encapsulation (Figure). The interaction between drugs and dendrimers.[33]

(a)   (b)   (c)
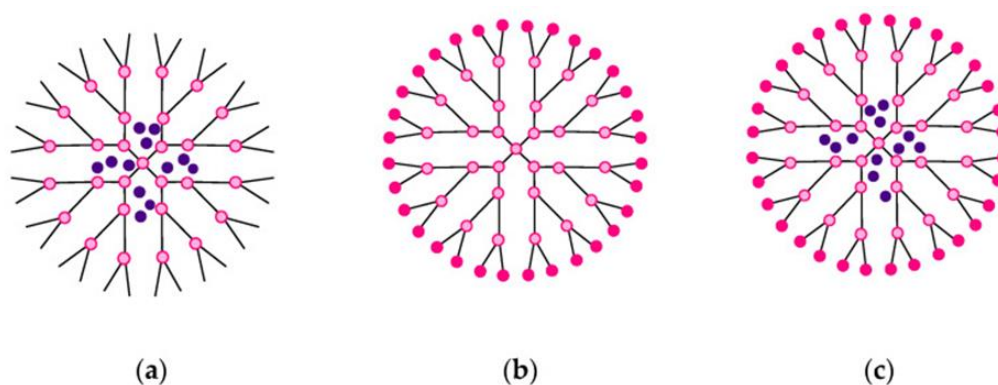
Figure 4.2 The schematic representation illustrates three methods of complexing or conjugating drug molecules with a dendrimer: (a) peripheral attachment, (b) encapsulation within internal cavities, and (c) simultaneous encapsulation within internal cavities and peripheral attachment. Reprinted with permission from Janaszewska, A., Lazniewska, J., Trzepiński, P., Marcinkowska, M., Klajnert-Maculewicz, B., Biomolecules, 2019, 9, 330–331.

Dendrimers serve as beneficial ligands for delivering drug molecules to tumor tissues through different biological compartments, thereby maximizing their pharmacodynamic activity at the target site. This advantageous carrier capacity of dendrimers makes them a significant approach in cancer therapy. The release of drugs from dendrimer complexes is regulated by mechanisms such as degradable spacers and controlled variations of terminal groups. Dendrimers exhibit unique properties, such as high hydro solubility, which are associated with their specific surface structure and functionalities. These characteristics enable the encapsulation or conjugation of multiple entities, both in the central structure and on the surface, making dendrimers excellent carriers for a variety of anticancer drugs. In the literature, there are numerous examples of drugs that have related to dendrimers. Dendrimers (PAMAM) have frequently been combined with different drugs that are used to treat neoplastic illnesses,

Doxorubicin (DOX), a medication employed in the treatment of lung cancer and brain tumors, has been linked to fifth generation PAMAM dendrimers (G4).[34] This conjugation was achieved by utilizing pH-controlled DOX-PEG-PAMAM dendrimers, forming arylhydrazone bonds on the dendrimer surface. The conjugation of DOX to the dendrimer led to enhanced therapeutic efficacy and increased specificity of action against lung neoplasms. Similarly, Imatinib (IMT), another drug used in lung cancer treatment, can form a complex with PAMAM dendrimers through electrostatic interactions, similar to other hydrophobic acid molecules. The non-polar groups of dendrimer branches can also act as micelles, thereby improving the solubility of the drug.
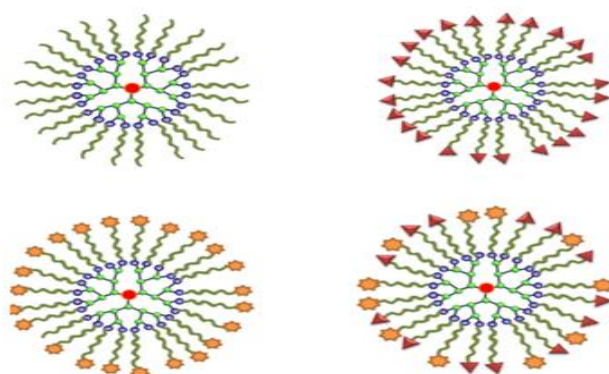
Figure 4.3 The illustration displays various PAMAM dendrimers, including PEGylated PAMAM dendrimers, PEGylated PAMAM dendrimers with attached targeting ligands, PEGylated PAMAM dendrimers with drug conjugation, and PEGylated PAMAM dendrimers with both targeting ligands and drugs.

By conjugating IMT with a PEGylated PAMAM G5 dendrimer, the drug's water solubility was increased, and its ability to target and eliminate cancer cells was enhanced. In the treatment of hypertension, the combination of ramipril and hydrochlorothiazide has proved to be helpful. Using PAMAM dendrimers, these two medicines were combined in two distinct processes. The first phase included the trapping of both medicines independently, and the second step involved the combination of both complexes into a single formulation, resulting in the formation of a hybrid drug–dendrimer complex.[34]
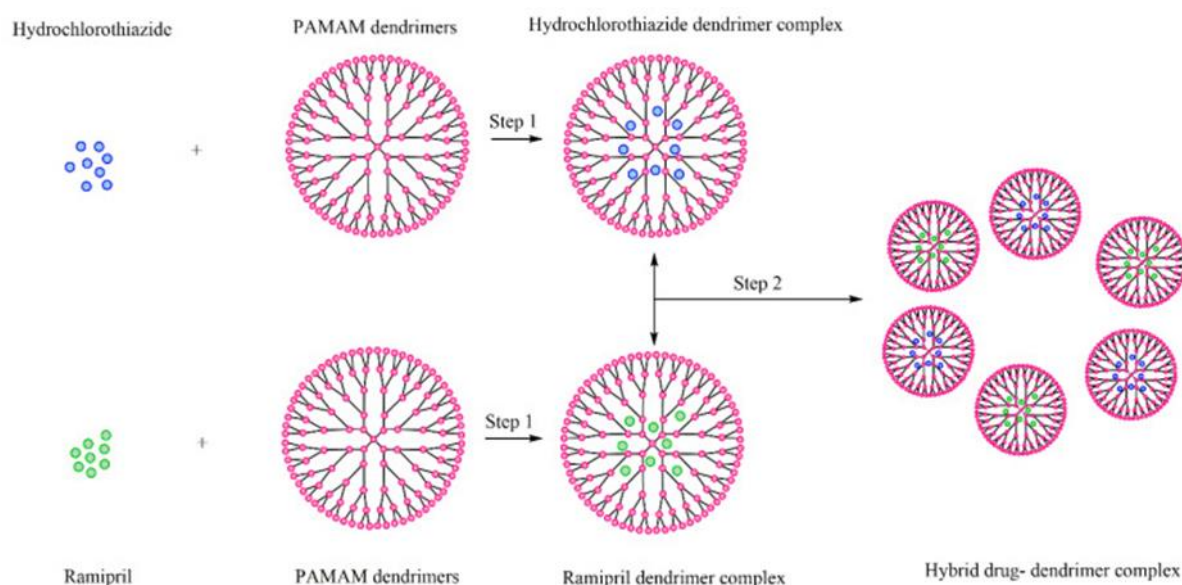

Figure 4.4 The formation of a hybrid drug-dendrimer complex involves a two-step process. Reprinted with permission from Chis, A. A., Dobrea, C., Morgovan, C., Arseniu, A. M., Rus, L. L., Butuca, A., Juncan, A. M., et al. Molecules, 2020, 25, 3982.
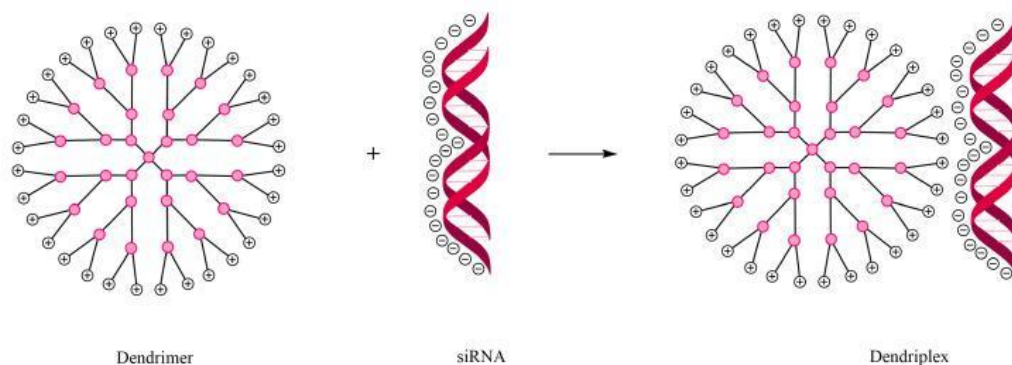
Figure 4.5 The generation of dendriplex, which refers to the complex formed between siRNA (small interfering RNA) and a dendrimer, involves a non-covalent. Reprinted with permission from Chis, A. A., Dobrea, C., Morgovan, C., Arseniu, A. M., Rus, L. L., Butuca, A., Juncan, A. M., et al. Molecules, 2020, 25, 3982.

The formulation of a hybrid complex involving Ramipril and hydrochlorothiazide with dendrimers has the potential to enhance drug loading, solubility, dispersion, and stability, thereby improving the therapeutic applications of these medications. Cationic dendrimers and quaternary ammonium salts, often referred to as quats, share a common mechanism for antibacterial activity. Both exhibit their antimicrobial effects primarily through electrostatic interactions with negatively charged bacteria. Cationic dendrimers, possessing positively charged moieties, interact with the negatively charged bacterial cell membranes, leading to membrane disruption and potential bacterial cell death. Similarly, quaternary ammonium salts, such as quats, leverage their positively charged quaternary ammonium groups to disrupt bacterial cell membranes, destabilizing their structure and contributing to their antibacterial efficacy. These electrostatic interactions are central to the bactericidal properties of both cationic dendrimers and quats. At low concentrations, they have a bacteriostatic effect by slightly altering membrane permeability. At higher concentrations, they disrupt membrane proteins and penetrate the lipid bilayer, resulting in potassium ion leakage and eventual bacterial membrane disintegration, leading to a bactericidal effect. PAMAM dendrimers of higher generations (4 or higher) offer several advantages, including efficient loading of active drug molecules through chemical interactions, enhanced interaction between drug molecules and tertiary amine groups within the

dendritic cavities, increased conjugation capacity due to a higher number of terminal groups, and heightened expectations regarding the efficacy of higher generation PAMAM dendrimers.[36]

4.2.3 Hyper branched polymers (HBPs)

Hyperbranched polymers are polydisperse structures, three dimensional and present a high number of terminal groups and internal spaces. In contrast to dendrimers, their linear branching and dendritic group distribution are random throughout their structure. The core is connected to linear and dendritic units with functional terminal end groups. If these branches join perfectly or if any unit is absent, dendrimers are generated; Consequently, HBPs are analogous to dendrimers in their globular structure, albeit with a more irregular shape. As a result they exhibit comparable physical and chemical characteristics that can be utilised for medication delivery.[38]
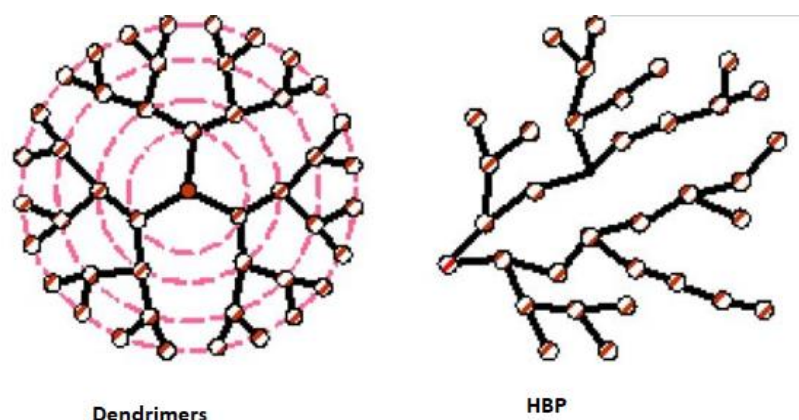
Figure 4.6 A schematic representation of Hyperbranched Polymers (HBPs) and dendrimers reveals their structured architectures. HBPs typically exhibit a highly branched, three-dimensional network, while dendrimers showcase a well-defined, symmetric, and ordered tree-like structure.

4.3.3 HBPs in drug delivery

HBPs have garnered significant attention due to their versatile structure. Scientists have been exploring ways to modify HBPs to enable selective response to various environmental stimuli, including changes in redox potential, pH, enzyme/protein interactions, and temperature. These modifications induce a

conformational change in the HBPs, leading to the release of non-covalently bound drugs. Like dendrimers, the abundance of terminal functional groups in HBPs allows for the formation of covalent drug complexes.[38]

A recent study conducted by Amanda K. Pearce and colleagues examined the impact of HBPs incorporating Doxorubicin on the regression of prostate tumors. The HBPs were modified with glutamate urea targeting ligands, which have an affinity for specific antigens found on prostate cells, thus improving the localization of Doxorubicin within the tumor. Extensive analysis of long-term regression demonstrated a significant reduction in the number of prostate tumors. Moreover, the study confirmed that HBPs loaded with DOX exhibited superior therapeutic efficacy compared to both Doxorubicin alone and a control polymer.[38]

Overall, it is clear that Hyperbranched Polymers (HBPs) share characteristics with dendrimers, making them comparable in certain aspects. However, in our research, our specific aim is to compare these macromolecules like for like as we have not come across similar studies in the existing literature.

4.4 Aims

Despite similarities in architecture, dendrimers and HBPs are fundamentally distinct from one another. The structure of dendrimers is controlled by the stepwise synthesis which generates structures that are well defined and perfectly branched. On the other hand, HBPs are much easier to synthesise and can be obtained in a single synthetic step.[39] However, this leads to molecules that are polydisperse in molecular weight, size, and structure. This leads to structures with random and imperfect branching (possessing both linear and dendritic units within their structures). Despite these differences, the two systems exhibit comparable physical and structural features. As such, the question we want to ask is, "it is worth the cost and effort to develop dendrimer-based systems, if HBPs can be just as effective".[40] There have been several studies that have compared the drug delivery potential of dendrimers' and HBPs' through simple encapsulation and release studies. However, these have not included like-for-like systems. That is, studies have not looked at dendrimers and HBPs that have the same functionality and connectivity. This is essential, as these features are important with respect to encapsulation and release. For example, a dendrimer or HBP connected by internal amides, will bind hydrogen bonding guests significantly stronger than an equivalent dendrimer or HBP connected by simple ether or ester links.[41]

- ⬭ encapsulation of drug in dendrimer via electrostatic and hudrogen bonding
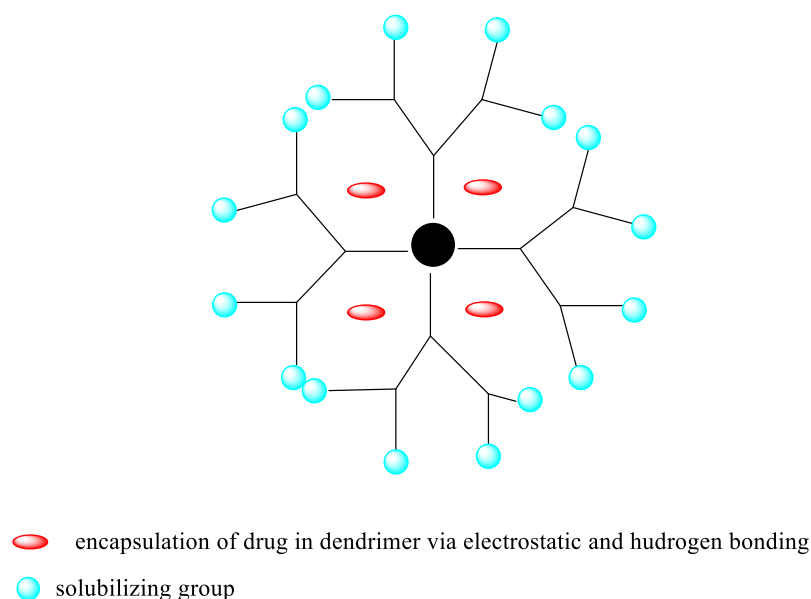- ○ solubilizing group

Figure 4.7 A cartoon illustration of dendrimer being used as a delivery agent.

Therefore, the aim of this part of this thesis will be to synthesise a dendrimer and a HBP that have the same connectivity and to compare their ability to bind and release guest species such as Ibuprofen and porphyrins. The proposed systems (dendrimer and HBP) should include amides and basic amine to encourage H-bonding and ion pairing to guest species (containing reciprocal groups). Once synthesised and characterised, a series of encapsulation experiments will be carried out to determine maximum loading capacities and any loading effects related to concentration of the proposed system. The next section will outline our decision-making process when selecting the dendrimer, HBP and guest species.[42]

4.5 Results and Discussion of Dendrimers and Hyperbranched Dendrimers

Selection of Dendrimers and HBPs for Use as Solubility Enhancers and for Drug Delivery

The aim of this work is to compare drug delivery properties of a dendrimer and HBP with the same functionality and to examine the characteristics of HBPs and dendrimers play a significant role in drug delivery applications as both have excellent solubility. To achieve these aims, we must decide what specific molecules to study. Specifically, we need to select an appropriate dendrimer and HBP a suitable drug for the encapsulation and release studies. For this work we decided to use PAMAM systems for both dendrimers and HBP.[43] As part of our selection process, we also considered the group's previous experience in synthesising and studying PAMAM dendrimers. The polyamidoamine (PAMAM) dendrimers are one of the better-known macromolecules with several existing applications. Internal amine groups and amide a spherical, homogeneous structure characterise dendrimers, which can interact and encapsulate many acidic and hydrogen bonding. Amine-terminated PAMAM dendrimers are water soluble; nonetheless, depending on concentration, they may be protonated and charged and exhibit cytotoxicity and hepatotoxicity in a physiological setting. Ester-terminated PAMAM dendrimers groups are less toxic, but the problem is that they are not soluble in water. However, rapid hydrolysis takes place in the physiological conditions, resulting in the formation of carboxylic acids that aid in solubilization. Nevertheless, these acids carry a negative charge. which may hinder attachment to cells

(which also have a negative charge). To meet the requirements of drug delivery carriers, conversion of terminal groups into neutral polar terminal groups is therefore a necessity.

In this research, a modified approach based on the method initially established by Newkome et al. was +employed to transform ester-terminated PAMAM dendrimers into hydroxyl-terminated PAMAM dendrimers with a neutral charge.[44] A similar process was employed in earlier studies by the Twyman group, and the conversion outcomes were successful. The next step involved a decision about the specific HBP to be used. To compare the HBP and the dendrimers fairly, we needed one with functional groups comparable to those of the dendrimer. HBP should contain internal amines and amide groups that resemble those found in dendrimers. Furthermore, it should be possible to include hydroxyl functional groups on the surface.[45] Thus, we selected the HBP previously synthesised by Twyman et al. as shown in Figure 4.8 Although this HBP contains terminal amine units, these can be converted to hydroxyl groups using the same two steps to convert amine ended PAMAM dendrimers to OH terminated groups. Even considering these extra steps, the proposed HBP appeared easy leading to important internal and external functionality that would enable us to carry out an encapsulation study using like-for-like dendrimers and HBPs.
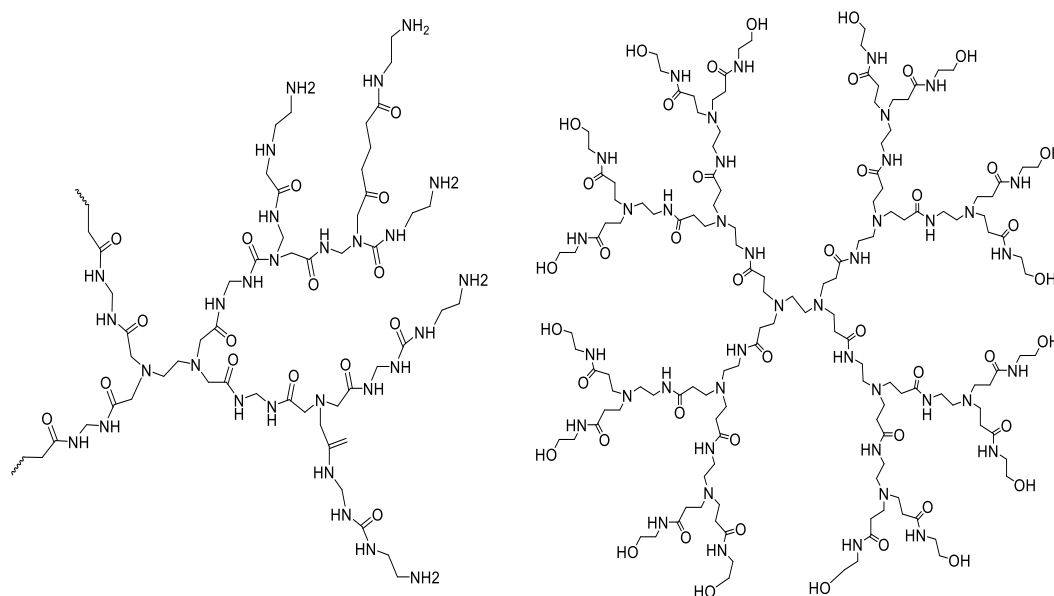

Figure 4.8 Comparison between PAMAM dendrimers and HBPs and both structures containing amine group.

Finally, the drug selected for the encapsulation study was Ibuprofen, a commonly employed non-steroidal anti-inflammatory drug (NSAID), was utilized in drug delivery experiments, was selected as the model drug for encapsulation in our study. The structure of ibuprofen is depicted in Figure 4.9. Ibuprofen is recognized for its limited solubility, typically in the range of approximately 60 mg/L, being nearly insoluble in water., resulting in limited bioavailability. However, its UV activity allows for quantification of its solubility in a solution using UV-Vis spectroscopy, with maximum absorbance observed at 273 nm. Ibuprofen contains a carboxylic acid functional group (-COOH) that can interact with basic amines and amides it can interact through hydrogen bonding. Ibuprofen exists as a chiral molecule with R- and S-enantiomers. The chirality of ibuprofen is crucial in dendrimer-based drug delivery, as the S-enantiomer is primarily responsible for its therapeutic effects, while the R-enantiomer is less active and can lead to side effects. Dendrimer design should prioritize selective encapsulation of the active S-enantiomer to optimize the drug's therapeutic efficacy. Considering chirality is essential for enhancing dendrimer-based drug delivery systems for chiral drugs like ibuprofen.
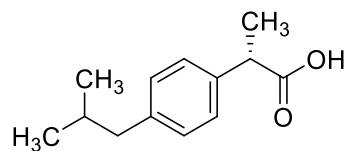
Figure 4.9 The Structure of Ibuprofen

4.5.1 Synthesis and Characterization of Neutral PAMAM Dendrimers

As mentioned earlier, PAMAM dendrimers possess a precisely branched structure and are categorized as monodisperse macromolecules. Based on existing literature, they can effectively enclose small organic and hydrophobic compounds either within their hydrophobic core or on their surface, creating an interaction between the dendrimers and the drugs. In addition, the internal functionality can be used to interact with specific functionality on the drug molecules, leading to cooperativity and improved encapsulation. PAMAM dendrimers have either an amine or ester (which can easily be converted to carboxylic acid) terminal groups. These polar groups give the dendrimer

its solubility in water. However, these groups are charging, which is not ideal for drug delivery.[45] The synthesis of PAMAM dendrimers started with the G0.5 dendrimer (1), which was obtained by combining ethylene diamine (EDA) with methyl acrylate at ambient temperature. This reaction involved the nucleophilic conjugate addition of the amine group in ethylene diamine to the α-β unsaturated carbonyl group in methyl acrylate, as shown in Figure 4.10. (EDA). EDA is composed of two amine groups, each with two hydrogens. As a result, EDA can form the G 0.5 dendrimer by reacting with four molecules of methyl acrylate (1). To guarantee full nucleophilic addition, a small excess of methyl acrylate was employed. The excess solvent and methyl acrylate were removed using a rotary evaporator.
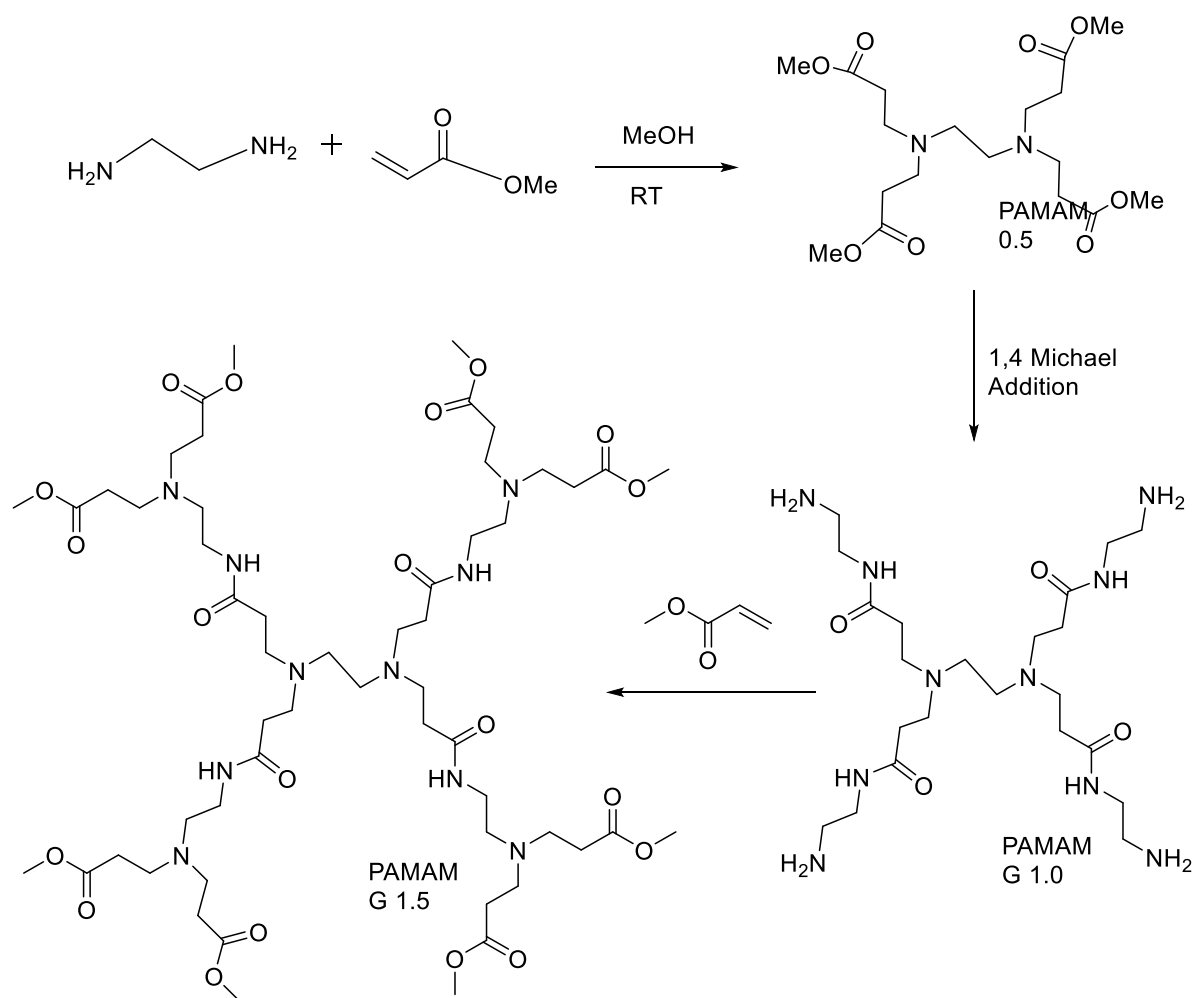
Figure 4.10. Route of the half and full generation of PAMAMs
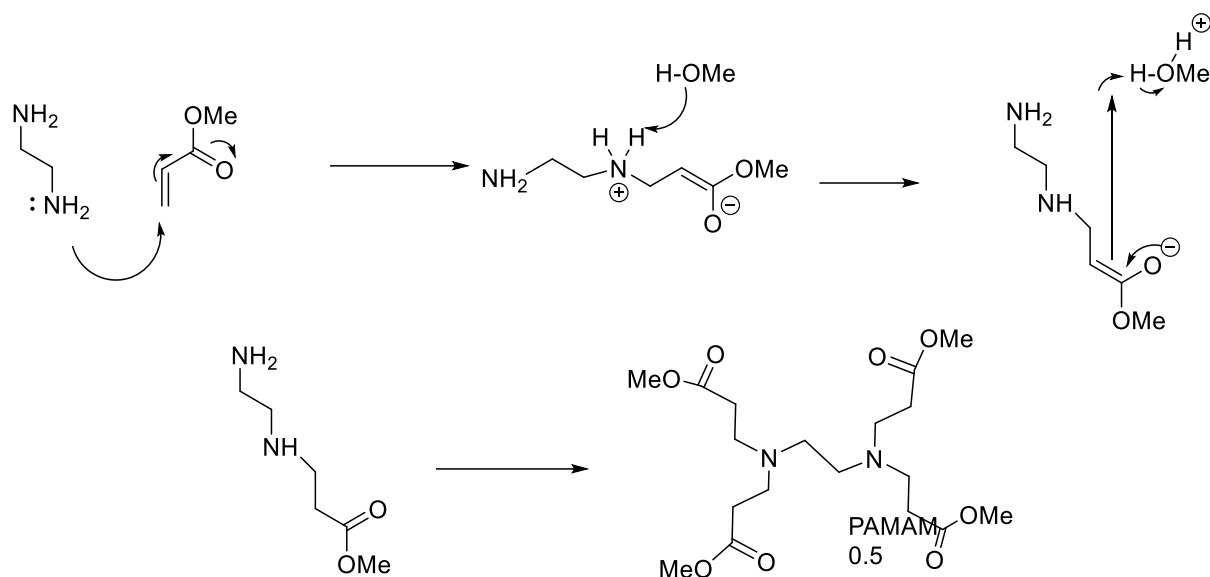
Figure 4.11 Mechanism for the synthesise half-generation dendrimers (ester terminated PAMAM)
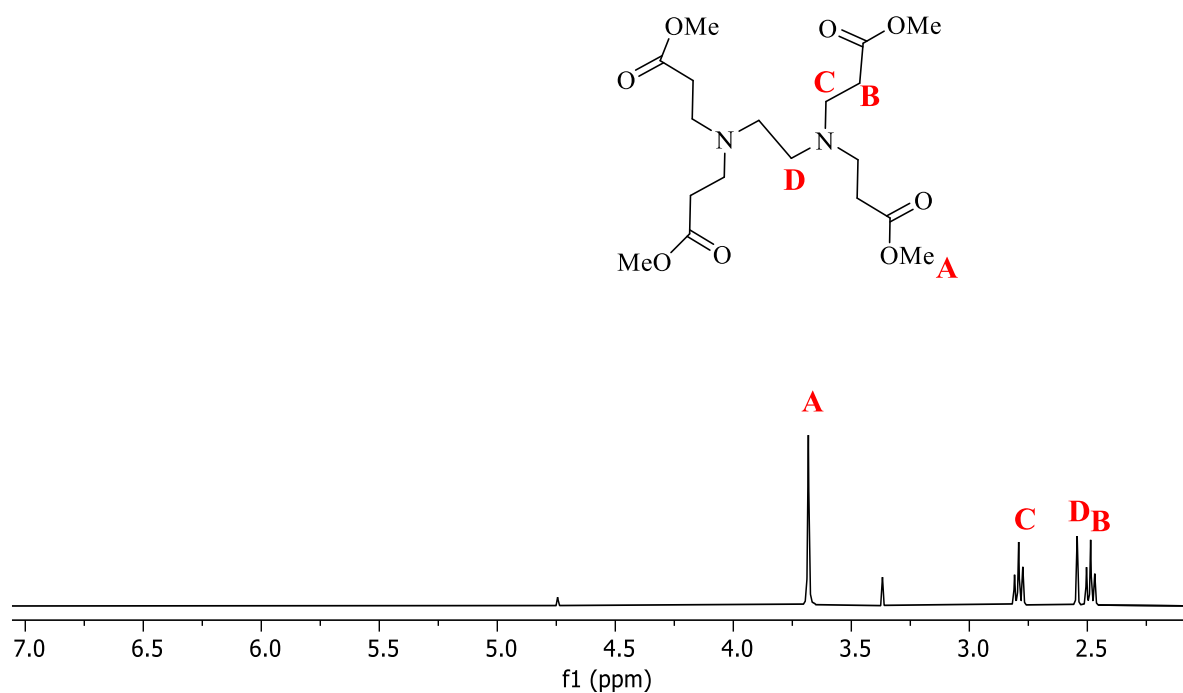
Figure 4.12 The ^{1}H NMR analysis of G 0.5 PAMAM dendrimer showed the absence of any remaining signals corresponding to methyl acrylate in the alkene region.

The ^{1}H NMR spectrum of the G0.5 dendrimer is shown in the Figure 4.12, which confirms that the reaction had finished. The methoxy peak appeared as a singlet at 3.67 ppm in the NMR spectrum, and the core EDA protons were assigned to a second singlet at 2.52 ppm, which integrated to 4H. As no

115

vinyl peaks were detected at 5-6 ppm, we were certain that, the excess methyl acrylate had been fully eliminated. The ester C=O peak was found in the ^{13}C NMR and FTIR spectra at 173 ppm and 1730 cm^{-1} respectively. The structure was supported by the mass spectrum, with the molecular ion visible at 404 (MH). The full-generation dendrimers were synthesized by reacting half-generation dendrimers with an excess of EDA. The lone pair on the nitrogen atoms of EDA reacted with the electrophilic carbonyl ester, leading to the substitution of the methoxy group with EDA.
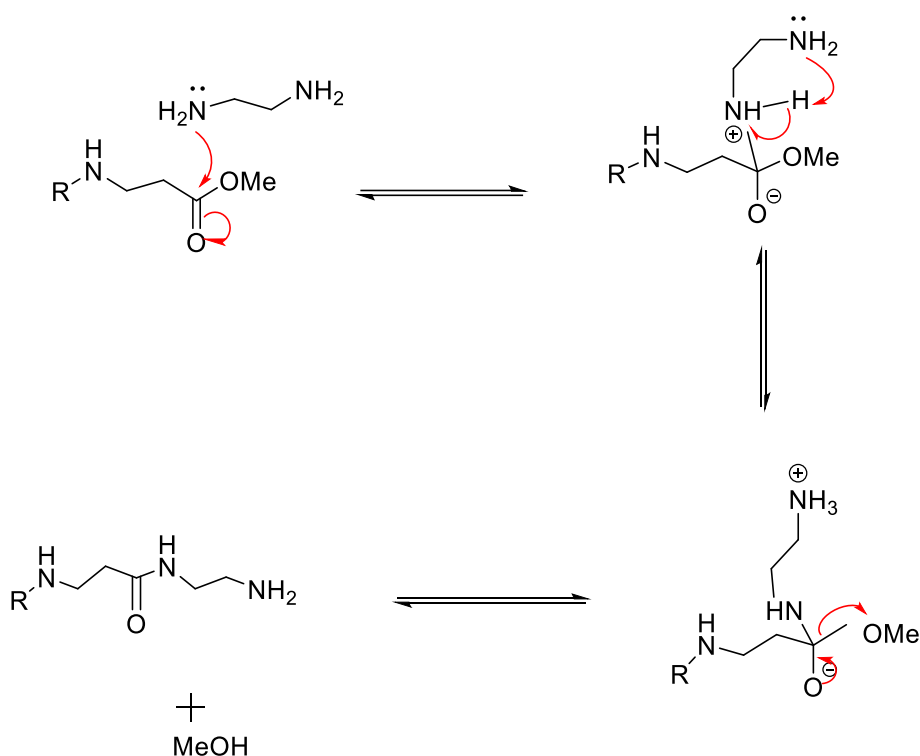
Figure 4.13 Amidation reaction of full-generation PAMAM
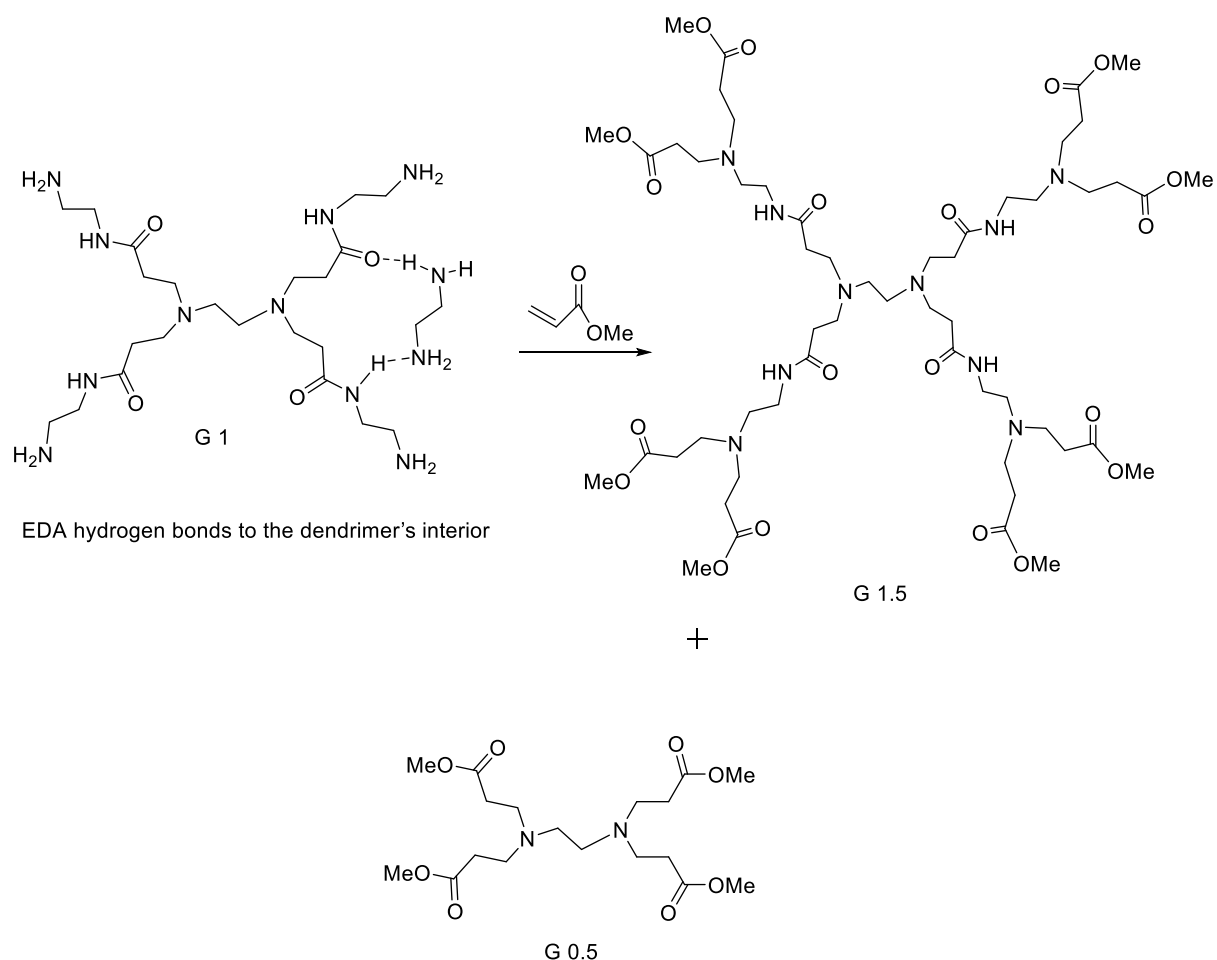
Figure 4.13. Partial elimination of ethylenediamine (EDA) and its associated by-products

To guarantee that the reaction would evolve up to completion and prevent side products caused by intra and intermolecular reactions, an excess of EDA was used. These side reactions include both intra and inter molecular reactions with EDA, as shown in the figure 4.14. The excess EDA was eliminated by using an azeotropic mixture of toluene and methanol (1:9 v: v), which is an effective hydrogen bonding rival for EDA, with a higher boiling point than EDA. The EDA peak at 2.71 ppm was monitored using ^{1}H NMR to ensure that it had been entirely eradicated (Figure 9). This is important, as any remaining EDA will react with methyl acrylate during the next step and form a G 0.5 dendrimer.
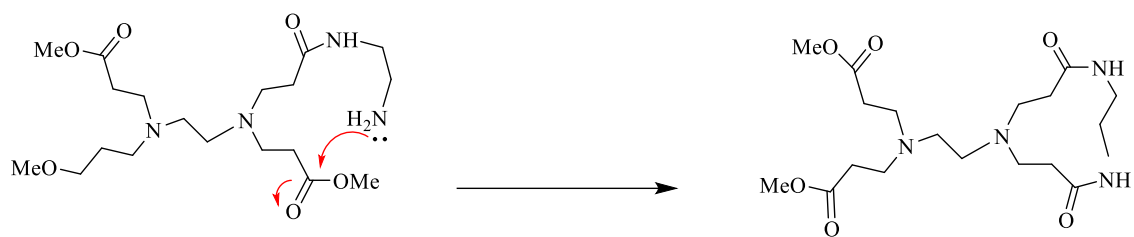
Intramolecular reaction with EDA
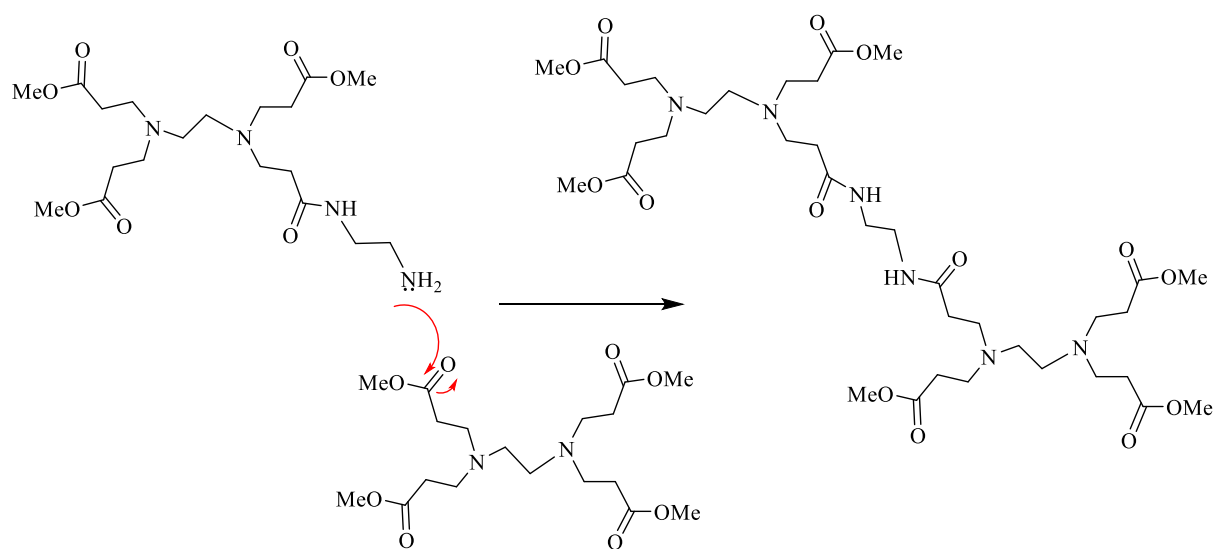
Intermolecular reaction with EDA

Figure 4.14 Structural defects can arise from various side reactions that occur during the synthesis of PAMAM dendrimers.
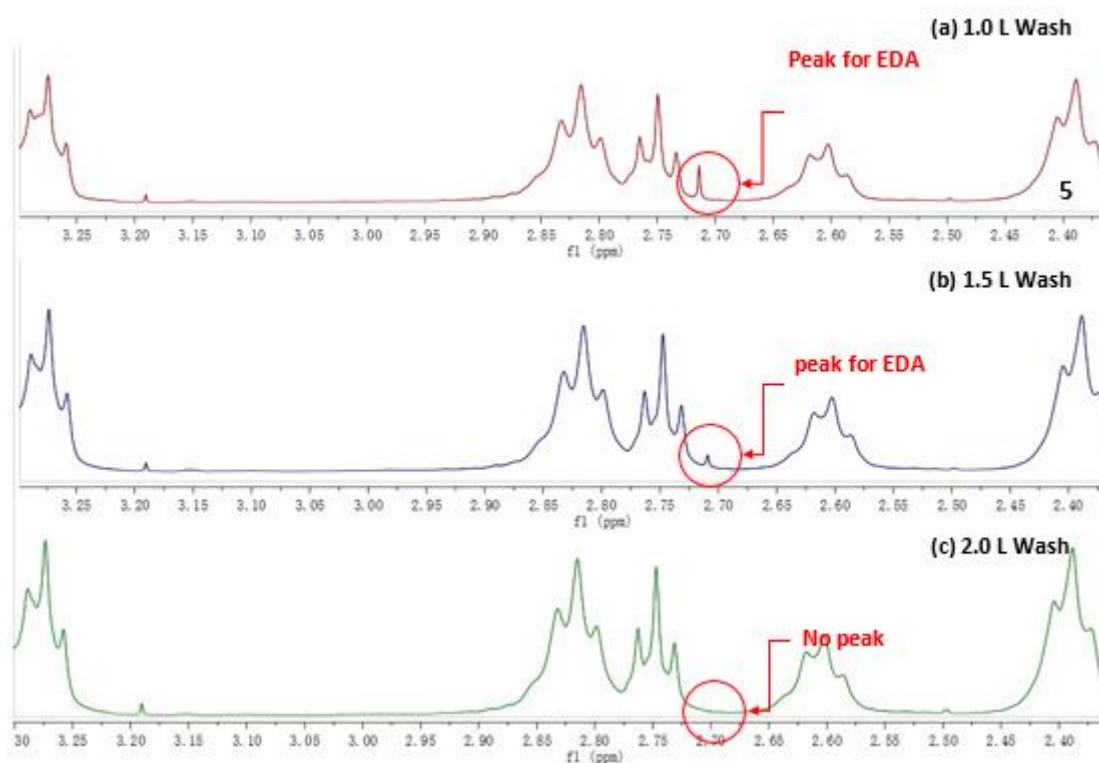
Figure 4.15 Generation 3 after washing with Azeotropic solution.

The ^{1}H NMR spectra of the new amine terminated G1.0 dendrimer indicated that the singlet peak for the excess EDA at 2.71 ppm was no longer present in the molecule. The C=O ester could be seen in the FTIR at 1736 cm^{-1} and the ^{1}H NMR signal at 3.68 ppm for the methoxy group was no longer discernible. Electrospray ionization mass spectrometry (ESI-MS) was employed to analyse smaller dendrimer generations (G0.5 - G2) with molecular weights below 2500 g mol^{-1}. larger generation dendrimers (G2.5 - G4.5) were examined using matrix-assisted laser desorption ionization (MALDI), as detailed in Table 1. Researchers observed that ESI mass spectra become increasingly complex as dendrimer generations rise, attributed to the generation of multiple charged species during the electrospray process. However, for PAMAM dendrimers of the third generation and beyond, ESI-MS struggles to detect these multiple charged molecules due to limitations in unit resolution mass analysis. And the dendrimers are shown in the figures 4.16 and 4.17.

Table 4.1 The molecular weight of PAMAM dendrimers

Dendrimer Generation	Molecular Formula	Terminal Groups	Calculated M_r (g mol^{-1})	Molecular Ion Peak (m/z)
G0.5	$C_{18}H_{32}N_2O_8$	4	405	427
G1.0	$C_{22}H_{48}N_{10}O_4$	4	517	539
G1.5	$C_{54}H_{96}N_{10}O_{20}$	8	1204	1227
G2.0	$C_{62}H_{128}N_{26}O_{12}$	8	1430	1428
G2.5	$C_{126}H_{224}N_{26}O_{44}$	16	2805	2809
G3.0	$C_{142}H_{288}N_{58}O_{92}$	16	3255	3257
G3.5	$C_{270}H_{480}N_{58}O_{92}$	32	6010	6054
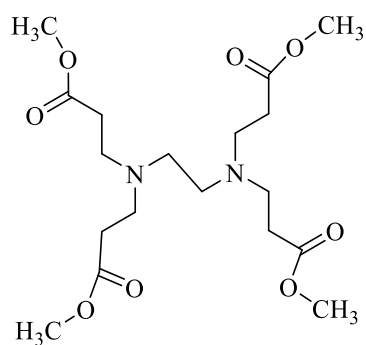
G 0.5 PAMAM
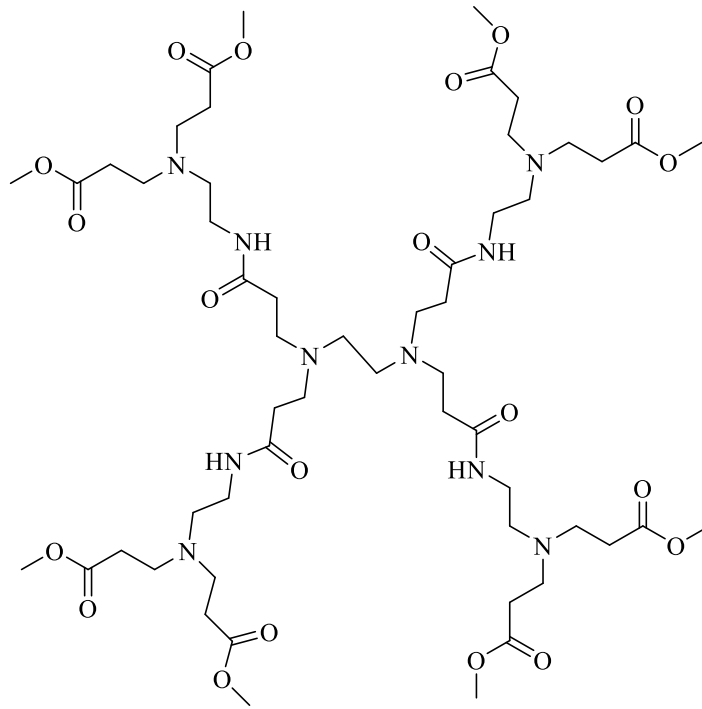
G 1.5 PAMAM
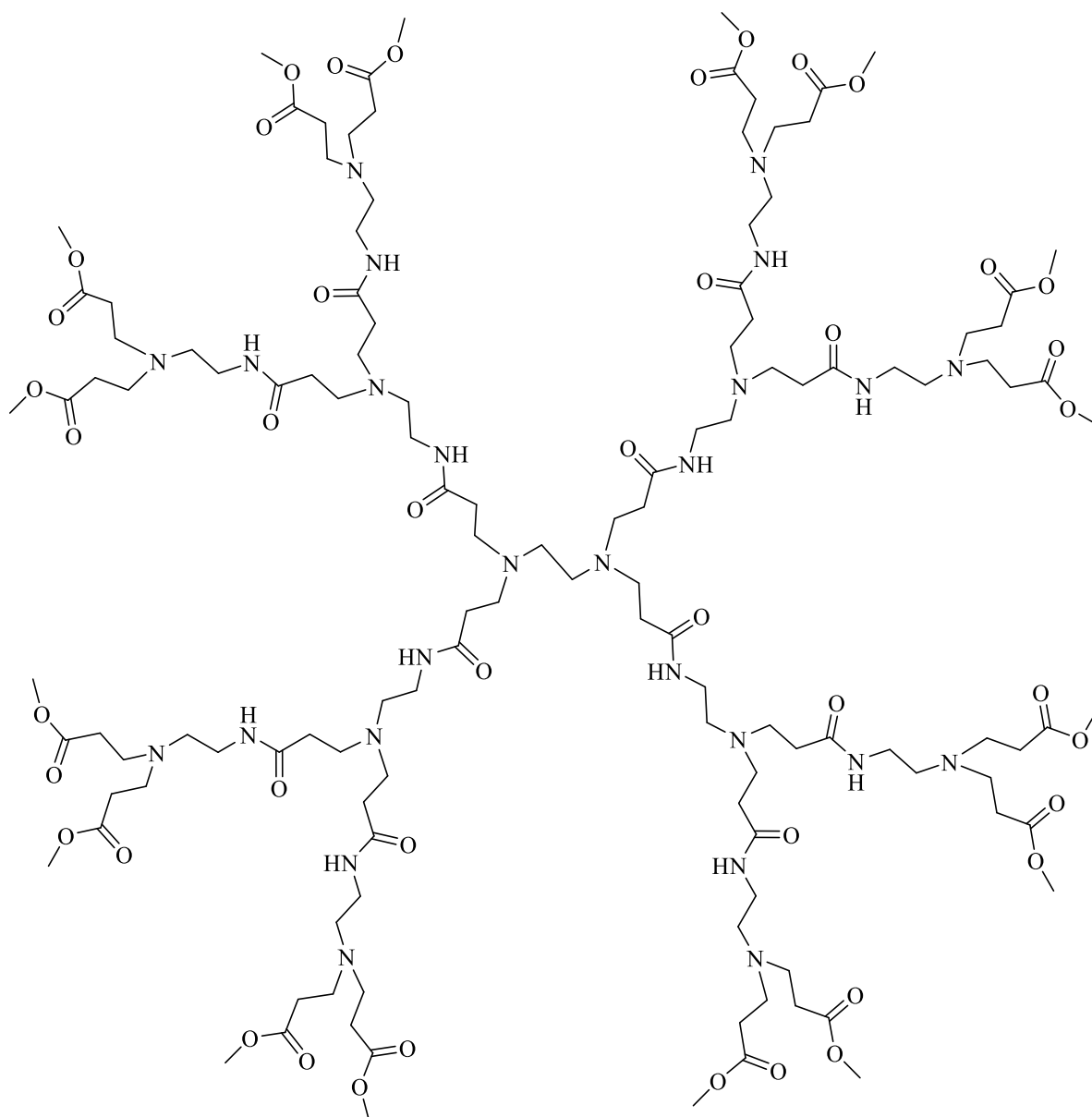
G 2.5 PAMAM
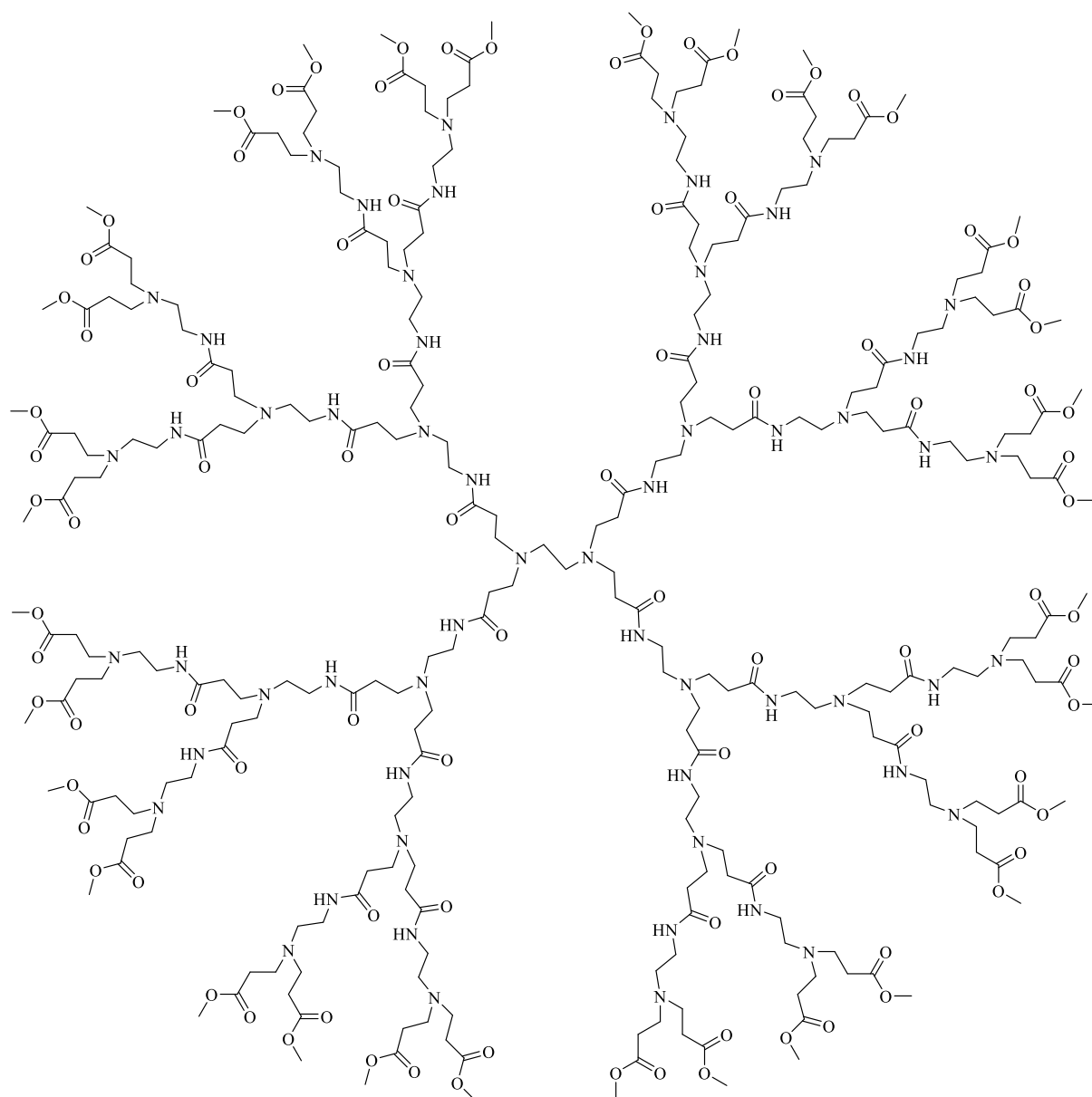
G 3.5 PAMAM
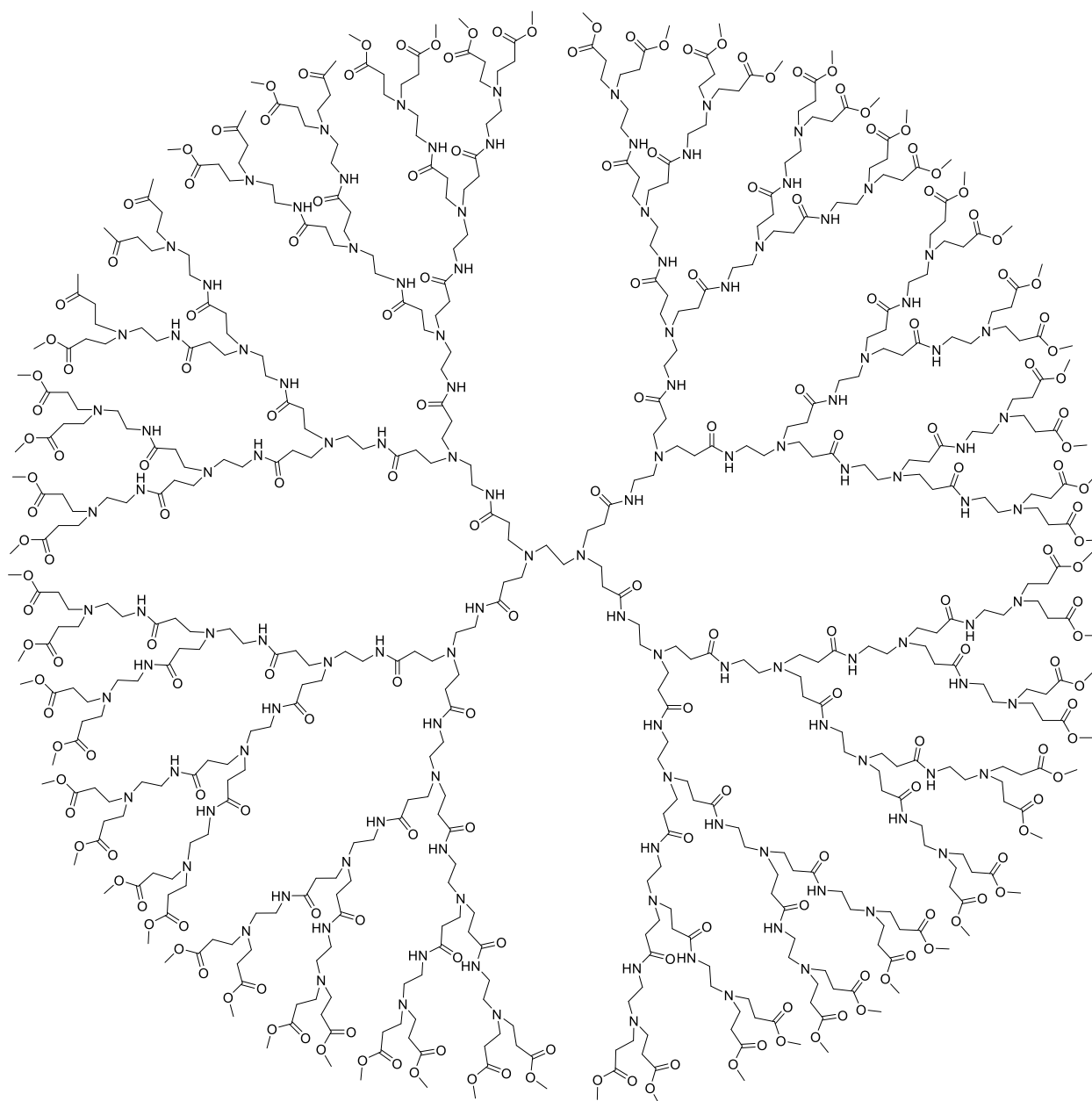
Chemical Formula: $C_{558}H_{992}N_{122}O_{183}$
Molecular Weight: 12338.75

G 4.0 PAMAM

Figure 4.16 Ester terminated dendrimers synthesized for this project.

G 1 PAMAM

G2 PAMAM

125
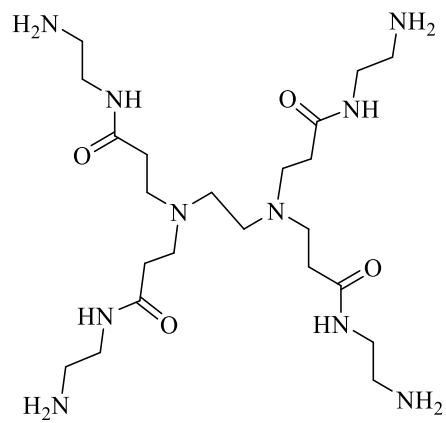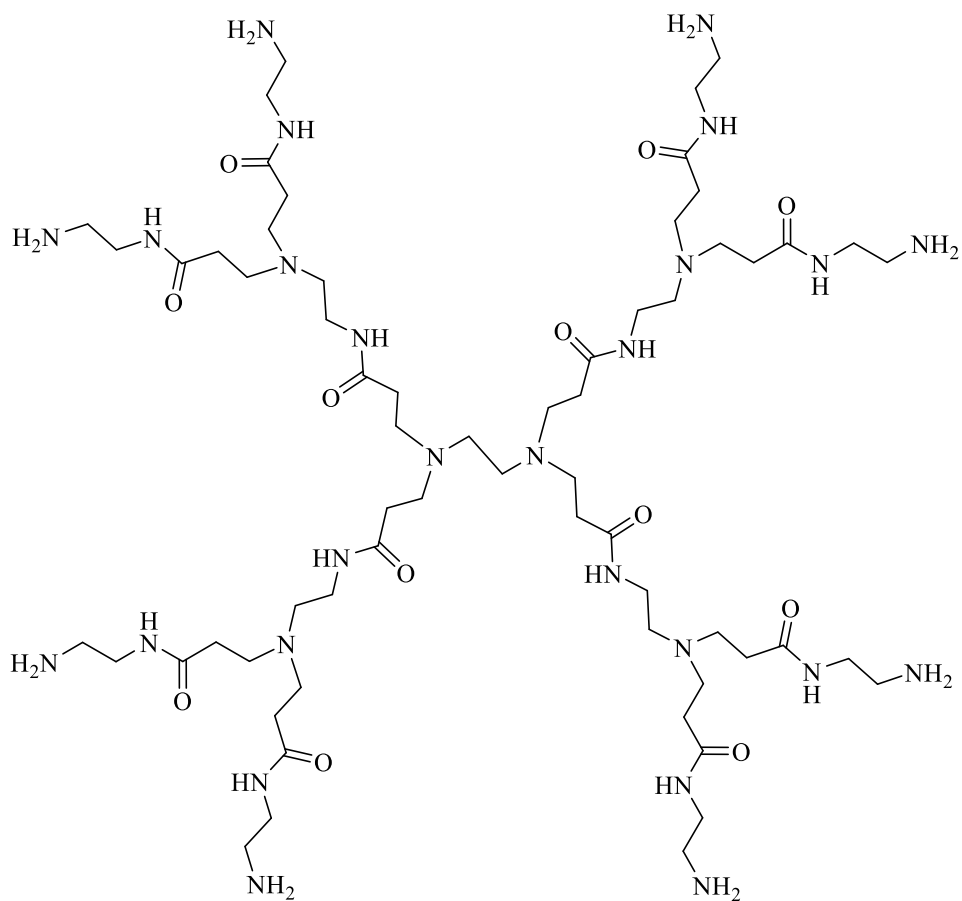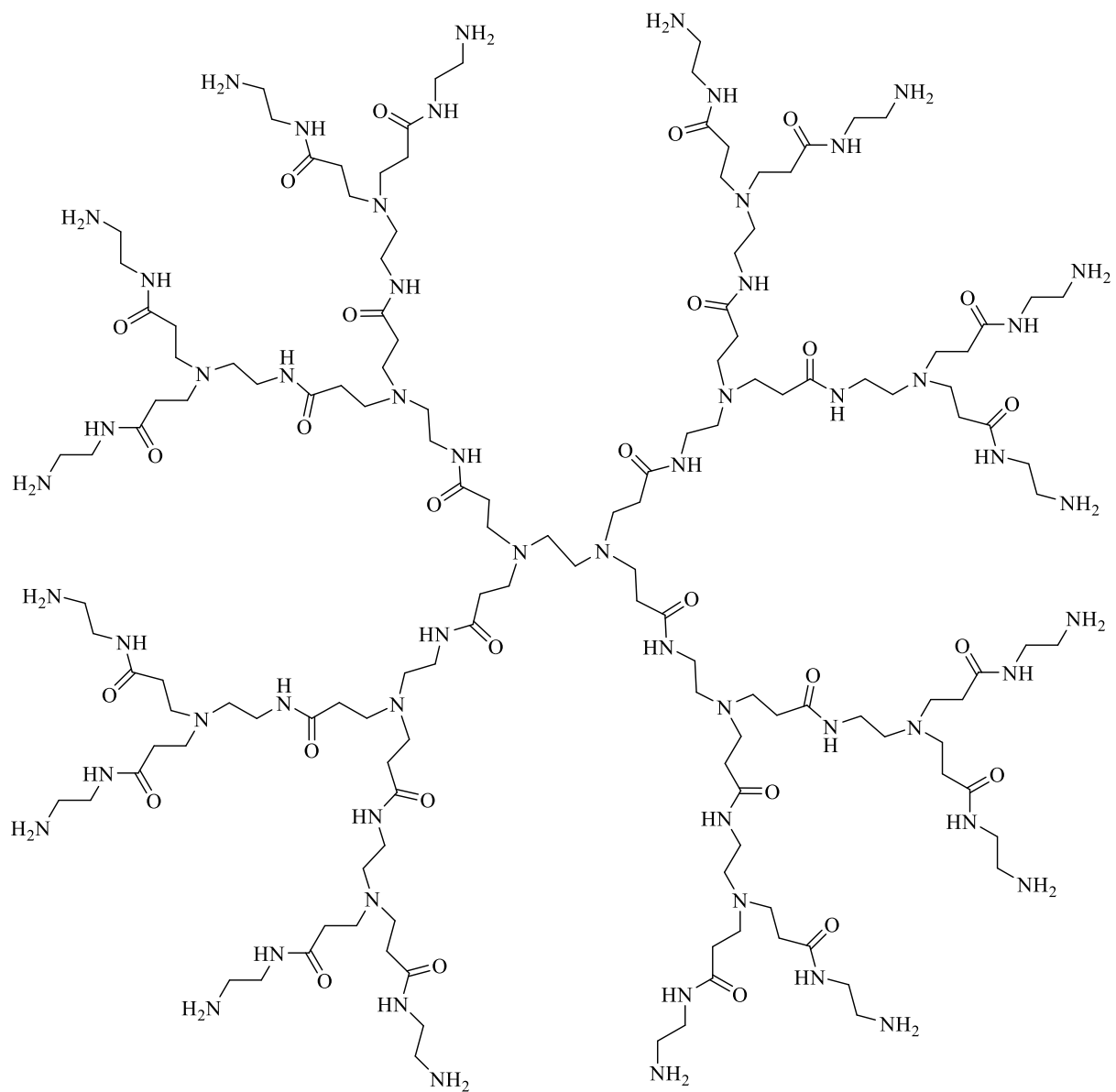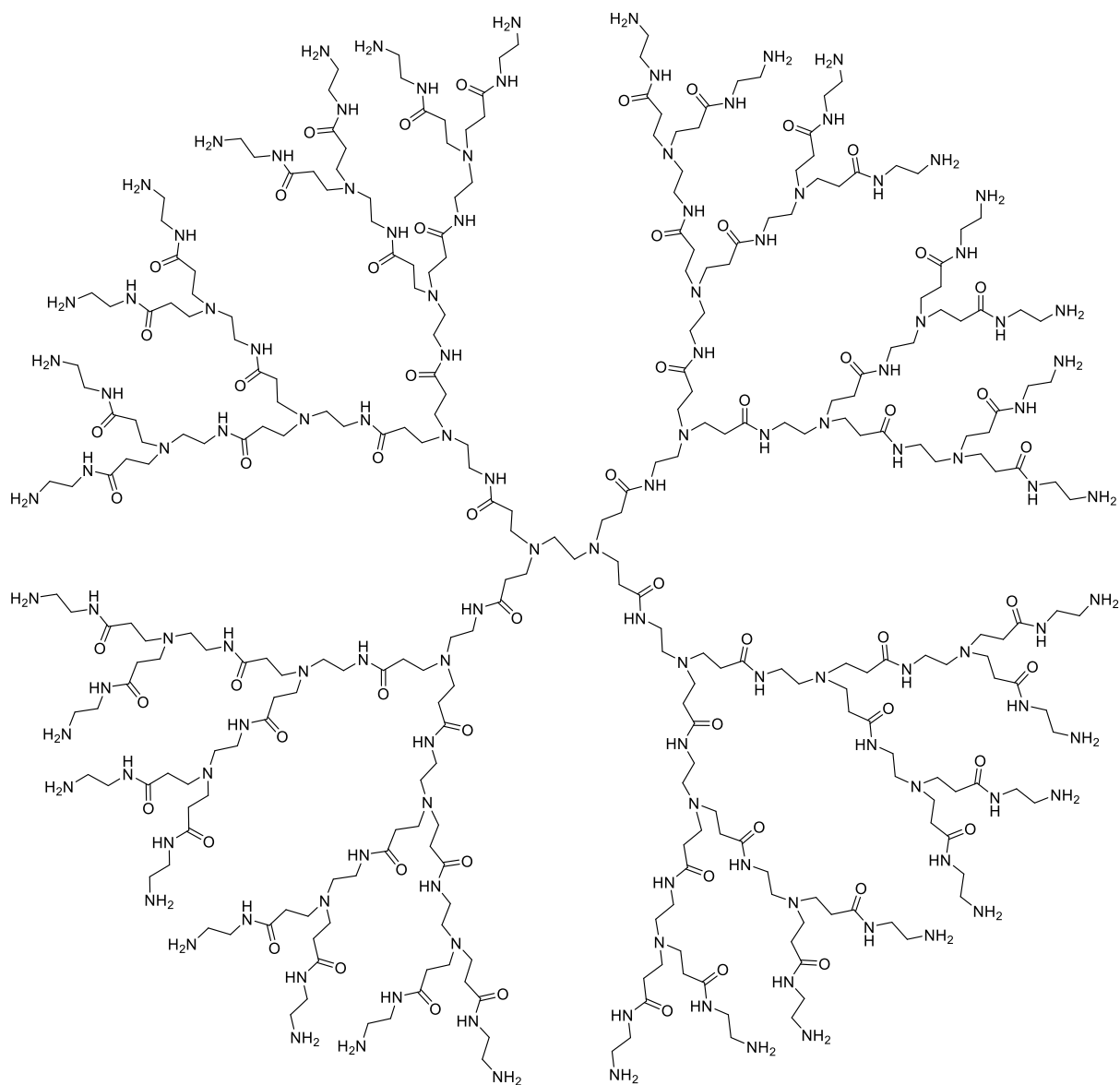
G 3.0 PAMAM

G 4.0 PAMAM

Figure 4.17 Amine Terminated dendrimers synthesized for this project.

Table 4.2 IR OF Dendrimers Generations

	IR (cm^1)	
Dendrimer Generation (G)	C=O	C=O
G 0.5 dendrimers	1733	-
G1.0 dendrimers	-	(1640)
G1.5 dendrimers	(1734)	(1648)
G2.0 dendrimers	-	(1639)
G2.5 dendrimers	(1733)	(1644)
G3.0 dendrimers	-	(1635)
G3.5 dendrimers	(1734)	(1645)

4.5.2 Synthesis of PAMAM Dendrimers with a Hydroxyl Group

 The amine-ended dendrimers were changed to hydroxyl end groups to neutralise the PAMAM dendrimers and make them less hazardous. Half-generation PAMAM dendrimers that were dissolved in DMSO and reacted with an excess of potassium carbonate and ethanolamine, to convert the ester groups into amide groups, and provide the terminal hydroxyl groups. The reaction is like the EDA step, with the lone pair attacking the electropositive carbonyl of the ester. However, the presence of a base is required to deprotonate the intermediate since the terminal OH group is not sufficiently basic for this purpose.
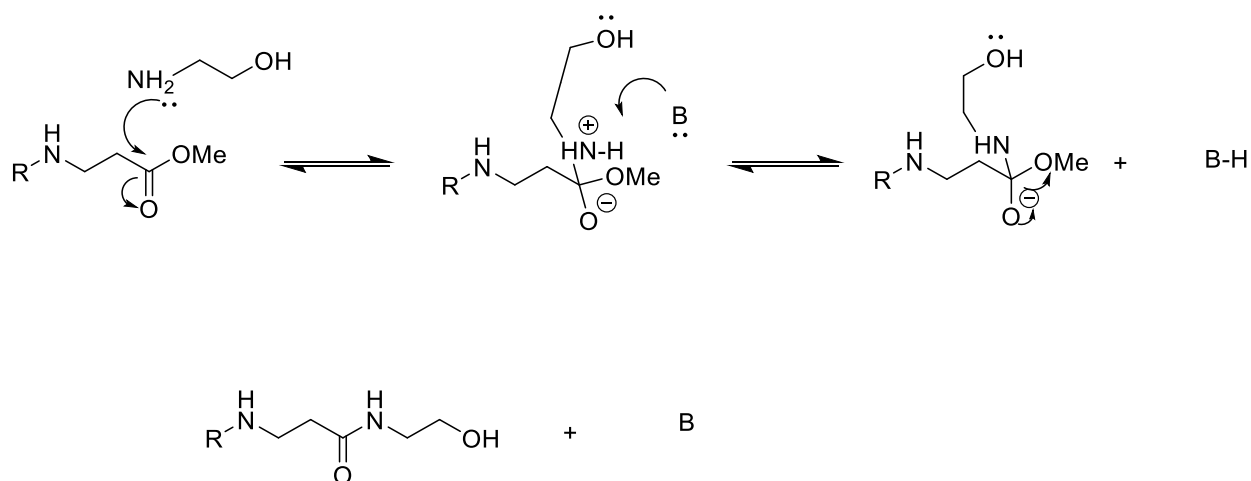
Figure 4.18 Synthesis of PAMAM Dendrimers with a Hydroxyl Group

4.5.3 Characterisation of Hydroxyl-Terminated PAMAM Dendrimers

Many spectroscopic approaches were used to characterise the hydroxyl terminated PAMAM dendrimers. All half-generation dendrimers, as previously mentioned, displayed a significant singlet peak at 3.68 ppm in their ^{1}H NMR spectra, due to the terminal methoxy group. This peak was not discernible in the spectra for G2.5-OH and G3.5-OH. Furthermore, we anticipated additional peaks between 63.7 and 52.34 ppm in the ^{13}C NMR hydroxyl. These signals were attributed to the carbons near the hydroxyl groups, as observed in the ^{13}C NMR spectra of G2.5 and G3.5 (C-O) dendrimers. Expected that the C=O stretch at 1735 cm^{-1} would no longer be present and for a new amide stretching at around 1600 cm-1 and a wide OH stretch of approximately 3000 cm-1 would be seen. Both IR spectra support these hypotheses.

In our research, we encountered challenges when attempting to obtain reliable mass spectrometry (mass spec) data for the NH2 and OH dendrimers. This is due to issues related to aggregation and multiple charges, that complicate the analysis.[46]
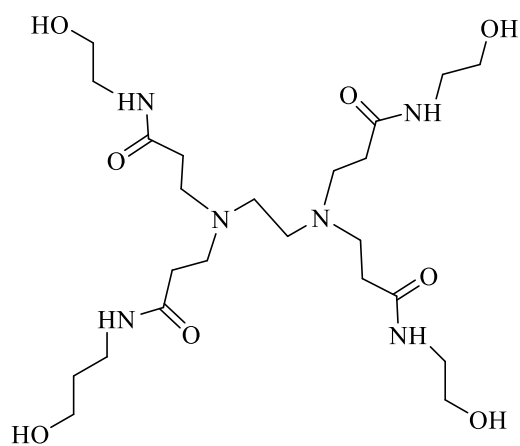
G 1.0-OH
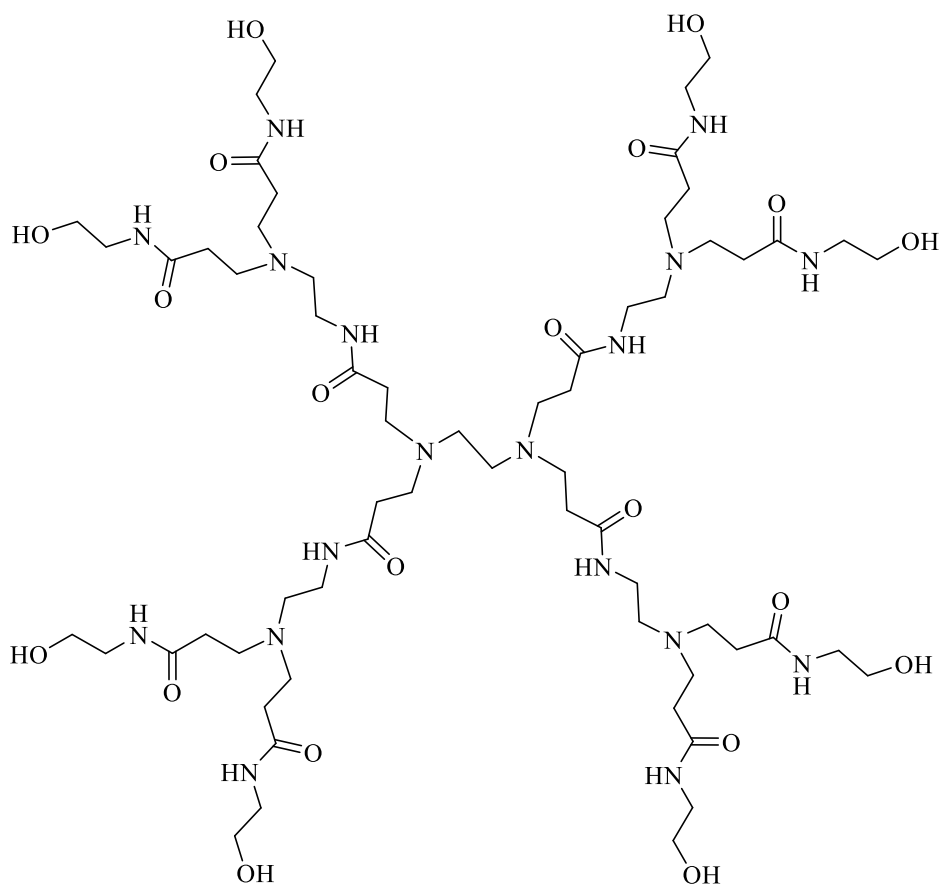
G 2.0-OH
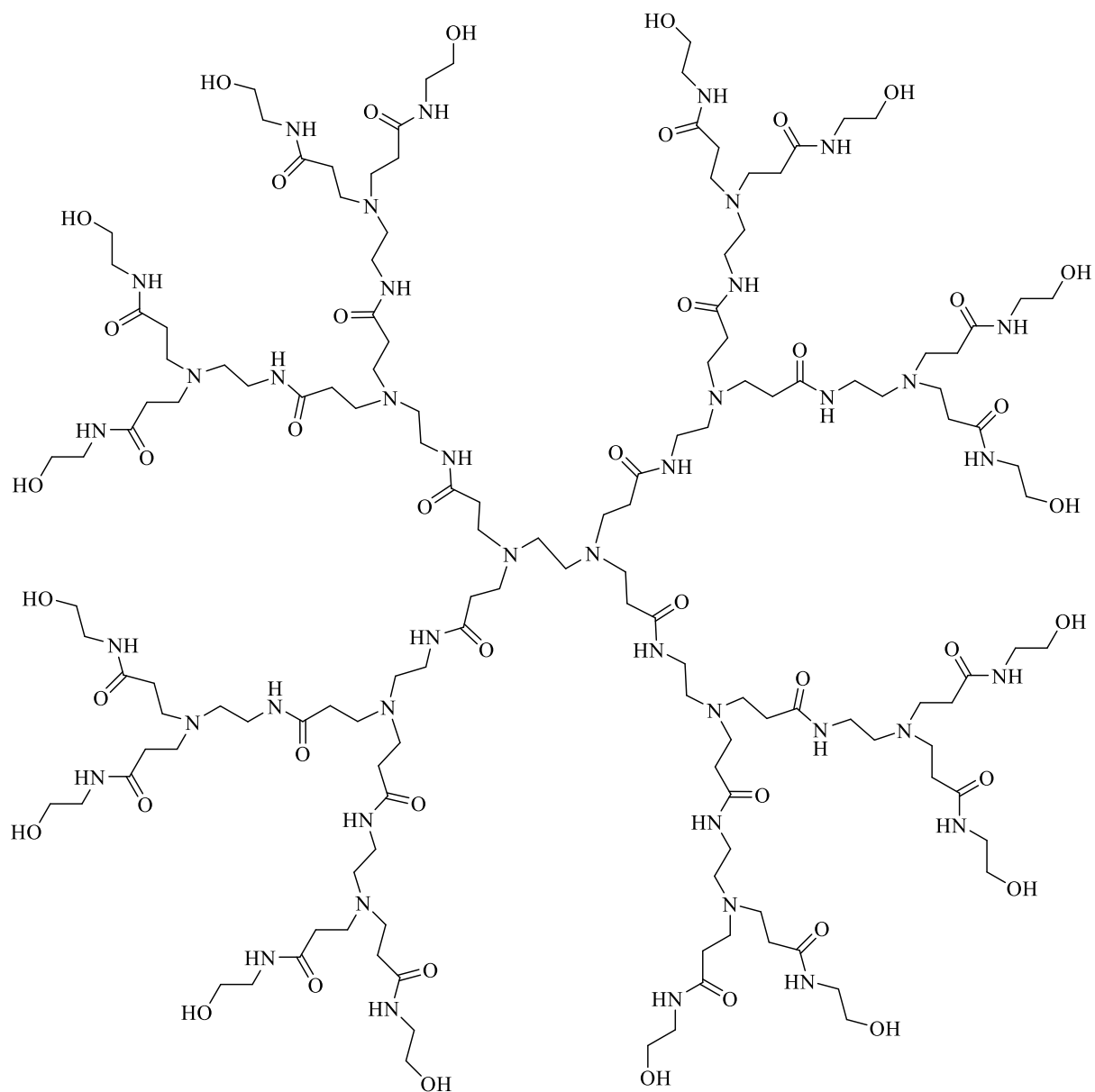
G 3.0-OH
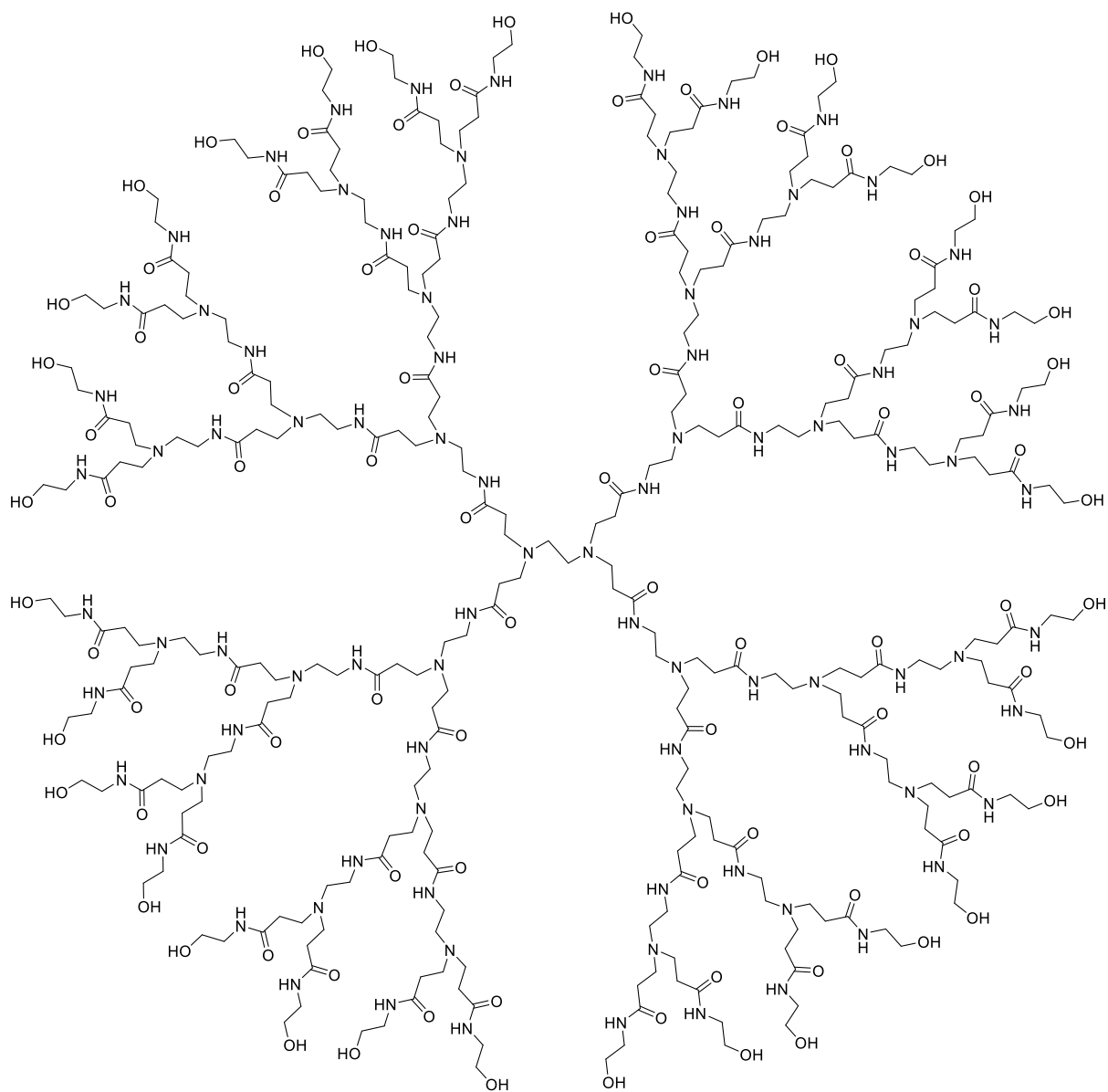
G 4.0-OH

Figure 4.19 Structures of neutral PAMAM

4.5.4 The process of encapsulating hydrophobic particles using water-soluble PAMAM dendrimers.

The main objective of this experiment was to compare the drug delivery capability of dendrimers and HBPs. A secondary aim, however, was to discover whether HBPs can encapsulate and transport pharmaceuticals as efficiently as dendrimers in order to help measure the drug baseline. Prior research showed that acidic guest molecules were successfully encapsulated using pH-dependent binding, and that those with H-bonding groups could also be enclosed. Nonetheless, the most effective encapsulation was achieved with guests containing both acidic and H-bonding groups, with neutral and hydrophobic guests demonstrating lower encapsulation rates. Ibuprofen was selected for this investigation because of its structure and commercial availability, along with the fact that it possesses an acid group that may combine with dendrimers to generate H-bonds, salts, or both. Moreover, ibuprofen is UV-active, making it simple to determine the concentration of its solution. The extinction coefficient of ibuprofen was thus determined by constructing a Beer-Lambert plot using the absorbance peak at 273 nm. As ibuprofen has low solubility in water, methanol was selected as the initial solvent for analysis.
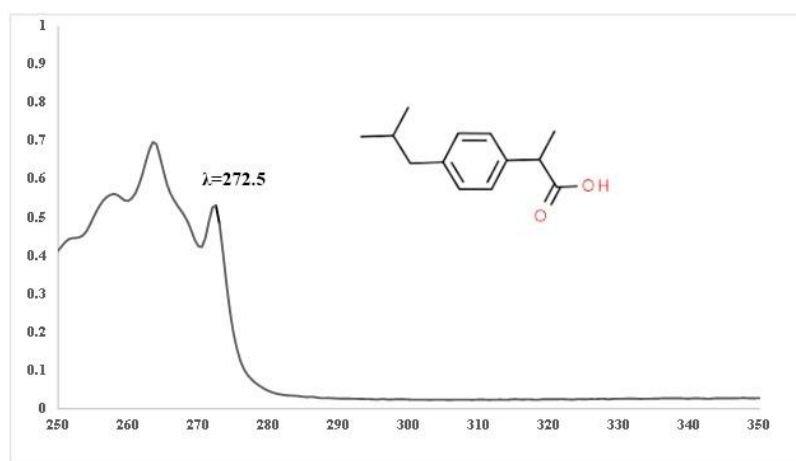
Figure 4.20 The chemical structure and UV vis spectrum of Ibuprofen and the peak highlighted at 272.5 nm was selected for our encapsulation experiments.

The objective of the initial experiment was to determine the highest concentration of ibuprofen that could be achieved in a buffer solution (pH 7.4) without the presence of dendrimers. To ensure that only ibuprofen that had been encapsulated was assessed, this value was then deducted from all subsequent dendrimer measurements. UV-vis absorption was used to measure the absorption, and using this with

the relevant Beer Lambert plot, the maximum saturation concentration of ibuprofen was calculated to be 7.72E-4 mol dm^{-3}. The host/guest complex for encapsulation experiments was then prepared using a co-precipitation technique. The ibuprofen and dendrimer were initially dissolved in methanol and subsequently removed to yield a co-precipitated complex. The addition of a phosphate buffer allowed for the removal of any insoluble or non-encapsulated ibuprofen through filtration: as dendrimers are soluble in phosphate buffer, they remained in solution along with any encapsulated ibuprofen molecules. Absorbance measurements were then taken for each complex, though to account for baseline drift, only absorption values between 274 and 276 nm were calculated. The Beer-Lambert analysis was then repeated using the same Δ Abs values. The results demonstrated a significant enhancement in ibuprofen solubility as facilitated by PAMAM dendrimers, shown in Figure 4.21. The final concentrations of encapsulated ibuprofen were then determined using equations A and B.

A
$$[\text{concentration of Ibuprofen}] = \frac{\text{Absorbance}}{\varepsilon_{\text{Ibuprofen}}}$$

B
$$[\text{encapsulated ibuprofen}] = [\text{Ibuprofen concentration}] - [\text{Free Ibuprofen}]$$
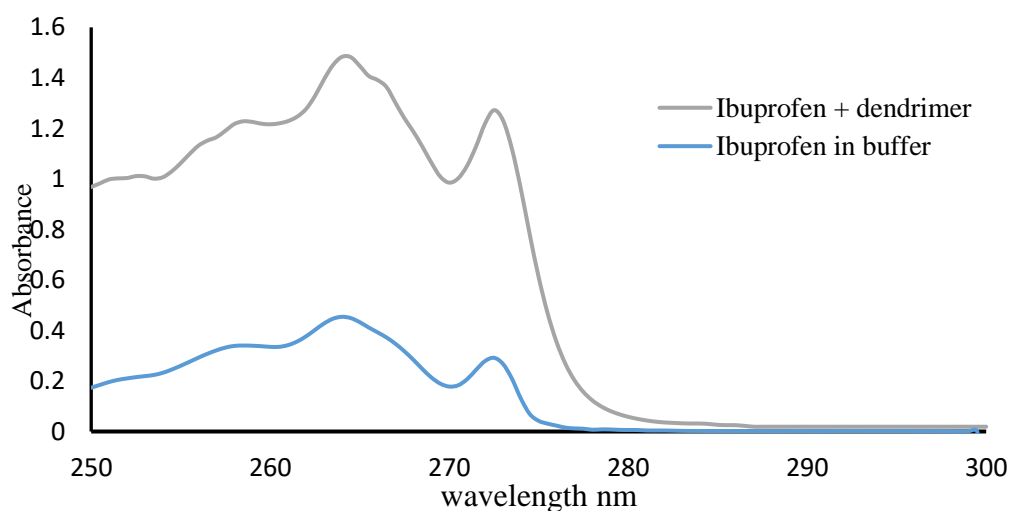
Figure 4.21 UV-visible spectra of ibuprofen and ibuprofen encapsulated in G 3-OH PAMAM dendrimer at a concentration of 1×10^{-4}M.

To evaluate the efficiency of drug encapsulation using PAMAM-OH dendrimers, two different generations of PAMAM-OH dendrimers were used, namely G3.0-16OH and G4.0-32OH. To ensure encapsulation of an excess amount of ibuprofen, the PAMAM dendrimers were used at a concentration of 1×10^{-4} M in the encapsulation experiment. By applying Beer-Lambert analysis and the calculations described above, the quantity of ibuprofen encapsulated within each PAMAM dendrimer was calculated. Initially, the identified peaks were exceptionally intense, indicating a high degree of encapsulation, leading to the application of a 10-fold dilution. The resulting ultraviolet spectra are illustrated in Figure 4.22. To calculate the loading per mole, the concentration of encapsulated ibuprofen was then divided by the concentration of dendrimer.
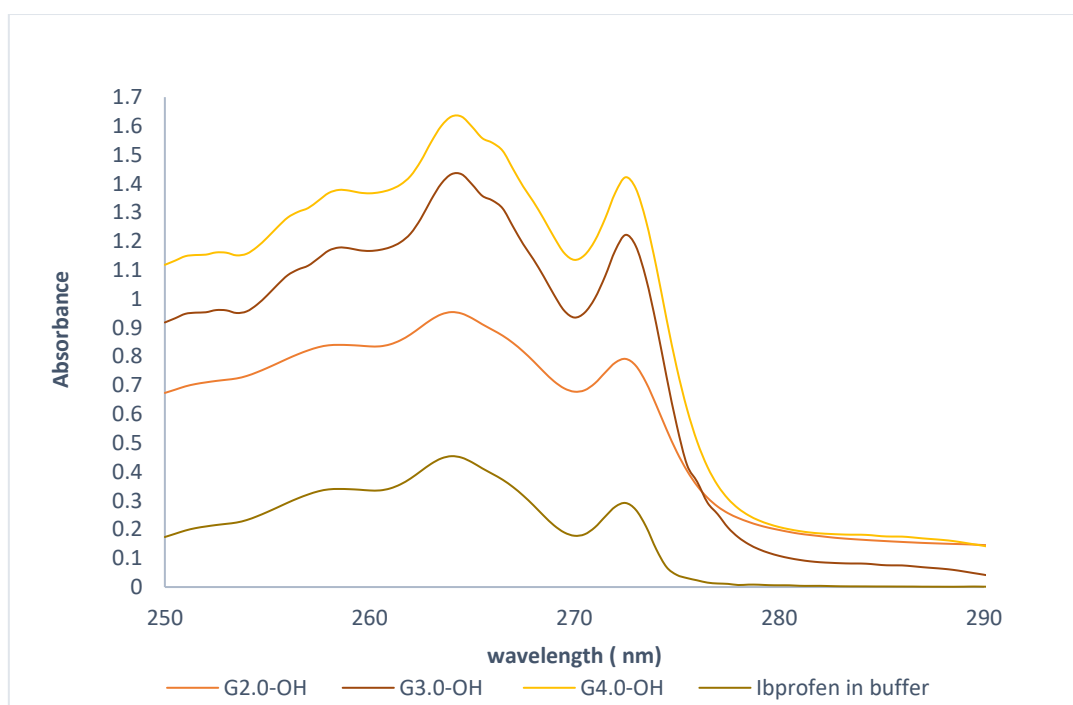
Figure 4.22 UV absorbance measurements before and after the encapsulation of ibuprofen in different generations of neutral dendrimers.

Table 4.3 Encapsulation of ibuprofen in PAMAM-OH dendrimers of different generations (G 2-OH, G 3-OH, and G 4-OH).

PAMAM-0H	Absorbance	[D] ×10-4 M	[Total Ibup] M	[Encap Ibu] M	Dendrimer loading
G2	0.036		1.24E-03	4E-04	4.0±0.4
G3.0	0.049	1E-04	1.68E-03	8.9E-04	10±0.55
G4.0	0.043		1.48E-03	7.73E-04	8.0±0.4
Maximum free ibuprofen concentration in buffer = 7.72E-04 M 10-fold dilution performed to obtain the correct concentration. All data was obtained as an average of three experiments.					

Based on the data from Table 4.3 and Figure 4.22. It can be concluded that dendrimer size has an obvious influence on ibuprofen solubility. The G2.0, with eight OH groups, could encapsulate four moles of ibuprofen, while the G3.0 with 16 OH groups encapsulated 10 moles of ibuprofen, and the G4.0 with 32 OH groups trapped only eight moles of ibuprofen inside the dendrimer. The solubility of hydrophobic molecules in dendrimer solutions thus clearly depends upon the dendrimer generation. The initial increase in solubility was due to an increase in the number of internal groups and the size of internal cavities available for interaction with ibuprofen molecules. As dendrimer concentrations increase with dendrimer size, a large increase in loading for higher-generation G4.0-OH was thus expected; however, only 8 moles were loaded, far lower than expected. This is believed to be due to steric crowding within the structure, which decreases the amount of organised space and leads to reducing binding. These results suggest that G3.0-OH is the most suitable generation for encapsulating hydrophobic molecules.

Based on these findings, the investigation then examined how dendrimer concentrations relate to drug encapsulation.
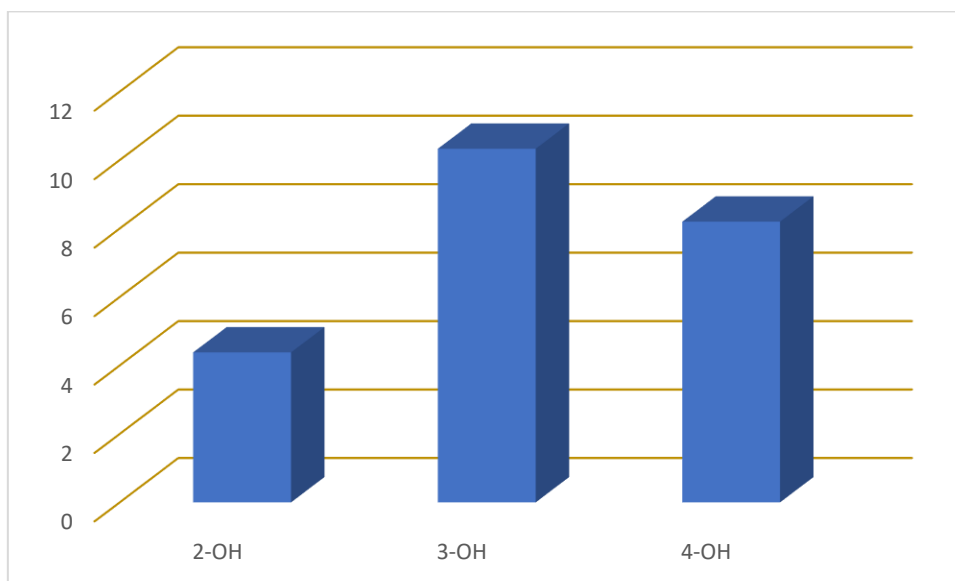
Figure 4.23 Average concentration of encapsulated ibuprofen as compared among three types of PAMAM-OH dendrimers: G2-OH, G3-OH, and G4-OH.

4.5.5 Synthesis and Characterisation of Hyperbranched PAMAM Polymers

In order to allow for fair comparison with the PAMAM dendrimers, a neutral HBPAMAM was made. In contrast to dendrimers, which are made using laborious production procedures and thus have lengthy reaction times, hyperbranched polymers can be made with quicker synthesis methods, reducing times, procedure complexity, and costs.

To compare a HBPAMAM and a dendrimer fairly requires the HBPAMAM to have functional groups comparable to those within the dendrimer. As a result, the synthesised HBPAMAM had to contain terminal and internal groups that resembled those found in target dendrimers. To mimic this functionality, an OH-terminated HBPAMAM that possessed the same internal functionality was required, with appropriate internal amide and amine groups. Meeting these conditions was seen as the minimum requirement for comparison.

A suitable PAMAM hyperbranched polymer was found using a literature search. The molecule chosen was a hyperbranched PAMAM developed by Patel et al.[47] that offered simple synthesis following a similar Michael addition methodology to that used in standard PAMAM dendrimer synthesis. Although the HBPAMAM as developed contained NH_2 terminal groups, it was believed that these could be

converted to OH groups using the same steps previously used to obtain the neutral PAMAM dendrimers. The method shown in the figure 4.24 was thus applied with the help of an MSc student, Letting Chen. The HBPAMAM was thus created using a one-pot process and a reaction between an A_2 B_4 monomer was triggered to create the amine-terminated HBPAMAM**.** MBA and EDA were the A_2 and B_4 monomers, respectively. The EDA, however, included two amine groups that could each react twice with the two conjugated alkenes of the MBA A_2 unit. The molar ratio of MBA to EDA was fixed at 1:1 to give both amine and alkene reacting functional groups with a molar ratio of 1:2 to ensure that the terminal groups were amines.

MBA(A$_2$ monomor)

22

EDA (B$_4$ monomor)

1

60 OC/30 min

23

MA

ETA

25

24

Figure 4.24 The proposed method for synthesising HBPAMAM using MBA and EDA monomers based on the original synthesis by Tomalia.

The mass spectrum and ^{1}H NMR spectrum of the HBPAMAM**.** The ^{1}NMR spectrum indicates a complete reaction of MBA in this process, as no alkene peaks are visible around 5 to 6 ppm. In addition, The EDA repeat units exhibit a singlet peak at 2.8 ppm, while the peak at 3.32 ppm corresponds to the CONHCH$_2$NHCO group seen in the structure of HBPAMAM. The MBA repeat unit is responsible for the presence of triplets at 2.94 ppm and 3.26 pp. The mass spectra show clusters between 1,200 and 1,400 and 1,500 and 1,600 m/z pointing to the existence of a small HBPAMAM. Mass spectrometry is not the best method for detecting high molecular weight polymers in the presence of lower molecular weight polymers due to the increased difficulty in ionising higher molecular weight molecules relative to smaller ones. Additional characterisation using GPC could not be performed, however, as HPAMAM is only soluble in water and not in the organic solvents available for GPC tests.

4.5.6 Modification of HBPAMAM-NH$_2$ using Methyl Acrylate

The conversion of terminal amines to esters was accomplished using a reaction with methyl acrylate, followed by a subsequent reaction with ethanolamine, with the aim of obtaining hydroxyl ended HBPAMAM. The experimental procedure was conducted at room temperature, involving the reaction of small quantities of HBPAMAM with methyl acrylate in methanol for a duration of 30 minutes.

The ^{1}H NMR spectra of the modified HBPAMAM samples were indistinguishable, featuring four distinct peaks. Notably, a distinctive signal at 3.66 ppm, corresponding to the methoxy protons, was observed exclusively in the modified product; this was absent in the standard HBPAMAM spectrum. The appearance of triplets at 2.78 ppm and 2.48 ppm corresponded to the two methylene groups, while the peak at 2.53 ppm was attributed to the EDA repeat units. However, no peaks originating from the polymer were detectable.

When subjected to GPC analysis in THF, the modified product exhibited a molecular weight (Mn) of only 400, notably less than the initial polymer, contrary to expectations. Multiple repetitions of the experiment consistently yielded this result, however, suggesting that the reaction of HBPAMAM with

MA does not lead to the intended ester terminated HBPAMAM. However, upon closer examination of the NMR data, a familiar spectrum emerged that closely resembled that of the G 0.5 PAMAM dendrimer. This observation suggests the potential formation of the G 0.5 dendrimer because of HBPAMAM degradation in the presence of methanol and EDA. The EDA produced may then undergo a 1,4 Michael addition reaction with MA. Subsequent mass spectrometry analysis confirmed the formation of the G 0.5 dendrimer, shedding light on the discrepancy in GPC data in THF; this formation was consistently conducted after attempted conversion to the ester.

It was speculated that this is possible due to the reversible nature of the initial polymerisation, which appears to be faster than the predicted reaction between MA and the HBPAMAM terminal amines. As such, the MA reacts with the EDA as it is produced during the reversible polymerisation process to give the G 0.5 dendrimer.
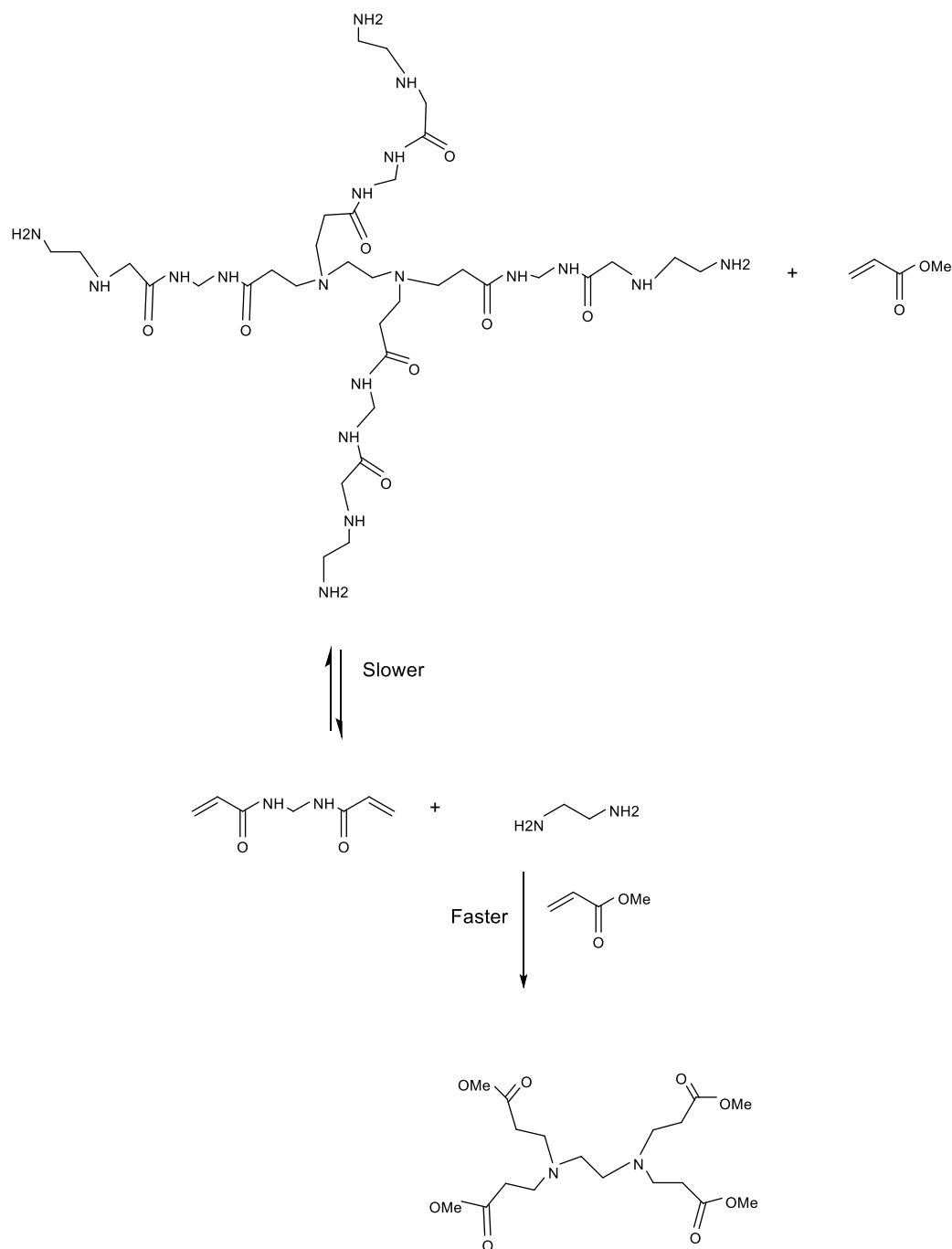
Figure 4.25 Theoretical process, based on the reversible nature of the initial polymerisation based on the original synthesis by Tomalia.

This did, however, prevented the generation of an HBPAMAM with the same internal and external functional groups as the PAMAM dendrimer. However, as the aim was to establish whether HBPAMAM-NH$_2$ could be used in place of structurally similar dendrimers, which required only a simple proof of concept, these systems were not required to be ready for clinical application at this stage.

Accepting this limitation facilitated the use of any dendrimer/HBPAMAM combination sufficiently structurally and functionally similar. Two molecules that were already available were thus used, namely the G 2.0 NH$_2$-ended PAMAM dendrimer and HBPAMAM NH$_2$.

4.5.7 Encapsulation Studies Using HBPAMAM-NH$_2$

From the data reported above, the dendrimer can encapsulate several different drug molecules. As such, the expectation was that a hydrophobic drug molecule such as ibuprofen could successfully be encapsulated within the HBPs internal cavities, due to the fact that, as previously discussed, ibuprofen has H-bonding groups and acidic groups that can form secondary interactions with the polymer's internal functionality.

The amine-ended HBPAMAM-NH2 is polydispersed and therefore does not have a discrete and specific molecular weight, which makes the use of molar concentration unreliable. As such, the mass of the resulting compound was used to measure concentration and compare the encapsulation efficiency of the two systems. Although the dendrimer and HBPAMAM-NH$_2$ did not possess the same structures, this concentration method was selected to enable a more accurate comparison to be made between the dendrimer and HBPAMAM-NH$_2$.

The encapsulation studies were carried out in collaboration with an MSc Student, Tianamo Xu. The encapsulation of HBPAMAM-NH$_2$ was performed at two concentrations, with mass/volume concentrations of 0.05 mg/ml and 0.75 mg/ml used to investigate the ability of HBPAMAM to encapsulate ibuprofen at both high and low concentrations. In the first step, the extinction coefficient of ibuprofen (ε Ibuprofen = 290 dm^3 mol-1 cm-1) was calculated, and the maximum free concentration of ibuprofen was thus seen to be approximately 7.72E-4 mol dm^{-3}. The Δ Abs absorption value was then set to 276 nm to compensate for potential baseline drift.

Table 4.4 Encapsulation data for ibuprofen at low and high concentrations.

[HBPAMAM-NH2] mg/ml	Δ Abs	[average of total Ibu] M	[* average of encapsulated Ibu] M
0.005	0.56	1.93E-03	9.01E-04 ±3.65E-04
0.75	0.421	1.45E-03	7.80E-04±1.46E-04
* Concentration of encapsulated ibuprofen after substruction with 7.72E-04 M			

It is clear that HBPAMAM-NH$_2$ can encapsulate ibuprofen and thus improve its solubility. The ibuprofen concentration was raised to 9×10^{-4}M at 0.005 mg mL^{-1} polymer concentration. When the polymer concentration was increased to 0.75 mg mL^{-1}, the expectation was thus for an increased loading potential linearly related to the change in HBPAMAM-NH$_2$ concentration such that, when increasing the HBPAMAM-NH$_2$ concentration by a factor of 150 (from 0.05 mg/mL to 0.75 mg/mL), the encapsulated concentration of ibuprofen might be expected to also rise by a factor of 150, giving a predicted encapsulation concentration of 0.135 M. However, a significantly smaller concentration of encapsulated ibuprofen was observed at the higher concentration, and in fact, the amount of ibuprofen encapsulated was smaller than that recorded for the HBPAMAM-NH$_2$ used at a lower concentration. It was thus postulated that this was due to different structure of the HBPAMAM-NH$_2$ at higher concentrations., which causes the polymer to have less available space. This may occur due to aggregation via H-bonding interactions between the HBPs internal amides, as if this occurs, then most internal space will be occupied by other branches of the HBPAMAM-NH$_2$ molecules.

DLS experiments were done for HBPAMAM-NH$_2$ at two different concentrations to cover the range studied for encapsulation (0.01 mg/mL, 0,02mg/mL). The DLS spectra are shown in Figure 4.26.
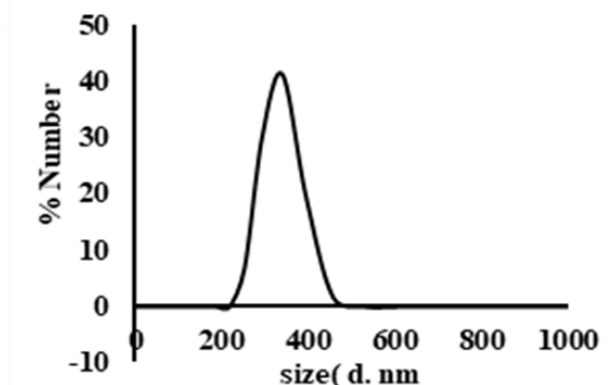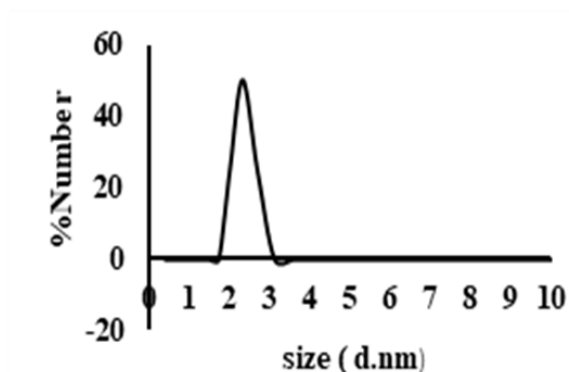
Figure 4.26: DLS data for HBPAMAM-NH$_2$ at different concentrations (**a**) polymer at 0.01 mg/mL; (**b**) polymer at 0.02 mg/mL; (**c**) polymer at 0.04 mg/mL; (**d**) polymer at 0.06 mg/mL.

The DLS data in Figure x shows increases in polymer concentration as the hydrodynamic radius increases in stages. At 0.01 mg/mL the diameter size was 2.3 nm, which increased to around 30 o 40 nm at 0.02 mg/mL. This broadly overlaps with the encapsulation data, and the ideal scenario is thus as sketched in Figure 4.27. This implies that the simple HBPAMAM-NH2 can encapsulate drug molecules as expected.

2.3 nm
0.01 mg/mL

28 nm
0.02 mg/mL
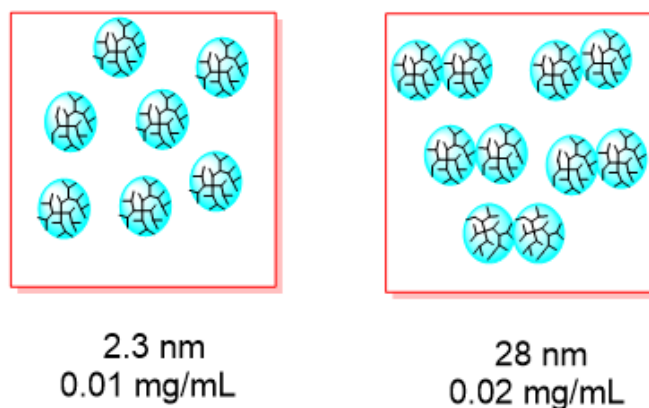
Figure 4.27 The expected cause of decrease in encapsulated ibuprofen at high concentrations.

4.5.8 Comparing the Encapsulation Efficiencies of a G 2.0 PAMAM Dendrimer and HBPAMAM-NH$_2$

To compare the encapsulation abilities of the two developed systems under similar conditions, it was first necessary to select an appropriate dendrimer and concentration method. Although a GPC of the HBPAMAM-NH$_2$ was not available, the mass spectrum indicated a molecular weight in the region of

1,500 g mol^{-1}. Considering the difficulties in obtaining other good data, mass spectrometry data for the poly-disperse samples (such as HBPAMAM-NH$_2$) was used and compared with that for the G2.0 amine terminated PAMAM dendrimers (molecular weight of 1,429 g mol^{-1}). An extinction coefficient ε of 290 dm^3 mol^{-1} cm^{-1} and a maximum free concentration of 7.72E-4 mol dm^{-3} had already been determined for ibuprofen. The difference in absorption at 276 nm was thus used to determine encapsulated concentrations, with Δ Abs used to compensate for potential baseline drift. A concentration of 0.14 mg/mL was used for both of the amine terminated systems, corresponding to the previous dendrimer concentration of 1×10^{-4} M, and the encapsulation data for the amine terminated dendrimer and HBPAMAM-NH$_2$.

Table 4.5 Comparative ability of G2 dendrimers and HBPAMAM-NH2 dendrimers to encapsulate ibuprofen.

Host System	Experiment one			Experiment two		
	Δ Abs	[Total Ibu] M	*[Encap Ibu] M	Δ Abs	[Total Ibu] M	*[Encapsulated Ibu] M
PAMAM G2	0.427	1.47E-03	7.00E-04	0.418	1.44E-03	6.69E-04
HBPAMAM-NH$_2$	0.445	1.53E-03	7.64E-04	0.436	1.50E-03	7.33E-04

Host System	Average [Encapsulated Ibu] M
G2	6.85E-04
HBPAMMA-NH$_2$	7.48E-04
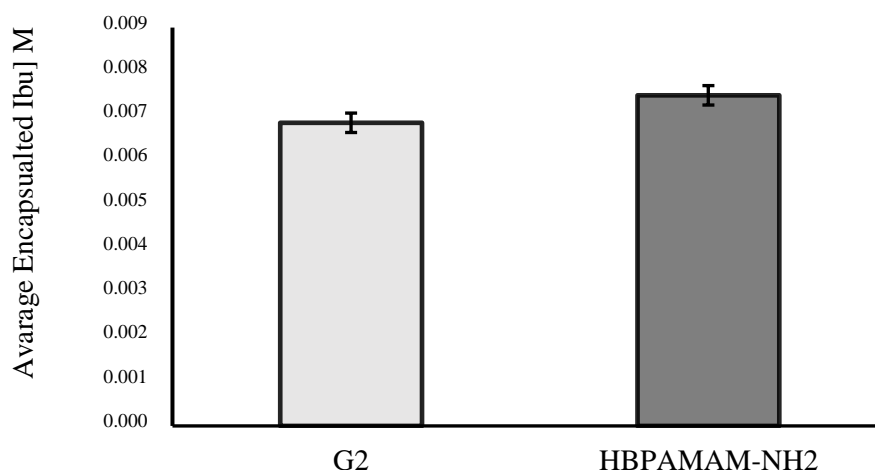
Figure 4.28. Comparison between G2 and HBPAMAM-NH2 regarding the average concentration of encapsulated ibuprofen at a concentration of 0.143 mg/mL.

Surprisingly, at the lower concentration, HBPAMAM-NH2 displayed a greater capacity for encapsulating ibuprofen than the G2 dendrimer, which was primarily attributed to the HBP's larger molecular weight and size, which offer more encapsulation space. However, considering encapsulation relative to polymer concentration made it apparent that the same HBP demonstrated significantly higher ibuprofen binding at the lower concentration of 0.14 mg/mL. This result aligns with earlier observations regarding aggregation's adverse effect on encapsulation. What is less apparent how the smaller dendrimer at 0.14 mg/mL was able to bind more ibuprofen. Nevertheless, these findings underscore the potential of using the simpler and more accessible HBPs as efficient drug delivery systems. In comparison to functionally similar dendrimers, HBPs showed promise in terms of encapsulating greater quantities of small drug molecules. Nevertheless, the extent of aggregation significantly impacts drug encapsulation: thus, while amine-ended systems serve as valuable models for preliminary evaluations, they may not be suitable for clinical use due to the potential protonation of terminal amines in aqueous solutions, which can result in densely packed surface charges and homolysis.

4.8 References

1- G. S. Banker, *The Theory and Practice of Industrial Pharmacy*, Vol. 1, Chapter 4, pp. 19106-19108, Philadelphia, 1970.

2- R.P. Dash, N. R. Srinivas, *Drug Dev. Ind. Pharm.*, 2019, 45, 1421-1429.

3- M. Jabbari, F. Teymoori, J. *Mol. Liquids.*, 2018, 262, 1-7.

4- H. Alhadi, S. Emami, Eur. *J. Med. Chem.* 2020, 187, 111970.

5- D. A. Snider, W. Addicks, *Adv. Drug Deliv. Rev.* 2004, 56(3), 391-395.

6- K. T. Savjani, A. K. Gajjar, *Int. Scholarly Res.* 2012, 3, 231-234.

7- L. Ito, A. Ito, J. *Drug Deliv. Sci. Technol.* 2019, 50, 201-207.

8- A. C. Anselmo, S. Mitragotri, J. Control. Release 2014, 190, 15-28.

9- P. R. Rao, P. V. Diwan, *Drug Dev. Ind. Pharm.* 1998, 24(4), 327-336.

10- D. Brambilla, P. Luciani, J. C. Leroux. *J. Control. Release* 2014, 190, 9-14.

11- R. F. Donnelly, T. R. R. Singh, M. J. Garland, K. Migalska, C. McCrudden, and A. D. Woolfson. *Adv. Funct. Mater.* 2012, 22(23), 4879-4890.

12- Y. Tang, Y. Cao, *Pharmaceutics.* 2021, 13(3), 422.

13- W. D. Rhine, D. S. Hsieh and, R. Langer, *J. Pharm. Sci.* 1980, 69(3), 265-270.

14- A. K. S. Chandel, D. Bhalani, and N, Kumar, *Bioavailability.* 2022, 3, 15-17.

15- R. Walther, J. Rautio, and A.N. Zelikin, *Adv. Drug Deliv. Rev.* 2017, 118, 65-77.

16- J. McMillan, E. Batrokva, H. E. Gendelman. *Prog. Mol. Biol. Transl. Sci.* 2011, 104, 563-601.

17- H. A. Maeda, Y. Matsumura, *Crit. Rev. Ther. Drug Carrier Syst.* 1989, 6(3), 193-210.

18- J. Nichols, Y.H. Bae, *J. Control. Release* 2014, 190, 451-464.

19- K. Greish, J. Fang, T. Inutsuka, T. Nagamitsu, H. Maeda, *Clin. Pharmacokinet.* 2003, 42, 1089-1105.

20- S. Taurin, H, Nehoff, K. Greish, *J. Control. Release* 2012, 164(3), 265-275.

21- R.R. Wakaskar, *Int. J. Drug Dev. Res.* 2017, 9(2), 37-41.

22- S.D. Li, L. Huang, *Biochim. Biophys. Acta (BBA)-Biomembranes.* 2009, 1788(10), 2259-2266.

23- C. Buzea, I.I. Pacheco, K. Robbie, *Biointerphases.* 2007, 2(4), MR17-MR71.

24- M. Mohammady, G. Yousefi, *J. Pharm. Sci.* 2020, 109(11), 3235-3247.

25- H.M. Ding, Y.Q. Ma, *cellular delivery.* 2015, 11(9-10), 1055-1071.

26- J. Dolai, K. Mandal, N.R. Jana, *ACS Appl. Nano Mater.* 2021, 4(7), 6471-6496.

27- D. Brambilla, D. Luciani, J.C. Leroux, *J. Control. Release* 2014, 190, 9-14.

28- M. D. Chavanpatil, A. Khdair, Y. Patil, H. Handa, *J. Pharm. Sci.* 2007, 96(12), 3379-3389.

29- A. Prokop, J.M. Davidson, *J. Pharm. Sci.* 2008, 97(9), 3518-3590.

30- L. J. Twyman, A.E. Beezer, R. Esfand, M.J. Haerdy, *Tetrahedron Lett.* 1999, 40(9), 1743-1746.

31- M. Xinpeng, M. Zhuxian, J. Erlei, S. Qihang, *J. Pharm. Sci.* 2012, 4, 213-216

32- A. E. Beezer, A. S. H. King, I.K. Martin, *Tetrahedron.* 2003, 59(22), 3873-3880.

33- A. Janaszewska, J. Lazniewska, P. Trzepinski, *Biomolecules.* 2019, 9(8), 330.

34- Q. Zhong, S. R. Rocha, *Mol. Pharmaceutics* 2016, 13(3), 1058-1072.

35- A.A. Chis, C. Dobrea, C. Morgovan, A.M. Arseniu, *Molecules* 2020, 25(17), 3982.

36- D.M. Shadrack, H.S. Swai, J.J. Munissi, E.B. Mubof, S.S.S Nyandoro, *Molecules* 2018, 23(6), 1419.

37- L.J. Twyman, A.S King, J. Burnett, *Tetrahedron Lett.* 2004, 45(2), 433-435.

38- A. K. Pearce, J. D. Simpson, N. L. Fletcher, Z. H. Houston, *Biomaterials.* 2017, 141, 330-339.

39- S.N. Abdullah, G. Mann, L.J. Twyman, *Molecules.* 2021, 26(22), 6850.

40- L.J. Twyman, A. Ellis, P.J. Gittins, *Macromolecules.* 2011, 44(16), 6365-6369.

41- F. Chiba, T. Chou, L.J. Tyman, M. Wagstaff, *Chem. Commun.* 2008, (36), 4351-4353.

42- J.M. Frechet, *Proc. Natl. Acad. Sci.* 2002, 99(8), 4782-4787.

43- F. Chiba, T.C. Hu, L.J. Twyman, M. Wagstaff, *Macromol. Symp.* 2010, 287(1), 37-41.

44- G. R. Newkome, Z. Yao, G.R. Baker, V.K. Gupta, *J. Org. Chem.* 1985, 50(11), 2003-2004.

45- I. K. Martin, L.J. Twyman, *Tetrahedron Lett.* 2001, 42(6), 1119-1121.

46- P. J. Gittins, L.J. Twyman, *Supramol. Chem.* 2003, 15(1), 5-23.

47- J. Patel, K. Garala, B. Basu, M. Raval, A. Dharamsi, *Int. J. Pharm. Investig.* 2011, 1(3), 135.

Chapter 5

Conclusions and future work

Future work involves addressing the challenge of functionalizing HBPAMAM by exploring innovative approaches. The ongoing project aims to synthesize a Hyperbranched Polymer (HBP) with both internal and terminal functionalities, resembling the structure of PAMAM dendrimers. Specifically, we plan to create an Aromatic Hyperbranched Polymer (Ar-HBPAMAM) enriched with amide groups, internal and terminal amines, mimicking the multifunctionality observed in PAMAM dendrimers. Moreover, we anticipate that the terminal amines in Ar-HBPAMAM can undergo strategic modifications to yield hydroxyl groups, resulting in an HBP with functionality comparable to OH-terminated PAMAM dendrimers. This strategic approach seeks to significantly enhance the versatility and functionalization potential of hyperbranched polymers, opening up new possibilities for a myriad of applications in materials science, drug delivery, and other fields. The ultimate goal is to contribute to the advancement of hyperbranched polymer technology, providing a platform for tailored properties and functionalities that can be tailored for specific applications.

The synthesis of the Ar-HBPPAMAM monomer entails a meticulous two-step process. In the first step, the monomer preparation is initiated through a well-established approach using conventional PAMAM techniques. Starting with 4-aminomethyl benzoic acid, the introduction of MA facilitates the formation of a diester. The reaction is carefully conducted, allowing the mixture to undergo stirring for 48 hours at room temperature, ensuring the completion of the process. Subsequent to this reaction period, the diester is subjected to purification steps, marking a critical phase in the synthesis to yield the purified Ar-HBPPAMAM monomer. This methodical approach is designed to produce a high-quality monomeric precursor with precision and reproducibility for subsequent stages in the synthesis process.
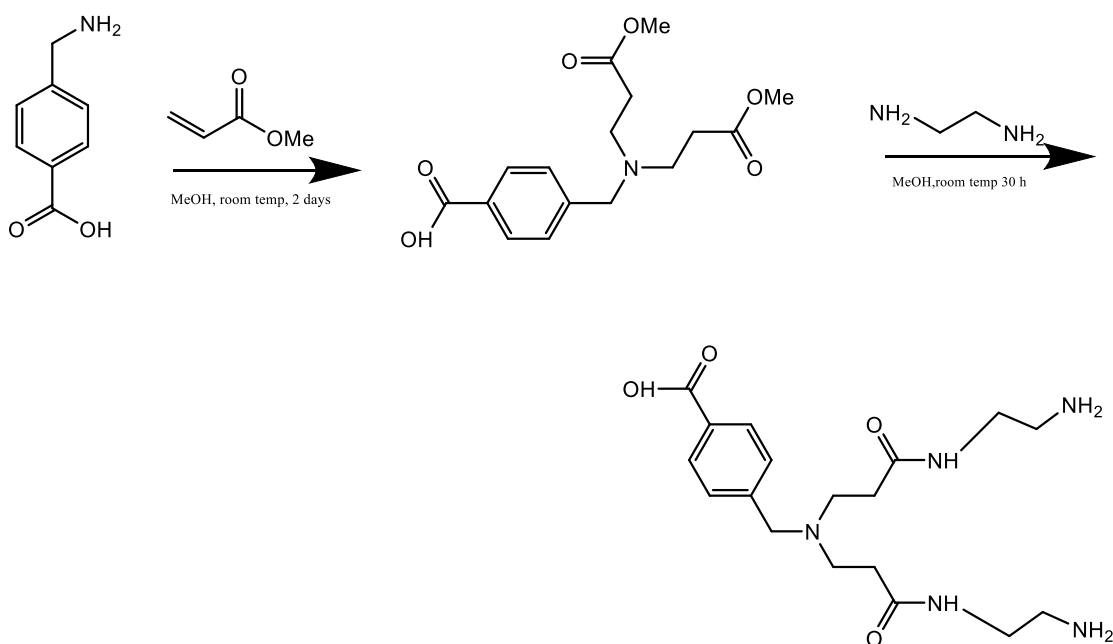
Figure 5.1 The monomer for Ar-HBPPAMAM was synthesized in two steps: first by preparing monomer through conventional PAMAM synthesis using 4-aminomethyl benzoic acid, followed by the addition of MA to produce diester.

In the subsequent reaction, a methodology akin to dendrimer amidation is employed. Diester is combined with a substantial excess of ethylenediamine to yield monomer, The use of an excess of EDA is imperative to prevent the previously mentioned side reactions The second step entails subjecting monomer to heating at 165°C for 30 hours under vacuum. This process culminates in the formation of a honey-colored glassy solid, indicative of the completion of the polymerization and the production of the hyperbranched polymer.

Synthesis of hydroxyl-terminated aromatic hyperbranched PAMAM polymer involves the conversion of terminal amines (Ar-HBPMAM) to hydroxyl groups using a procedure analogous to that employed for PAMAM dendrimers. The initial step entails modifying the amine group to ester terminal groups, resulting in Ar-HBPAMAM-OMe, through treatment with methacrylate. To confirm the conversion from Ar-HBPAMAM-OMe to Ar-HBPAMAM-OH, characterization will essential. The anticipated outcome involves the disappearance of the ester methyl peak, coupled with the emergence of new peaks corresponding to the methylene protons, serving as indicators of successful transformation.

152

Encapsulation of Ibuprofen will be carried out utilizing the synthesized aromatic hyperbranched PAMAM polymer (Ar-HBPAMAM-OH). Aqueous GPC analysis will be conducted to estimate the molecular weight, with the average determined by GPC being utilized for this purpose. Subsequently, the encapsulation ability of Ar-HBPAMAM-OH for drug molecules will be investigated at two concentrations. Based on the outcomes observed for HBPAMAM-NH2, it is anticipated that the concentration of encapsulated ibuprofen will exhibit a twofold increase with a corresponding twofold increase in polymer concentration.
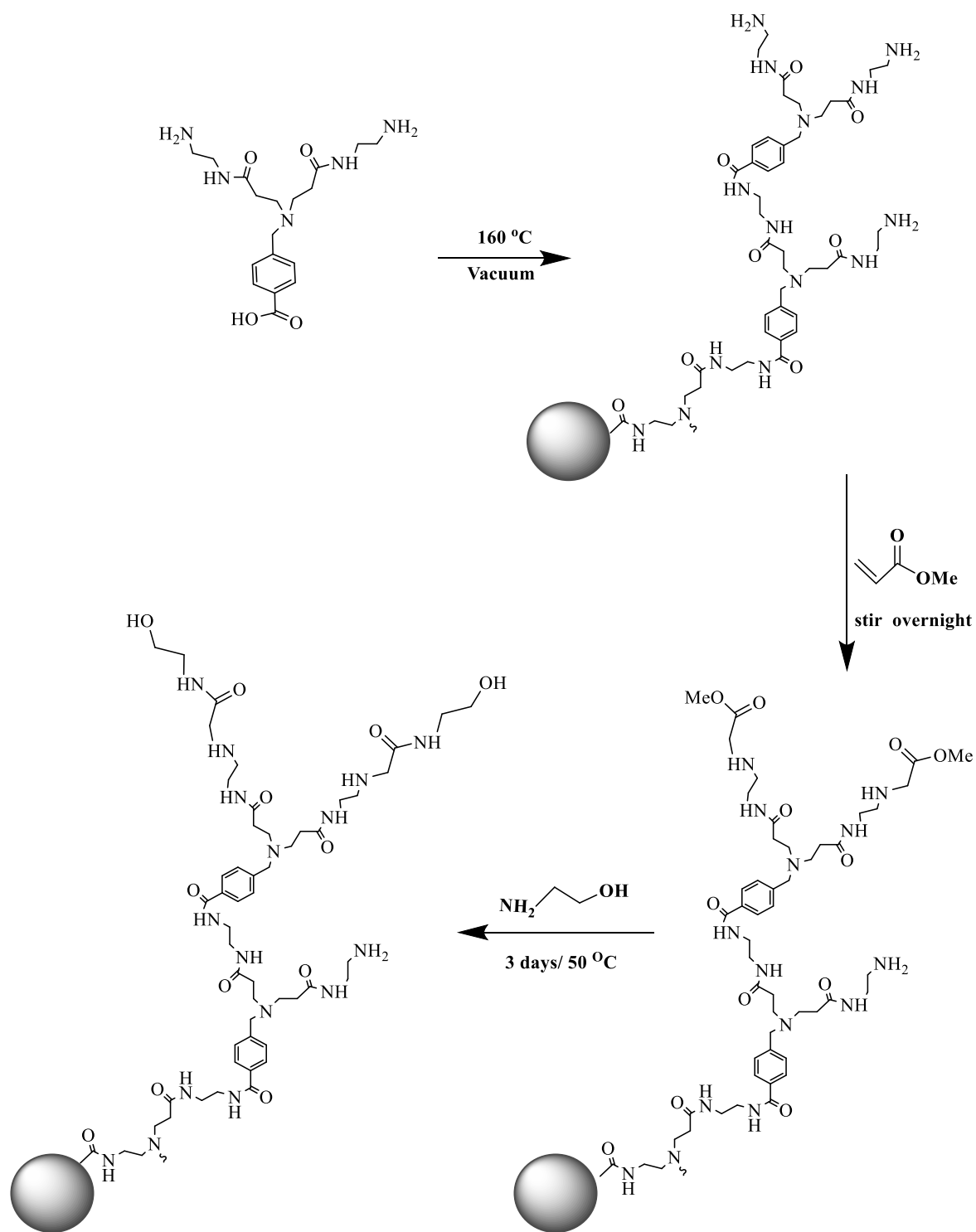
Figure 5.2 illustrates the synthesis of Ar-HBPAMAM. Firstly, reaction of monomer to give amine terminal Ar-HBPAMAM. Then the ester-terminated Ar-HBPAMAM will obtain by react with MA. Finally, product will react with ethanolamine to synthesis the hydroxyl terminated Ar-HBPAMAM-OH

Future scientific investigations also synthetic strategy is proposed for crafting a thiol-terminated dendrimer and incorporating amino acids with thioester functionality. This approach includes showcasing the thiol/thioester exchange reaction occurring on the surface of a minute dendrimer. The study further aims to develop multivalent dendrimer-chain complexes, incorporating diverse amino acids that can be presented on the dendrimer's surface. Additionally, a dynamic combinatorial approach will be explored, enabling the synthesis of functionalized dendrimers with different amino acid chains capable of forming cross-links, either with each other or with the dendrimer itself, especially in the presence of a protein. This dynamic approach seeks to enhance ligand binding opportunities at the dendrimer's binding surface, even in the absence of a protein template, and offers a promising avenue for versatile applications in various control reactions.
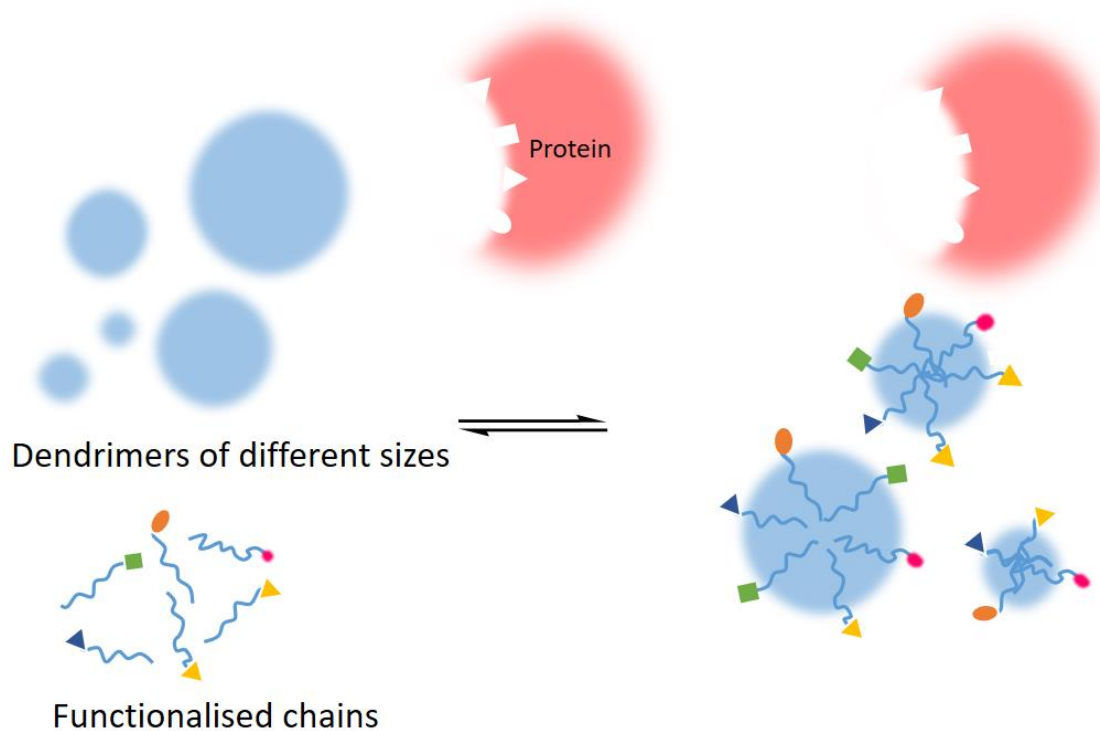
Figure 5.3 Shows Dynamic Combinatorial Library to self-selected dendrimer-protein complex.

Moving forward, further research is imperative with respect to in vitro studies to provide a more comprehensive comparison of the delivery capabilities of HBPs and dendrimers. Such studies should offer a deeper understanding of how both systems may enhance the delivery and therapeutic efficacy of

the drugs they transport, which is crucial for advancing the field of drug delivery. Another promising avenue for future investigation involves the further development of concepts related to solubilisation and site-specific delivery of photosensitisers for photodynamic therapy (PDT). This area of study holds the potential to revolutionise PDT by enhancing the selectivity and effectiveness of this therapy, offering new horizons in the treatment of various diseases, especially in the context of cancer.

In this case, the goal was to assess the improved protein-binding capabilities of functionalised Graphene Oxide (GO) as compared to unmodified GO, which is already recognised for its strong protein surface binding. The aim was thus to enhance this binding and potentially achieve selectivity by introducing functional groups, such as glutamic acid, with the latter being selected due to its significant role in protein-protein and protein-surface interactions.

Additionally, the impact of various factors, including the degree of functionalisation, the thickness of the surface modification, and the influence of spacers provided by oligomers on protein binding, were explored. Using an EDC coupling technique with unprotected glutamic acid, GO with an oligomeric layer of glutamic acid was successfully synthesised in a single step. A monomeric functionalised Graphene Oxide (GO) was also created using a slight modification of the same procedure, though this involved two steps. This process included the EDC-mediated introduction of C-protected Glutamic acid, followed by hydrolysis to eliminate the protective group. All GO configurations, encompassing both the monomeric and oligomeric layers, demonstrated the capacity to hinder chymotrypsin activity, signifying proficiency with protein binding. Upon reviewing the initial rate data, however, the oligomeric system displayed the most substantial inhibition, thereby demonstrating the most robust binding. This was nearly four times superior to that of unfunctionalized GO. Consequently, the monomeric system was deemed less efficient in inhibiting chymotrypsin activity as compared to the oligomeric functionalized GO. Typically, monomeric systems exhibit a limited number of accessible functional groups for interacting and binding with target molecules or processes. This reduced availability of binding sites can lead to weaker or less stable interactions, ultimately resulting in reduced inhibitory effects.

Additionally, within a monomeric system, functional groups often function independently, lacking the cooperative or synergistic effects observed in the oligomeric system. This contrasts with the tyrosine system, which can cooperatively bind to the protein surface. In the case of glutamic acid (Glu), there is no competition between protein binding and GO binding. This research has thus demonstrated the strong binding capability of functionalized GO with chymotrypsin, as well as confirming that the degree of oligomerisation plays a significant role in influencing binding affinity. The ongoing objective is thus to leverage these findings to develop innovative protein ligands and enzyme inhibitors with enhanced selectivity in their binding. Ongoing research thus focused on applying this methodology and the insights gained to designing and creating new GO inhibitors.

Successful synthesis of 3-trityl sulfanyl propanoic acid was achieved by combining trithylthiol with 3-bromopropionic acid in tetrahydrofuran (THF) at room temperature. Characterisation of the synthesised compound was carried out using various spectroscopic techniques, including ^{1}H and ^{13}C nuclear magnetic resonance (NMR) spectroscopy and infrared (IR) spectroscopy, which confirmed the presence of CH_2 and phenyl groups within the molecular structure. However, the attempt to synthesise N-(2-acetamidomethyl)-3-(triphenyl 4-sulfanyl) propenamide using a one-step synthesis utilising ethyl(dimethylaminopropyl) carbodiimide (EDC) as a coupling agent faced challenges and failed to yield the desired pure product despite multiple efforts to enhance yield and purity. As a result, a two-step procedure was explored, involving the synthesis of an acid chloride intermediate, which could then be reacted with the corresponding amine. Unfortunately, however, even after numerous attempts, no product was isolated using this two-step approach.

In recent years, dendrimers have shown significant promise as drug carriers. They possess the remarkable ability to encapsulate small host molecules within their spherical structures, especially at higher generations. Their capacity for functional modification also provides opportunities for both active and passive drug targeting, helping mitigate many associated side effects. However, it is important to acknowledge that dendritic systems are not without their limitations, as previously discussed.

Consequently, both the academic and industrial sectors have begun exploring alternative macromolecules for drug delivery, seeking options that may offer simplicity in synthesis, often achieved by using a one-pot process, unlike dendrimers. This project thus aimed to provide a comprehensive, like-for-like comparison of HBPs and dendrimers in terms of size and functionality, addressing a notable gap in the existing literature.

To achieve this, a series of PAMAM dendrimers, spanning from G 0.5 to G3.5, were synthesised. This synthesis involved the sequential repetition of Michael addition and amination steps to construct the desired dendrimers. A water-soluble PAMAM dendrimer (OH-ended PAMAM) was then created by converting the ester terminal groups into hydroxyl groups, resulting in OH-ended dendrimers (8OH, 16 OH, and 32 OH).

The initial investigation aimed to assess the dendrimers' capability with respect to encapsulating drug molecules, taking into account the dendrimer size and potential dense packing effects. This involved a focus on three generations of dendrimers, namely G2.0-OH, G3.0-OH, and G4.0-OH, each at a concentration of 1×10^{44} M. The dendrimers' ability to encapsulate the drug molecule was found to be contingent on the size of the PAMAM dendrimer generation; in particular, G 3.0-OH demonstrated the most efficient encapsulation of ibuprofen. The G4.0-OH, a higher dendrimer generation, was limited to encapsulating due to its densely packed structure. Consequently, the G2.0 and G3.0-OH dendrimers was identified as the most appropriate generation for the encapsulation of small hydrophobic drugs.

A study on concentration limits concerning the G2.0-OH dendrimer was then conducted at various concentrations ranging from 1.0×10^{3} to 1.0×10^{6} M. The results revealed that the amount of ibuprofen that the G3.0-OH dendrimer could encapsulate increased approximately linearly up to a dendrimer concentration of 2.5×10^{4} M. Beyond this concentration, the loading capacity remained constant, plateauing. Dynamic light scattering (DLS) measurements then indicated that dendrimers at concentrations exceeding 2.5×10^{4} M exhibited significantly larger sizes compared to those measured at lower concentrations (200 nm vs. 5 nm, respectively). A study conducted to measure the size

distribution for G2.0-OH at 1.0×10^4 M further substantiated the hypothesis that the observed decrease in encapsulation ability resulted from dendrimer aggregation at higher concentrations. This suggests that it is crucial to maintain concentrations below 2.5×10^4 M for future encapsulation experiments, particularly when making comparisons with equivalent HBPs.

The stability of the ibuprofen-dendrimer complexes was investigated over a ten-day period, under conditions of exposure to light and in darkness. This part of the study aimed to assess how dendrimer size influences the stability of complexes; thus, G2.0-OH, G3.0-OH, and G4.0-OH dendrimers were all tested. In the absence of light, it was observed that the stability of the drug complexes was approximately 50% greater than in those exposed to light, with degradation rates of 1.0×10^4 M and 5.0×10^5 M, respectively.

HBPs (HBPAMAM-NH_2) were also successfully synthesised; however, these exhibited instability under specific reaction conditions, preventing the conversion of their terminal groups to hydroxyl-ended groups. Nevertheless, encapsulation studies were conducted for both polymers, and these were compared to similar dendrimers, based on terminal groups. In the case of HBPAMAM-NH_2, the concentration of ibuprofen increased linearly until it reached 0.04 mg/mL, after which it plateaued. Dynamic light scattering (DLS) analysis indicated a more gradual aggregation in HBPs, as opposed to the more discrete aggregation observed in the dendrimers.

The final phase of this project, fulfilling one of its primary objectives, involved a comparative assessment of the encapsulation capabilities of similar HBPs and dendrimers, with the aim of evaluating the formers' potential as drug delivery systems. To begin this process, the encapsulation performances of HBPAMAM-NH_2 and G2 PAMAM NH2 dendrimers were examined. The findings for this revealed that the encapsulation abilities of HBP-NH2 and G2 dendrimers for drug molecules were not significantly different. For instance, the G2 PAMAM dendrimer and its equivalent could encapsulate ibuprofen to maximum concentrations of 6.85×10^3 and 7.48×10^3, respectively.

Overall, it is evident that HBPs represent viable and cost-effective alternatives to dendrimers when used in drug delivery systems. Nevertheless, it is important to note that dendrimers offer a regular and well-balanced monodisperse structure that readily meets the stringent size and dispersity requirements of drug approval agencies and potential clinical applications. In contrast, HBPs often exhibit high polydispersity in terms of molecular weights and structures, making it more challenging to produce the narrowly dispersed materials demanded by drug approval agencies. In order for HBPs to serve reliably as drug delivery systems, there is thus an ongoing need to enhance both synthesis and purification techniques.

Chapter 6

Materials and Methods

6.1 Instrumentals

Infrared (FTIR) Spectroscopy

Infrared spectroscopy relies on the principle that molecules absorb specific frequencies of infrared light, inducing molecular vibrations. This analytical method is adept at recognizing and examining chemicals based on their infrared absorption. The fundamental premise involves molecules absorbing particular infrared light frequencies, indicative of their structural characteristics. These frequencies correspond to the energy needed to excite the molecule from one vibrational level to another. When a sample is exposed to infrared radiation, specific frequencies are absorbed, causing the molecule to vibrate, such as stretching or bending, contingent on the bond type and molecular structure. The remaining light the pass through the sample and is detected on the other side. Through scrutinizing the absorbed light frequencies, valuable insights into the sample's molecular bonds and structure can be gleaned. The foundation of IR spectroscopy is rooted in quantum mechanics, positing that molecules can solely absorb energy in discrete units known as quanta. The energy of an absorbed infrared light photon is directly proportional to its frequency. Consequently, as a molecule absorbs an infrared photon, it acquires a specific amount of energy, inducing vibration. The frequency of the absorbed light corresponds to the energy disparity between two molecular vibrational levels. In practical terms, an IR spectrometer generates an absorption spectrum, portraying the intensity of absorbed light against frequency. Each peak in the spectrum aligns with a distinct molecular vibrational mode. By comparing the spectrum with reference spectra of known substances, the chemical compounds within the sample can be identified. In summary, the core principle of IR spectroscopy revolves around molecules selectively absorbing specific infrared light frequencies linked to their vibrational energy levels, ultimately aiding in the identification of bonds and molecular structures in the sample. FT-IR spectrometer was used, and the spectra was analysed by a Perkin Elmer.

NMR Spectroscopy

Nuclear Magnetic Resonance (NMR) operates on the principle that many nuclei possess spin and carry an electrical charge. If an external magnetic field is applied, an energy transfer occurs from the base energy to a higher energy level, typically a single energy gap. This transfer transpires at a wavelength corresponding to radio frequencies. Subsequently, as the spin returns to its original level, energy is emitted at the same frequency. The signal corresponding to this energy transfer is measured and processed to generate an NMR spectrum for the relevant nucleus. In the mechanism of nuclear magnetic resonance (NMR) Spectroscopy, the sample is positioned within a magnetic field, and the NMR signal is generated by exciting the nuclei with radio waves, leading to nuclear magnetic resonance. This resonance is then detected using sensitive radio receivers. The intramolecular magnetic field surrounding an atom in a molecule alters the resonance frequency, offering insights into the electronic structure of the molecule and its individual functional groups. Due to the uniqueness or high specificity of these fields to individual compounds, NMR spectroscopy stands as the definitive method for identifying monomolecular organic compounds. Beyond identification, NMR spectroscopy provide details about the structure, dynamics, reaction state, and chemical environment of molecules. While proton and carbon-13 NMR spectroscopy are the most prevalent types, the technique is applicable to any sample containing nuclei with spin. ^{1}H NMR and ^{13}C NMR spectra were measured using Brucker AVX400 MHz, Brucker HD400 MHz and Brucker AV1400 MHz.

Mass Spectrometry

Matrix Assisted Laser Desorption Ionization Time of Flight (MALDI-TOF) Spectrometry relies on the synergistic action of matrix-assisted laser desorption ionization and time-of-flight mass spectrometry. In MALDI-TOF, a crystalline matrix is crucial in facilitating the ionization of large biomolecules. When exposed to a laser beam, the matrix absorbs energy and transfers it to the analyte molecules, causing their ionization. The resulting ions are then accelerated through a vacuum tube by an electric field, and

the time taken to traverse a fixed distance correlates with the mass-to-charge ratio of the ions. High mass resolution and accuracy are achieved, enabling precise determination of molecular weights. This technique is widely employed in proteomics, genomics, and clinical diagnostics for analyzing biomolecules like proteins, peptides, nucleic acids, and carbohydrates. Electrospray Ionization Mass Spectrometry (ESI-MS) operates on the principle of generating ions from a solution through an electrospray process. In ESI-MS, a sample solution containing analyte molecules is sprayed through a fine capillary at a high voltage. The electric field causes the solvent to evaporate, leading to the formation of charged droplets. As these droplets further disintegrate, ions are produced, and the analytes are carried into the mass spectrometer. The resulting ions are then separated based on their mass-to-charge ratio, and the detector records their abundance. ESI-MS is particularly suitable for analyzing large biomolecules such as proteins and nucleic acids, and it has become a cornerstone in various fields, including biochemistry, pharmaceuticals, and environmental analysis, due to its sensitivity and ability to handle complex samples.

UV/Vis spectroscopy

UV-Visible Spectroscopy operates on the fundamental principle of light-matter interaction, specifically the absorption of ultraviolet (UV) or visible light by chemical compounds, leading to the generation of distinctive spectra. This analytical technique plays a pivotal role in elucidating the electronic structure of molecules and is rooted in the absorption of light energy by the electrons within the matter. The interaction between light and matter initiates processes of excitation and de-excitation, ultimately manifesting as a spectrum. When a chemical compound absorbs ultraviolet radiation, the electrons within it undergo excitation, transitioning from a ground state—characterized by a relatively low energy level—to an excited state marked by a higher energy level. This electron excitation is a direct consequence of the absorption of ultraviolet or visible radiation. Notably, the energy difference between the ground state and the excited state corresponds precisely to the amount of energy carried by the absorbed radiation. This principle is consistent with the basic tenets of quantum mechanics, where

discrete energy levels are associated with electron transitions. Expanding on this principle, the UV-Visible Spectroscopy technique involves illuminating a sample with a broad spectrum of UV or visible light and measuring the extent of light absorption at different wavelengths. The resulting spectrum, known as an absorption spectrum, is a graphical representation of the absorption characteristics of the compound under scrutiny. Peaks and troughs in the spectrum correspond to specific electronic transitions, providing valuable insights into the molecular structure and composition of the substance. UV-Visible Spectroscopy hinges on the absorption of light by chemical compounds, leading to electronic excitation and the production of characteristic spectra. This technique's ability to unravel the intricacies of molecular electronic transitions has made it an indispensable tool in fields ranging from chemistry and biology to materials science and environmental analysis. Through the lens of UV-Visible Spectroscopy, researchers gain a deeper understanding of the electronic properties and behavior of diverse chemical entities. And the measurement was carried out by Analytik Jena AG Specord S600 and recorded by the Software (WinASPECT).

The Raman spectroscope

Raman Spectroscopy, a powerful analytical technique, is grounded in the theory of inelastic scattering of light, known as the raman effect. When monochromatic light, typically emitted from a laser, interacts with a sample, a small fraction of photons undergoes inelastic scattering due to interactions with the molecular vibrations, rotations, and other low-frequency modes within the sample. The raman effect results in scattered photons with frequencies that differ from the incident photons, revealing valuable information about the vibrational and rotational properties of the molecules. The key principle lies in the energy exchange between incident and scattered photons during molecular transitions. When the energy of scattered photons is lower than that of the incident photons, it leads to Stokes scattering. Conversely, in anti-Stokes scattering, the scattered photons have higher energy than the incident photons. The energy differences, quantified as the Raman shift, are unique to each molecular interaction, producing a distinct spectrum. Raman Spectroscopy is renowned for its ability to provide detailed

insights into molecular structures, making it an invaluable tool across various scientific disciplines, from chemistry and biology to materials science and beyond. And raman spectra of samples were recorded from 500 to 3500 cm^{1} on a Renishaw in Via Raman Microscope using a green laser operating at wavelength of 514.5 nm and laser power at 20 mV.

X-ray photoelectron spectroscopy (XPS)

X-ray Photoelectron Spectroscopy (XPS), also known as Electron Spectroscopy for Chemical Analysis (ESCA), stands as a highly valuable quantitative spectroscopic technique specifically designed for surface chemical analysis. Operating on the principle of measuring both the kinetic energy and the number of electrons emitted when a sample is exposed to a beam of X-ray radiation under high vacuum conditions, XPS offers unparalleled insights into the elemental composition, empirical formula, chemical state, and electronic state of the material's constituting elements. In the XPS process, X-ray radiation interacts with the sample, leading to the emission of photoelectrons. By precisely measuring the kinetic energy of these emitted electrons, valuable information about the binding energy levels and the chemical environment of the atoms in the sample is obtained. The resulting XPS spectra serve as a rich source of data, enabling the qualitative, quantitative, or semi-quantitative analysis of the sample. This technique is particularly surface-sensitive, providing detailed information about the top few nanometers of a material. The elemental sensitivity of XPS is due to the distinct binding energies associated with different elements, allowing for the identification and quantification of individual elements present in the sample. Furthermore, the chemical state information provided by XPS sheds light on the electronic configuration and bonding environment of the analyzed elements. XPS has found widespread applications in diverse scientific fields, including materials science, catalysis, and surface chemistry, making it an indispensable tool for researchers seeking comprehensive insights into the composition and properties of surfaces and thin films. X-ray photoelectron spectroscopy measurements were performed using monochromatic Al- kα radiation (hν = 1486.69 eV). Casa XPS v 2.3.16 software was used to record curve fitting and to calculate the atomic concentrations.

Thermal conductivity analysis (TGA)

Thermogravimetric Analysis (TGA) is a powerful analytical technique designed to measure the weight changes in a material as a function of temperature or time under controlled atmospheric conditions. The fundamental principle of TGA finds applications in various aspects, including assessing a material's thermal stability, determining filler content in polymers, quantifying moisture and solvent content, and analyzing the percent composition of components within a compound. TGA plays a crucial role in a multitude of applications, providing insights into critical parameters such as the filler content of polymer resins, residual solvent content, carbon black content, decomposition temperature, moisture content in organic and inorganic materials, plasticizer content in polymers, oxidative stability, and the performance of stabilizers. It is particularly effective in identifying low molecular weight monomers in polymers, contributing to a comprehensive understanding of material composition. The principle of TGA operation involves subjecting a sample to a gradual increase in temperature within a furnace while concurrently measuring its weight using an analytical balance located outside the furnace. Mass loss is observed during thermal events that involve the release of volatile components, with chemical reactions like combustion contributing to measurable mass losses, whereas physical changes such as melting do not. The resulting data, typically represented as a plot of sample weight against temperature or time, offers a visual representation of thermal transitions within the material. This includes the loss of solvent and plasticizers in polymers, water of hydration in inorganic materials, and ultimately, the decomposition of the material. TGA, with its versatility and precision, serves as a cornerstone in material characterization, aiding researchers and industry professionals in unravelling the intricate thermal behaviours and compositions of diverse materials. Thermogravimetric Analysis (TGA) was conducted by employing a Perkin Elmer Pyris instrument, within the temperature range of 25°C to 800°C, under a controlled atmosphere of dry flowing nitrogen. The obtained data was subsequently analyzed using Origin software.

X-ray diffraction (XRD) patterns

X-ray Diffraction (XRD) operates on the fundamental principle of constructive interference between monochromatic X-rays and a crystalline sample, providing invaluable insights into the crystal structure of materials. The X-rays, initially generated by a cathode ray tube, undergo a meticulous process to ensure monochromaticity and directional focus before being directed towards the crystalline sample. To initiate the constructive interference, the incident X-rays interact with the crystal lattice of the sample, resulting in the production of a diffracted ray. This phenomenon is governed by Bragg's Law ($n\lambda = 2d \sin \theta$), which establishes a relationship between the wavelength of the incident X-rays, the diffraction angle (θ), and the lattice spacing (d) in the crystalline sample. The law dictates that under specific conditions, the diffracted X-rays will exhibit constructive interference, producing detectable peaks. The diffracted X-rays are then meticulously detected, processed, and counted. To comprehensively explore the crystal lattice's various orientations, the sample is systematically scanned through a range of 2θ angles. This approach ensures the attainment of all possible diffraction directions, especially crucial in the case of randomly oriented powdered materials. The conversion of diffraction peaks into d-spacings serves as a crucial step in the identification process, as each mineral possesses a distinct set of unique d-spacings. This identification is achieved by comparing the observed d-spacings with established standard reference patterns. Through this comparison, the mineral composition of the sample can be accurately deduced, making X-ray Diffraction an indispensable tool in material science, geology, and various other scientific disciplines. The precision and specificity of XRD in revealing the crystalline structures of diverse materials contribute significantly to our understanding of their properties. The X-ray diffraction (XRD) patterns were acquired using the Bruker D8 Advance diffractometer equipped with a copper target (CuKα = 1.54178 Å). The XRD measurements were conducted with a tube voltage of 40 kV and a tube current of 35 mA. The patterns were collected in the range of 5-100° at a scanning speed of 0.05°/min.

Elemental Analysis

Elemental Analysis (EA) is a critical analytical technique employed in chemistry to determine the elemental composition of chemical compounds and their complexes. This method facilitates the identification of present elements and quantifies the mass percentage of each chemical element in the tested substance, thereby establishing the empirical formula. While elemental analysis provides insight into the overall molecular weight, it does not reveal the molecular structure, or the specific arrangement of atoms connected by chemical bonds. The principle of elemental analysis involves controlled combustion of samples within a reactor and subsequent measurement of the corresponding oxides produced during this process. Samples undergo combustion in a column equipped with an oxidizing-reducing catalytic bed, maintaining an electronically controlled temperature. Elemental analysis focuses on determining the amounts of carbon (C), hydrogen (H), nitrogen (N), and sulfur (S). Oxygen content is often derived indirectly by calculating the difference between the total percentage and the sum of CHNS elements. However, for precise analyses, a separate procedure involving pyrolysis determines the oxygen content. In the CHNS + O procedure, samples are introduced in tin or silver crucibles under an inert atmosphere (He, Ar), with oxygen injected for combustion during CHN analysis. The catalytic bed, typically containing CuO or WO_3, yields evolved gases such as N_2, $NxOy$, CO_2, H_2O, SO_2, and SO_3. A reduction column eliminates excess oxygen, leading to the final calculation of N, C, H, S. The oxygen content is obtained separately through the pyrolysis process. Elemental analysis is a versatile technique providing essential information about the elemental composition of substances, contributing significantly to diverse scientific fields such as chemistry, material science, and environmental science. Its ability to determine the presence and percentage of key elements makes it a foundational tool in elucidating the chemical composition of various compounds. The elements analysed using a Vario MICRO Cube CHN/S analyser and solid samples were used.

Scanning electron microscope

The Scanning Electron Microscope (SEM) and Energy-Dispersive X-ray (EDX) analysis are complementary techniques that enable detailed investigations of materials at the nanoscale. Scanning Electron Microscope (SEM): The SEM utilizes an electron beam to achieve high-resolution imaging of samples down to the nanometer scale. The working principle involves the emission of electrons from a filament, collimation into a beam, and subsequent focusing on the sample surface by an electron column. The electron lenses within the column, including the condenser and objective lenses, manipulate the trajectory of the electrons using magnetic fields. The condenser lens converges the electrons into a focused beam, and the objective lens focuses this beam onto the sample surface. Scan coils control the scanning motion of the electron beam, generating detailed images by directing the beam in a raster pattern. The result is a comprehensive visualization of the sample's surface morphology at high magnification. SEM is invaluable for studying materials at the micro and nanoscale, providing insights into their structural features, topography, and composition. Whereas energy-Dispersive x-ray (EDX) Analysis is an elemental analysis technique that complements SEM. It operates by bombarding a sample with high-energy x-rays, inducing inner-shell ionization and the subsequent emission of characteristic x-rays from the sample's atoms. The energy-dispersive detector then measures the energies of these emitted x-rays, producing an energy spectrum known as the EDX spectrum. Peaks in the spectrum correspond to the characteristic x-rays of different elements present in the sample. Quantitative information about elemental composition is obtained by analyzing the intensity of these peaks. EDX is particularly effective when coupled with SEM, allowing for spatially resolved elemental analysis. By integrating these two techniques, researchers can not only visualize the surface morphology of a sample but also determine its elemental composition, offering a comprehensive understanding of the material's characteristics. SEM and EDX analysis work in tandem to provide a holistic approach to materials characterization. SEM facilitates high-resolution imaging, revealing surface details, while EDX analysis complements this by offering insights into the elemental composition. The combination of these techniques allows scientists to explore the intricate world of materials at the nanoscale, unlocking a wealth of information about their structure, morphology, and chemical composition. scanning electron

microscope (SEM) analysis was performed using a JEOL-7001F instrument operated at 15 kV. Solid samples were employed for both the SEM and energy-dispersive x-ray (EDX) analysis. The samples were placed in a vacuum and subsequently gold coated.

The principles and rationales governing the synthetic protocols devised for the functionalization of Graphene Oxide (GO) and the synthesis of Polyamidoamine (PAMAM) dendrimers. The strategic design of these protocols is grounded in the pursuit of precision, control, and reproducibility, essential for crafting advanced materials with tailored functionalities. In the realm of functionalized Graphene Oxide, a multi-step process involving the incorporation of amino acid methyl esters, such as tyrosine and valine, unfolds under ultrasonic oscillation and controlled reaction conditions. Triethylamine, DMAP, and EDC.HCl act as catalysts, ensuring uniform dispersion and high-yield product formation. The described synthetic protocol outlines the stepwise process for the production of functionalized graphene oxide (GO) and subsequent synthesis of PAMAM dendrimers of varying generations. The overall principles and rationale of the synthetic procedure are designed to achieve controlled functionalization of GO and the generation of PAMAM dendrimers with hydroxyl end groups. In the first section, the synthesis of graphene oxide involves the oxidation of graphite particles using a mixture of concentrated H_3PO_4 and H_2SO_4, along with $KMnO_4$. The resulting product undergoes several purification steps, including centrifugation, washing with water and HCl, and vacuum drying, ultimately yielding dark brown solid graphene oxide. Following the synthesis of graphene oxide, functionalization is performed with two different amino acids, tyrosine methyl ester (Tyr-OCH$_3$) and L-valine methyl ester. The functionalization involves the reaction of GO with triethylamine, DMAP, and EDC.HCl, resulting in two different functionalized graphene oxide derivatives. The resulting products are characterized by their color, yield, and structural analysis, demonstrating successful functionalization.Subsequently, the synthesis of a trityl thiol compound and its conversion to 3-trityl sulfanyl propanoic acid is described. This involves the addition of trityl thiol to NaH, followed by the addition of 3-bromopropionic acid. The resulting compound is characterized using NMR spectroscopy.

The synthesis then moves on to the preparation of N-(2-acetamidomethyl)-3-(triphenyl 4-sulfanyl) propanamide, where 3-(tritylthio) propionic acid reacts with N-(2-aminoethyl) acetamide in the presence of EDC, HOBt, DMAP, and DIPEA. The resulting product is purified and characterized. The subsequent sections detail the synthesis of PAMAM dendrimers of various generations (G0.5 to G4.0). The synthetic steps involve the reaction of ethylenediamine (EDA) with methyl acrylate and subsequent purification steps. Each generation of PAMAM dendrimer is characterized using various analytical techniques, including FTIR, NMR, and mass spectrometry. The final section describes the synthesis of neutral PAMAM dendrimers with OH-terminated groups. The synthesis involves the reaction of half-generation PAMAM dendrimers with DMSO, potassium carbonate, and ethanolamine. The resulting OH-terminated dendrimers are characterized using FTIR, NMR, and mass spectrometry. Overall, the synthetic protocol provides a comprehensive approach to the controlled synthesis of functionalized graphene oxide and PAMAM dendrimers, demonstrating the careful design and execution of each step to achieve the desired products. The use of various analytical techniques for characterization ensures the quality and purity of the synthesized compounds at each stage of the process.

6.1.2 Synthesis of Graphene Oxide (GO)

2.95 g (1.0 eq) of graphite particles were added to a 1:9 mixture of concentrated H_3PO_4/H_2SO_4 (40:380 V/V), and 18.0 g (6.0 eq) of $KMnO_4$. The mixture was stirred for 24 hours, allowing the reaction to cool at room temperature. The container was poured onto ice along with 4 mL of 30% H_2O_2. After centrifuging the crude product at 4000 rpm for 35 minutes, the supernatant was gathered. The crude product underwent multiple washes using 400 mL of water. The crude product was further treated by combining 400 mL of 30% HCl with 400 mL of ethanol until the pH of the solution reached a stable level. To induce coagulation, 400 mL of diethyl ether was added to the solution, and the resulting mixture was then filtered to separate the suspension. The precipitate collected on the filter was vacuum-dried at ambient temperature for 24 hours, resulting in a yield of 5.5 g (85%) as a dark brown solid.

6.1.3 Functionalized Graphene Oxide

Graphene oxide functionalized with methyl ester of tyrosine (Tyr-OCH3)

GO was diluted in 100 mL of deionized water using ultrasonic oscillation for 3 hours (0.25 g, 1 eq). Triethylamine (3.94 g, 39.0 mol), L-tyrosine methyl ester (2.5 g, 0.013 mol), DMAP (3.17 g, 0.026 mol), and EDC.HCl (4.98 g, 0.026 mol) were added to 10 eq of the mixture. The reaction mixture was stirred and refluxed at 75 °C for twenty-four hours, allowing the reaction to reach room temperature before proceeding to the next step. 100 mL of brine was used to rinse the raw product three times. After 45 minutes of centrifugation of the filtrate at 4000 rpm, the supernatant was drained off. Before being desiccated at 60 °C, the precipitate was washed with 2 L of water and ethanol once more. A black solid (0.40 g, 80%) was obtained.

Graphene Oxide – Valine -OCH3

GO (0.25 g, 1 eq) was dispersed in 100 ml of deionized water and sonicated with ultrasonic oscillation for 4 hours. The mixture was added to an excess of L-Valine methyl ester (2.17 g, 0.013 mol), followed by

Triethylamine (3.95 g, 0.039 mol), DMAP (3.17 g, 0.026 mol), and EDC HCl (5 g, 0.026 mol) added to 10 eq of the mixture. The reaction mixture was stirred and refluxed at 75 °C for 24 h. The reaction was allowed to cool to room temperature and washed with brine (100 ml × 4). The filtrate was centrifuged for 45 minutes (4000 rpm), and the supernatant produced was decanted off. The precipitate was washed again with water and ethanol. The product was dried at 60°C, and (0.41 g, 80%) of the product was obtained as a black powder.

3-trityl sulfanyl propanoic acid

Trityl thiol (3.1 g, 0.010 mol) in THF (10 mL) was added to NaH (440.0 mg, 0.010 mol) in THF (5 mL), which had been washed with pentane, at 0°C. The addition was performed gradually over a period of 5 minutes, followed by stirring the mixture at room temperature for 15 minutes. Subsequently, the mixture was placed in a cold bath, and 3-bromopropionic acid (2.19 g, 0.010 mol) was added. After stirring at room temperature for 40 minutes, the mixture was concentrated, and the resulting mixture was partitioned between EtOAc (25 mL) and H2O (15 mL). The organic layer was dried using MgSO4, and the solvent was evaporated under reduced pressure. The obtained yield was 4.06 g (90% yield): 4.06 g (90%). ^{1}H-NMR CDCL3):H 2.15 (2H, t, CH2), 2.38 (2H, t, CH2), 7.13-7.23 (12H, m, J 6.5 , H-PH), 7.37 (3H, d, H-PH). ^{13}C-NMR (CDCL$_3$),CNMR 26.48 (CH$_2$), 33.00 (CH$_2$), 55.77 (C(PH)3), 126.72 (PH), 127.93 (PH), 129.52 (PH), 146.93 (PH), 156.27 (C=O).

Synthesis of N-(2-Acetamidomethyl)-3-(Triphenyl 4-Sulfanyl) Propanamide

A stirred solution of 3-(Tritylthio) Propionic Acid (0.05 g, 0.20 mmol, 1.0 eq) in AcCN (2 mL) was combined with N-(2-Aminoethyl) Acetamide (0.04 g, 0.24 mmol, 1.2 eq), EDC (0.04 g, 0.20 mmol, 1.0 eq), HOBt (0.003 g, 0.020 mmol, 0.1 eq), DMAP (0.02 g, 0.20 mmol, 1.0 eq), and DIPEA (1 mmol, 5.0 eq) at 23°C. The progress of the reaction was monitored by TLC (eluent phase = acetone/hexane = 50%). After completion of the reaction, the solvent was evaporated by rotary evaporation and concentrated under reduced pressure. Subsequently, the reaction mixture was diluted with EtOAc, quenched with a saturated NaHCO3 solution, and extracted with EtOAc (2x100 mL). The combined organic extracts

were dried over anhydrous Na2SO4, filtered, and concentrated under reduced pressure. The crude compound was purified by column chromatography over silica gel (30% acetone/hexanes) to afford the pure product. The resulting yield was 40 mg (45%). (1H-NMR CDCL3): 1H: 0.71-0.83 (6H, 0.77 (q, J = 8.1 Hz), 0.77 (q, J,8.1 Hz)), 0.84-0.98 (6H, 0.90 (t, J,6.9 Hz), 0.90 (t, J, 6.9 Hz), 0.93 (t, J ,7.3 Hz), 1.37-1.50 (2H, 1.44 (t, J ,7.3, 6.9 Hz), 1.86 (3H, s), 2.29 (9H), 3.12-3.54 (t, J,7.2 Hz), 7.36 (15H, dd).

6.1.4 Synthesis of PAMAM Dendrimer

Synthesis of PAMAM dendrimer G 0.5

Over a period of 30 minutes, EDA (5 g, 0.08 mol) in methanol (150 mL) and methyl acrylate (42 g, 0.4 mol) were added. The mixture was stirred at ambient temperature for 23 hours. The excess solvent and unreacted methyl acrylate were removed and purified. The resulting product, G0.5, was obtained as a yellow oil with a yield of (50 g, 98%). The characterization of the product was carried out as follows: FTIR (cm^{-1}), 2950 (OCH_3), 1728 (C=O), 1445 (CH_2),1173 (CO), 1125, 1038 (C-N); ^1H NMR (400 MHz, MeOD), 3.69 (12H, Singlet, OCH_3), 2.76 (8H, t ,J 7.0 Hz, NCH2CH2CO), 2.52 (4H, s, CH2N), 2.49 (8H, t, J 7.0 Hz, NCH_2CH_2CO); ^{13}C NMR (100 MHz, MeOD), 173 (C=O), 52.0, 51.0 (CH_3), 48.5, 32.0 (CH_2); Mass spec (ES), 406

Synthesis of PAMAM dendrimer G 1.0

EDA (60 g, 0.99 mol) was added dropwise over a period of 45 minutes to a solution of PAMAM G0.5 (22 g, 0.04 mol) in methanol (120 mL). The mixture was allowed to react at room temperature for three days. Methanol and excess EDA were then removed under reduced pressure at 45°C. The resulting product was purified using an azeotropic solution (1.0 L of 1:9 toluene: methanol) and washed with methanol (100 mL). The purification process was repeated several times to extract all remaining EDA, and the product was subsequently dried under reduced pressure. G1.0 was obtained as a yellow oil with a yield of 70 g (95%). The product was characterized as follows: FT-IR spectroscopy showed characteristic peaks at 3285 cm^{-1} (N-H stretch), 2939 cm^{-1} (C-H stretch), 1647 cm^{-1} (C=O), 1565 cm^{-1}

(N-H bend), and 1463 cm^{-1}, 1442 cm^{-1} (C-H bend). ^{1}H NMR spectroscopy (at 400 MHz in MeOD) exhibited signals at 3.27 ppm (8H, t, J 6.5 Hz CONHCH$_2$), 2.76 ppm (8H, t, J 7.0 Hz, CH2NCH2), 2.74 ppm (8H, t, J 6.5 Hz, CH$_2$CH$_2$NH$_2$), 2.55 ppm (4H, s, CH$_2$N), and 2.38 ppm (8H, t, J 7 Hz, CH2CONH). ^{13}C NMR spectroscopy (at 100 MHz in MeOD) showed signals at 174.0 ppm (C=O), 52.0 ppm, 50.0 ppm, 42.0 ppm, 40.5 ppm, and 32.5 ppm (CH2). Mass spectrometry (ES) yielded a measured mass of 516 (calculated).

Synthesis of PAMAM dendrimer G 1.5

PAMAM G1.0 (30.7 g, 0.059 mol) was dissolved in 100 mL of methanol and stirred at 0°C for 45 minutes while methyl acrylate (103.2 g, 1.20 mol) was added dropwise. The mixture was allowed to react at room temperature for three days. After completion of the reaction, the solvent was concentrated under reduced pressure at 45°C. The resulting substance was dried and obtained as a yellow oil (63 grams, 87% yield). The product was characterized as follows: FTIR spectroscopy revealed characteristic peaks at 3312 cm-1 (N-H stretch), 2952 cm^{-1} (C-H stretch), 2876 cm^{-1}, 1735 cm^{-1} (C=O, ester), 1650 cm^{-1} (C=O), 1537 cm^{-1} (N-H), and 1436 cm^{-1} (CH2 bend). ^{1}H NMR spectroscopy (at 400 MHz in MeOD) exhibited signals at 3.68 ppm (24H, s, OCH3), 3.27 ppm (8H, t, J 6.5 Hz, NHCH$_2$), 2.80 ppm (24H, t, J 7.0 Hz, NCH$_2$), 2.57 ppm (12H, t, J 6.5 Hz, CH$_2$N), 2.48 ppm (16H, t, J 7.0 Hz, CH$_2$CO), and 2.41 ppm (8H, t, J 7.0 Hz, CH$_2$CO). ^{13}C NMR spectroscopy (at 100 MHz in MeOD) showed signals at 172.3 ppm (C=O), 171.4 ppm (C=O), 53.3 ppm, 52.5 ppm (CH$_3$), 51.0 ppm, 50.0 ppm, 49.5 ppm, 38.0 ppm, 33.5 ppm, and 33.0 ppm (CH$_2$). Mass spectrometry (ES) yielded a measured mass of 1205 (M), 1227 (MNa+), while the calculated mass for $C_{54}H_{96}N_{10}O_{2}0$ is 1205.

Synthesis of PAMAM dendrimer G 2.0

PAMAM G1.5 (40.70 g, 0.033 mol) and EDA (32.4 g, 5.39 mol) were added dropwise to a solution of methanol (100 mL) over a period of 45 minutes. The resulting mixture was allowed to react at room temperature for six days. The EDA was completely removed through purification using an azeotropic solvent (2.0 L mixture of 9:1 toluene: methanol) and subsequent rinsing with methanol (100 mL). The

substance was dried, resulting in the formation of G2.0 4 as a sticky yellow oil (47 g, 94% yield). The product was characterized as follows: FTIR spectroscopy showed characteristic peaks at 3286 cm^{-1} (N-H stretch), 2937 cm^{-1} (C-H stretch), 1647 cm^{-1} (C=O, amide), and 1561 cm^{-1} (N-H). ^{1}H NMR spectroscopy (at 400 MHz in MeOD) exhibited signals at 3.27 ppm (24H, t, J 6.0 Hz, NHCH2), 2.81 ppm (24H, t, J 7.0 Hz, NCH$_2$), 2.74 ppm (16H, t, J 6.0 Hz, CH$_2$NH$_2$), 2.60 ppm (12H, t, J 7.0 Hz, CH$_2$N), and 2.35 ppm (24H, t, J 6.5 Hz, CH$_2$CO). ^{13}C NMR spectroscopy (at 100 MHz in MeOD) showed signals at 174.0 ppm (C=O), 173.5 ppm (C=O), 52.5 ppm, 51.0 ppm, 50.0 ppm, 42.0 ppm, 41.0 ppm, 37.5 ppm, 33.2 ppm, and 32.5 ppm (CH$_2$). Mass spectrometry (ES) yielded a measured mass of 1430 (MH+), while the calculated mass for C$_{62}$H$_{128}$N$_{26}$O$_{12}$ is 1429.

Synthesis of PAMAM dendrimer G 2.5

PAMAM G2.0 (29.18 g, 20.42 mmol) was dissolved in 100 mL of methanol and stirred for 45 minutes while methyl acrylate (70.74 g, 0.82 mol) was added dropwise. The mixture was allowed to react at room temperature for five days. Excess methyl acrylate and solvent were removed at 45°C under reduced pressure. G2.5 5 (42 g, 72% yield) was obtained as a sticky yellow oil by drying the product under high vacuum. The characterization of the product provided the following results: FTIR spectroscopy revealed peaks at 3298 cm^{-1} (N-H stretch), 2954 cm^{-1} (C-H stretch), 1730 cm^{-1} (C=O, ester), 1640 cm^{-1} (C=O, amide), 1553 cm^{-1} (N-H, amide bend), and 1437 cm-1 (CH$_2$). ^{1}H NMR spectroscopy (at 400 MHz in MeOD) exhibited signals at 3.69 ppm (48H, s, OCH$_3$), 3.29 ppm (24H, t, J 6.5 Hz, NHCH2), 2.81 ppm (24H, t, J 7.0 Hz, NCH$_2$), 2.78 ppm (32H, t, J 7.0 Hz, NCH$_2$), 2.62 ppm (12H, t, J 7.0 Hz, NCH$_2$), 2.59 ppm (16H, t, J 6.5 Hz, CH$_2$N), and 2.47 ppm (32H, t, J 7.0 Hz, CH$_2$CO). ^{13}C NMR spectroscopy (at 100 MHz in MeOD) showed signals at 173.0 ppm (C=O), 172.0 ppm (C=O), 171.0 ppm (C=O), 53.0 ppm, 52.5 ppm, 52.0 ppm (CH$_3$), 50.0 ppm, 49.7 ppm, 49.5 ppm, 37.5 ppm, 37.0 ppm, 34.0 ppm, 33.5 ppm, and 32.0 ppm (CH$_2$). Mass spectrometry (ES) yielded a measured mass of 2806 (MH+), while the calculated mass for C$_{126}$H$_{224}$N$_{26}$O$_{44}$ is 2807.

Synthesis of PAMAM dendrimer G 3.0

In a 100 mL methanol solution, PAMAM G2.5 (24.78 g, 8.82 mmol) was stirred. Over a span of 45 minutes, EDA (104.48 g, 1.74 mol) was added dropwise. The resulting mixture was left to react at room temperature for 7 days. To eliminate EDA from the crude product, a 2.0 L mixture of toluene and methanol in a 1:9 ratio was utilized as an azeotropic solution at 45°C. The purification process was repeated, followed by a wash with 100 mL of methanol. The resulting product, G3.0 6, was obtained as a yellow oil weighing 28 g with a purity of 97%. The characterization of the product yielded the following data: FT-IR spectroscopy exhibited peaks at 3290 cm^{-1} (N-H stretch), 3089 cm^{-1} (C-H stretch), 1636 cm^{-1} (C=O), 1564 cm^{-1} (N-H), and 1486 cm^{-1} (CH$_2$). ^{1}H NMR spectroscopy (at 400 MHz in MeOD) showed signals at 3.27 ppm (24H, t, J 7.0 Hz, NHCH$_2$), 2.82 ppm (32H, t, J 6.0 Hz, CH$_2$N), 2.71 ppm (56H, t, J 7.0 Hz CH$_2$N), 2.58 ppm (32H, t, J 6.0 Hz, NCH$_2$), and 2.38 ppm (56H, t, J 7.0 Hz, CH2CO). ^{13}C NMR spectroscopy (at 100 MHz in MeOD) displayed signals at 175.5 ppm (C=O), 174.8 ppm (C=O), 174.6 ppm (C=O), 51.4 ppm, 49.1 ppm, 41.64 ppm, 39.9 ppm, 36.8 ppm, and 33.8 ppm (CH$_2$). Mass spectrometry (ES) yielded a measured mass of 3257 (MH+), while the calculated mass for C$_{142}$H$_{288}$N$_{58}$O$_{28}$ is 3256.

Synthesis of PAMAM dendrimer G 3.5

PAMAM G3.0 (24.98 g, 7.68 mmol) was dissolved in 100 mL of methanol and stirred. Dropwise additions of methyl acrylate (51.62 g, 0.60 mol) were made over a period of 45 minutes. The mixture was left to react for four days. Surplus methyl acrylate and solvent were removed at 45°C under reduced pressure. The product, G3.5, was obtained as a sticky yellow oil with a yield of 38 g (81%). The product was characterized using various techniques, and the obtained data are as follows: FTIR spectroscopy showed peaks at 3296 cm^{-1} (N-H stretch), 2952 cm^{-1} (C-H stretch), 2832 cm^{-1}, 1737 cm^{-1} (C=O, ester), 1643 cm^{-1} (C=O, amide), 1555 cm^{-1} (N-H bend), and 1445 cm^{-1} (CH$_2$). ^{1}H NMR spectroscopy (at 400 MHz in MeOD) exhibited signals at 3.69 ppm (96H, s, OCH$_3$), 3.29 ppm (24H, t, J 5.0 Hz, NHCH2), 2.86 ppm (32H, t, J 6.0 Hz, NCH$_2$), 2.78 ppm (56H, t, J 7.0 Hz ,NCH$_2$), 2.65 ppm (64H,t, J 7.0 Hz ,NCH$_2$), 2.58 ppm (32H, t, J 6.0 Hz ,CH$_2$N), 2.49 ppm (64H, t, J 7.0 Hz, CH2CO), 2.40 ppm (56H,

t, J 7.0 Hz ,CH_2CO).^{13}C NMR spectroscopy (at 100 MHz in MeOD) displayed signals at 173.5 ppm (C=O), 53.0 ppm, 52.5 ppm, 49.8 ppm, 49.5 ppm, 49.0 ppm (CH3), 37.4 ppm, 36.5 ppm, 33.5 ppm, 31.5 ppm (CH2).Mass spectrometry (ES) yielded a measured mass of 6014 (M), while the calculated mass for $C_{270}H_{480}N_{58}O_{92}$ is 6014.

Synthesis of PAMAM dendrimer G 4.0

PAMAM G3.5 7 (19.44 g, 3.23 mmol) was stirred in 100 mL of methanol. Dropwise additions of EDA (93.5 g, 1.56 mol) were made over a period of 45 minutes. The mixture was allowed to undergo a chemical reaction at room temperature for ten days. The crude product was purified using an azeotropic solution (2.5 L mixture of 9:1 toluene: methanol) at 45°C to ensure complete removal of EDA. The crude product was concentrated and washed with 100 mL of methanol. The product, G4.0 8, was obtained as a yellow oil with a yield of 21 g (92%). The product was characterized as follows: FTIR (vmax/cm^{-1}), 3282 (N-H, amide stretch), 3080, 2940 (C-H stretch), 1643 (C=O), 1558 (N-H bend), 1468 (CH2 bend); ^{1}H NMR (400 MHz, D_2O), 3.25 (56H, t, J 6.0 Hz ,$NHCH_2$), 3.15 (64H, t, J 6.0 Hz, NHCH2), 2.74 (120H, t, J 7.0 Hz ,NCH_2), 2.62 (64H, t, J 6.0 Hz ,NH_2CH_2), 2.53 (60H, t, J 6.5 Hz NHCH2), 2.34 (120H, t, , J 6.50 Hz, CH_2CH_2); ^{13}C NMR (100 MHz, D_2O), 175.0 (C=O), 51.5, 50.5, 42.0, 40.0, 36.5, 33.0, 32.5 (CH$_2$); Mass spec (ES), 6913 (M), ES-MS $C_{302} H_{608} N_{122}O_{60}$ = 6913 (calculated).

6.1.5 Neutral PAMAM dendrimer synthesis

The standard method for Synthesis of Neutral OH-terminated dendrimers:

In a 250 ml round-bottom flask, a solution containing half of the dendrimer generation was mixed with DMSO. Dropwise additions of potassium carbonate and ethanolamine followed in the mixture. The mixture was stirred and subjected to reflux at 0°C for a period of three days. To eliminate any remaining potassium carbonate, the solution was filtered under reduced pressure. The product was then purified by performing three consecutive soakings with 200 ml of acetone. The resulting oil product settled at

the bottom of the flask. The acetone layer was carefully decanted, and 5 ml of distilled water was added to dissolve the product. After allowing the product to precipitate and settle for an hour, the upper layer was removed. The resulting product was subsequently dried in a vacuum oven, leading to the formation of the PAMAM-OH dendrimer.

Synthesis of PAMAM G1.0 OH (8 OH)

In 10 mL of DMSO, the half-generation of PAMAM dendrimer (6 g, 14 mmol) was dissolved. The mixture was then treated with K2CO3 (7.80 g, 56.22 mmol) and ethanolamine (4.02 g, 65.6 mmol) at 50°C. The reaction mixture was agitated and refluxed for three days. The purification process followed the previously described method. The resulting product was dried, yielding a yellow oil known as G0.5-OH, with a yield of 6.7 g (53%). The ^{1}H NMR spectrum recorded in D_2O at 400 MHz exhibited signals at 3.58 ppm (8H, t, J 5.5 Hz, CH_2CH_2OH), 3.20 ppm (8H, m, $NHCH_2CH_2$), 2.76 ppm (8H, m, $N(CH_2CH_2)$), 2.57 ppm (4H, t, J 7.0 Hz, CH_2CH_2N), and 2.36 ppm (8H, t, J 7.0 Hz, CH_2CH_2CO). The ^{13}C NMR spectrum recorded at 400 MHz in D_2O showed peaks at 174.3 ppm (C=O), 173.5 ppm (C=O), 60.5 ppm, 55.5 ppm, 50.0 ppm, 48.0 ppm, 41.5 ppm, 37.0 ppm, 33.0 ppm, and 33.5 ppm (CH_2). In the FTIR spectrum, characteristic peaks were observed at 3294 cm^{-1} (N-H stretch), 3125 cm^{-1}, 2940 cm^{-1}, and 2850 cm$^{-1.}$

Synthesis of PAMAM G2.0 OH

The G1.5 PAMAM dendrimer (10.2 g, 8.31 mmol) was dissolved in DMSO, and a gradual addition of ethanolamine (4.90 g, 0.08 mol) and potassium carbonate (11.07 g, 0.08 mol) was carried out while stirring the mixture. The resulting mixture was refluxed at 50°C for three days. The crude product was purified using a Rota evaporator. G1.5-OH (18 g, 75% yield) was obtained by drying the substance overnight in an oven. The following characterization data were obtained: Mass Spectrometry (ES), 1437 (m/z); ^{1}H NMR (D2O), 3.50 (16H, t, , J 5.5 Hz, CH_2CH_2OH), 3.19 (24H, t, $NHCH_2CH_2$), 2.68 (24H, t, J 7.0 Hz ,$N(CH_2CH_2)$), 2.49 (12H,t, J 7.0 Hz), 2.32 (24H, t, J 7.0 Hz ,CH_2CH_2CO); ^{13}C NMR (100 MHz,

D2O), 175.5 (C=O), 172.5 (C=O), 62, 52.5, 51.0, 47.5, 41.0, 37.5, 33.5 (CH2); FTIR (cm^{-1}), 3294 (N-H), 3133, 2959, 2846, 1584 (C=O), 1565 (N-H), 1454 (CH2), 1374, 1312, 1214, 1048.

Synthesis of PAMAM G3.0 OH

In 10 mL of DMSO, a PAMAM G2.5 (6.2 g, 2.16 mmol) was dissolved. Potassium carbonate (5.85 g, 0.042 mol) and ethanolamine (2.66 g, 0.043 mol) were added in portions to the dendrimer solution. The mixture was refluxed at 50°C and stirred for 70 hours. Subsequently, a purification step was carried out according to the basic technique, resulting in a yield of 5.76 g (80%). Mass spec TOF MALDI-MS, 3272 (MH+); 1H NMR (400 MHz, D2O), 3.63 (32H, t, CH2CH2OH), 3.32 (56H, m, NHCH2CH2), 2.81 (56H, t, N(CH2CH2), 2.60 (28H, t, CH2CH2N), 2.40 (56H, t, J 7.0 Hz, CH2CH2CO); ^{13}C NMR (400 MHz, D2O), 175.5 (C=O), 174.5 (C=O), 60.0 , 51.5 , 49.0 , 41.5, 39.0 , 36.5 , 33.0 (CH2) ;FTIR (cm-1) , 3423 (N-H stretch), 2945, 1642 (C=O), 1565 (N-H), 1445(CH2), 1317, 1072, 1035.

Synthesis of PAMAM G4.0 OH

A solution of 5.20 grams (0.88 mmol) of G3.5 PAMAM dendrimer was prepared by dissolving it in 10 ml of DMSO in a flat-bottom flask. To this dendrimer solution, 2.09 grams (0.034 mol) of ethanolamine and 4.61 grams (0.033 mol) of potassium carbonate were added. The resulting dendrimer solution was stirred and refluxed at 50°C for a period of three days. The product was then purified and dried using the standard method. G3.5-OH (6.45 g, 98%) was obtained as a result. Mass Spec 6941 (MH +);1H NMR (400 MHz, D2O), 3.54 (64H,t,), 3.25 (120H, t, NHCH2CH2), 2.77 (120H, m, N(CH2CH2), 2.54 (60H, t, CH2CH2N), 2.40 (120H, CH2CH2N);^{13}C NMR (100 MHz, D2O), 176.5 (C=O), 174.0 (C=O), 59.87 , 60.3, 52.8, 49.5, 48.8, 42.3, 37.8, 32.5 (CH2);FTIR (CM^{-1}) , 3267 (N-H), 3075, 2915, 2825, 1650 (C=O), 1549 (N-H), 1439 (CH2), 1363.

Beer-Lambert law experiment:

To determine the solubility of ibuprofen, an excess amount of ibuprofen was added to a 100 ml conical flask containing 50 ml of phosphate buffer solution with a pH of 7.4. The flask was then shaken at a

temperature of 25 degrees Celsius for 35 minutes. After appropriate dilution, the sample was filtered through a syringe filter with a pore size of 0.45 μm. The concentration of ibuprofen in the filtered sample was measured using UV spectrophotometry. To prepare the standard solutions, a dosage of 205 mg of ibuprofen was placed in a 100 ml volumetric flask and mixed with methanol. This resulted in a stock solution with a concentration of 1×10^{-3} mol/ml. From the stock solution, standard solutions with known concentrations (0.1, 0.3, 0.4, 0.7, and 1 mM) were prepared. The absorbance of ibuprofen was measured using UV/Vis spectroscopy, and the change in absorbance (Δ absorbance) was calculated based on the data obtained at wavelengths between 273 and 278 nm.

Preparation of Buffer Solutions

A solution was prepared by dissolving 2.022 g of sodium phosphate dibasic and 0.35 g of sodium phosphate monobasic in 1.0 L of distilled water. The resulting solution was used to create a buffer solution with a concentration of 0.01 M. The pH of the buffer solution was adjusted to 7.4 using either HCl (hydrochloric acid) or NaOH (sodium hydroxide).

General Method for Encapsulations

PAMAM dendrimer solutions with hydroxyl terminal groups (G2, G3, and G4) were prepared in methanol with an excess of ibuprofen. The solutions were vigorously shaken for 10 minutes. Subsequently, the solvent was removed using a rotary evaporator. Any excess ibuprofen was then filtered out, and the dendrimer/ibuprofen complexes were dissolved in a 10 ml solution of phosphate buffer at pH 7.4. Finally, UV-Vis analysis was conducted on all samples.

Solutions of PAMAM dendrimers were prepared for experimental use. (G 2, G 3, and G 4 -OH)

In 100 ml of methanol, 15 mg of G2-OH (1×10^{-4} M) was dissolved to make a stock solution. In contrast, the G3-OH solution was made by adding 32 mg and dissolving it in 100 ml of volumetric flask containing methanol. While 70 mg of G4-OH were diluted in 100 ml of methanol to create the G4-OH solution.

6.1.6 Synthesis of hyperbranched Polymers (HBPAMAM-NH2)

The General procedures for synthesis HBPAMAM

EDA (1.08 g, 17.65 mmol) and 3.75 ml of water were combined in the synthesis of HBPAMAM, followed by the addition of MBA (2.75 g, 17.65 mmol). The reaction mixture was equipped with a condenser and magnetic stirrer, and the compound was slowly added. The mixture was then refluxed at 60°C for 24 hours. After cooling to ambient temperature, the mixture was precipitated in 200 ml of acetone. The resulting product was concentrated under high vacuum to yield a light-yellow oily product (HBPAMAM 1). This process was repeated with various variables for all polymers.

Converting of HBPAMAM-NH$_2$ 1 to HBPAMAM-OMe 1 g of HPAMAM 27 was added to 20 ml of methanol in each of four 100 mL round bottom flasks. The HBPs solutions were then given a dropwise addition of 5ml of methyl acrylate. Rotary evaporation was used to recover the methanol. Light-yellow oil was obtained.

Encapsulation of ibuprofen by HBPAMAM-NH2

To encapsulate ibuprofen using HBPAMAM-NH2. two different concentrations, 0.005 mg/mL and 0.075 mg/mL, were prepared by dissolving 0.05 g and 0.75 g of HBPAMAM-NH2 (17) in 100 mL of methanol, respectively.

The Method of encapsulating ibuprofen using HBPAMAM-NH2 1 was carried out using four different concentrations.

HBPAMAM was diluted to four different concentrations (0.01, 0.02, 0.004, and 0.06 mg/mL) in four (100 ml) volumetric flasks (0.1, 0.2, 0.4, and 0.6 g).

General procedure for comparison encapsulation Studies:

The Method for encapsulation of Ibuprofen by using NH$_2$ ended PAMAM dendrimers and HBPAMAM-NH$_2$

Preparation solutions for G3/ HBPAMAM-NH2:

To obtain a concentration of 0.32 mg/mL, 0.032 g of G3/HBPAMAM-NH2 was introduced into 100 ml volumetric flasks.

Preparation solutions for G2/ HBPAMAM-NH2

To obtain a concentration of 0.14 mg/mL, 0.014 g of G2/ HBPAMAM-NH2 was weighed out and added to 100 ml volumetric flasks.